SYNTHESIS AND CHARACTERIZATION OF IN SITU WHISKER-REINFORCED GLASS-CERAMICS

by

Kyoungho Lee

Dissertation submitted to the Faculty of the

Virginia Polytechnic Institute and State University

in partial fulfillment of the requirements for the degree of

DOCTOR OF PHILOSOPHY

in

Materials Engineering and Science

APPROVED:

J.J. Brown, Jr., Chairman

R.S. Gordon

G.V. Gibbs

D.A. Hirschfeld

W.T. Reynolds

April, 1993

Blacksburg, Virginia

SYNTHESIS AND CHARACTERIZATION OF IN SITU WHISKER-REINFORCED GLASS-CERAMICS

by

Kyoungho Lee

Committee Chairman: J.J. Brown, Jr.
Materials Engineering and Science

(ABSTRACT)

The effects of in situ TiO_2 whisker reinforcement on mechanical and thermal properties of glass-ceramics in the Li_2O-Al_2O_3-P_2O_5-SiO_2 system were investigated.

When TiO_2 whiskers, having an average aspect ratio of 28, are precipitated from the glass-ceramic matrix, $(Li_{0.4},Ca_{0.05})Al(Si_{0.75},P_{0.5})O_{4.5}$, flexural strength is improved from 72 to 134 MPa. Fracture toughness, K_{IC}, is increased from the 1.1 to 1.6 $MPa{\cdot}m^{1/2}$ due to crack deflection by the TiO_2 whiskers. In situ TiO_2 whisker-reinforced glass-ceramic exhibits rising fracture resisnce, K_R, with increasing crack extension. The fracture resistance, K_R, is increased from 1.89 to 2.5 $MPa{\cdot}m^{1/2}$ over the crack extension range range of 40 to 200 μm. The composite shows a narrow failure strength distribution compared to the glass-ceramic without TiO_2 whisker precipitation. The coefficient of thermal expansion (CTE) changes from $-2.8x10^{-7}$/°C to $-1.7x10^{-7}$/°C due to the precipitation of TiO_2 phase which has a positive CTE ($7.3x10^{-6}$/°C).

With the matrix composition, $(Li_{0.41},Mg_{0.035})Al(Si_{0.48},P_{0.52})O_4$, a three-fold increase in flexural strength was observed with a TiO_2 content of 12 wt%. CTE value of the composite increases linearly from a negative to a positive value with increasing TiO_2 content up to 12 wt%. The in situ composite containing 8~10 wt% TiO_2 exhibits near-zero CTE values up to 1000°C.

ACKNOWLEDGEMENTS

I would like to express great appreciation to Dr. Jesse. J. Brown for giving me the opportunity to work with him and for his constant guidance and support throughout the course of my studies. I am deeply grateful for the privilege he gave me to work with the Center for Advanced Ceramic Materials here at Virginia Polytechnic Institute and State University.

I also wish to express my thanks to Dr. Ronald S. Gordon, Dr. Gerald V. Gibbs, Dr. William T. Reynolds, and Dr. Deidre Hirschfeld for serving on my committee. I would like to give special thanks to Dr. Deidre Hirschfeld for her help and support during my research and her editorial assistance. I also wish to express my thanks to a special person, Nancy Brown, for her assistance in the preparation of numerous reports and presentations.

I would like to thank Mrs. Katie Hutchison and Mrs. Susan Fleming for their assistance and support during my studies.

I am thankful for my fellow graduate students within the center for their aid, support, and friendship.

I would like to thank my parents and parents-in-law for their steadfast support of all my undertakings.

I am deeply grateful to my loving wife, Keum-Jung, whose continual encouragement and support made this educational endeavor a reality.

Finally, my warmest gratitude and love are given to my daughter, Sowon, for her cheerful smile during the study.

TABLE OF CONTENTS

LIST OF TABLES

LIST OF FIGURES

CHAPTER I

INTRODUCTION

The development of materials with mechanical reliability at room temperature and for extended high temperature service has been the object of scientific inquiry for many years. One approach to the development of advanced materials with these characteristics is the formation of composite materials in which a low modulus, low strength material is reinforced by a high modulus, high strength second phase, typically in the form of fibers or whiskers with high aspect ratios. The strong and stiff second phase carries the applied load so that the overall strength and toughness of the composite are improved.

Reinforcing materials are usually prefabricated into a desired shape and size, and added to the matrix material during composite processing. In some cases, however, materials may be reinforced in situ. For instance, in binary eutectic compositions, in situ composite formation is common.[1,2,3] When the eutectic reaction is carried out unidirectionally, a planar solid-liquid interface may be produced, and one of the solid phases is formed into lamella or fiber shapes. Glass-ceramics are a type of in situ composite because, by careful time-temperature heat treatment, the crystal phase is precipitated throughout the glass matrix. Superior physical properties of glass-ceramics compared to those of base glasses have been reported by various researchers.[4,5,6]

In the present study, an in situ TiO_2 whisker-reinforced $AlPO_4$-modified β-eucryptite glass-ceramic composite was fabricated. Considerable data (which will be discussed in succeeding sections) indicate that the mechanical performance of a whisker-reinforced glass-ceramic composite is superior to that of the glass-ceramic which serves as the matrix. The effect of TiO_2 whiskers formed in situ on the mechanical and thermal properties of $AlPO_4$-modified β-eucryptite glass-ceramics will be discussed in this study in detail.

In situ composite fabrication offers a number of advantages over conventional composite processing techniques:

(a) Composite fabrication temperature is relatively lower so there is no thermal degradation of whisker during fabrication. Furthermore, rather than adding prefabricated whiskers, the whiskers are precipitated throughout the matrix, thus there is no whisker degradation during handling and blending. Therefore, theoretical mechanical strength and stiffness of the whiskers can be fully utilized.

(b) There is no prefabrication of whiskers involved, therefore the manufacturing cost of the reinforcement is eliminated.

(c) The potential health hazards associated with handling of reinforcing materials is eliminated.

Promising applications for these materials include use as electronic substrates, sealing frits for low-expansion materials, thermal shock resistance ceramics, and possibly structural ceramics.

CHAPTER II

GENERAL BACKGROUND

2.1 β-Eucryptite (β-$LiAlSiO_4$)

β-eucryptite, with a structure of high-quartz (space group $P6_222$), is a stuffed-derivative of SiO_2 in which half of the Si^{4+} ions are replaced by Al^{3+} ions, and the charge balance is maintained by the addition of Li^+ ions into the main channels of the structure, which are positioned parallel to the crystallographic **c** axis. Winkler[7] synthesized a single crystal of β-eucryptite and hypothesized that the Si and Al atoms were arranged in an ordered way in alternating layers, perpendicular to the **c** axis. Li atoms in the main channels of the structure should occupy the 4-fold coordination sites, which are surrounded by 4 oxygen atoms. Tscherry and Laves[8] confirmed the ordering of Al and Si layers and the oxygen coordination of Li atoms. Figure 2.1 shows the β-eucryptite structure projected along the **c** axis.

With increasing temperature, Li atoms in all channels tend to change from an occupied site to an unoccupied 4-fold or 6-fold coordination site. When an Li atom enters a 6-fold coordination site, the atom will push oxygen atoms along the **a** axis. The corresponding shifts of oxygen atoms are shown in Figure 2.2. Consequently, the framework around the Li atoms expands parallel to the **a** axis and contracts parallel to the **c** axis. In terms of the entire crystal, the **a** axis must be expanded and the **c** axis must be contracted.

Strong negative aggregate bulk coefficient of thermal expansion (CTE), from about -60×10^{-7}/°C to -90×10^{-7}/°C (20 to 850°C), for sintered bars of β-eucryptite has been determined by different researchers.[9,10] Three CTE values for the **a** axis and **c** axis of β-eucryptite reported by different researchers[11,12,13] are given in Table 2.1.

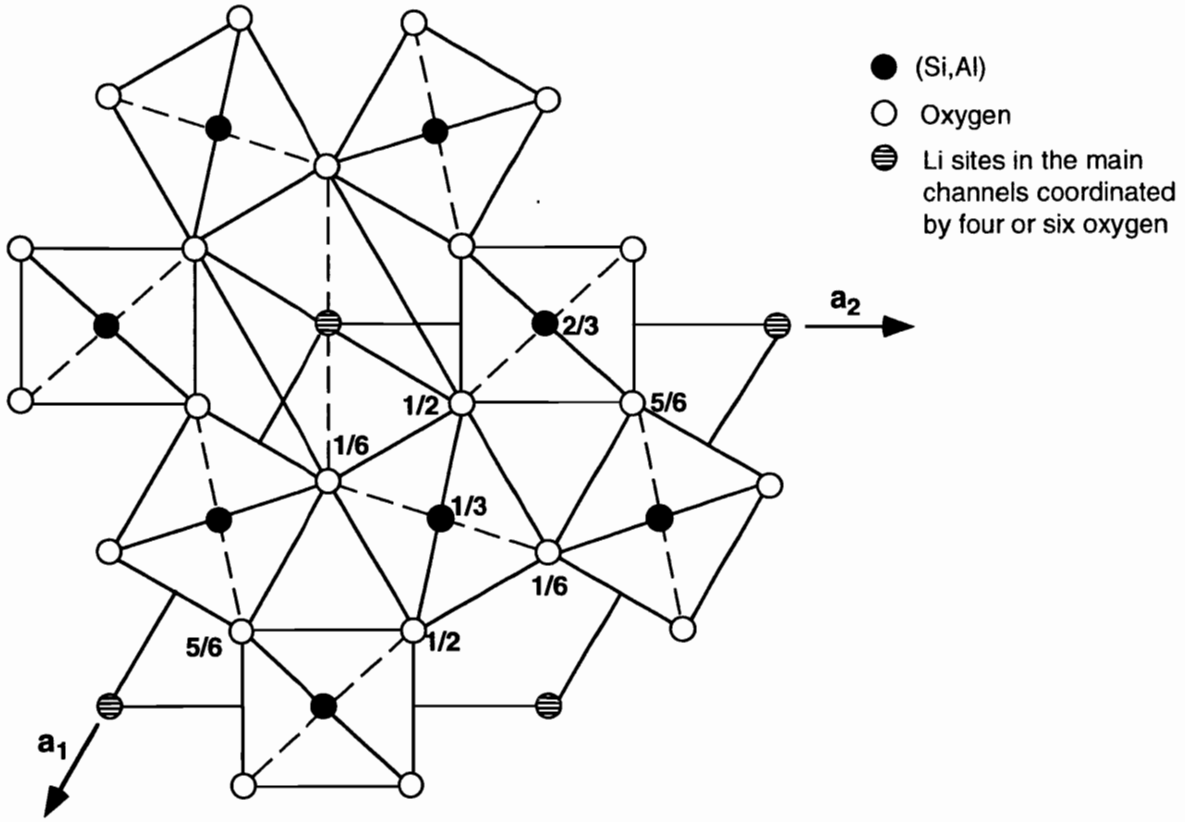

Figure 2.1 Schematic projection of β-eucryptite structure on (001). The numbers in the figure are the z-coordinates. The drawn LiO_4 tetrahedron contains lithium with z=1/3.[7]

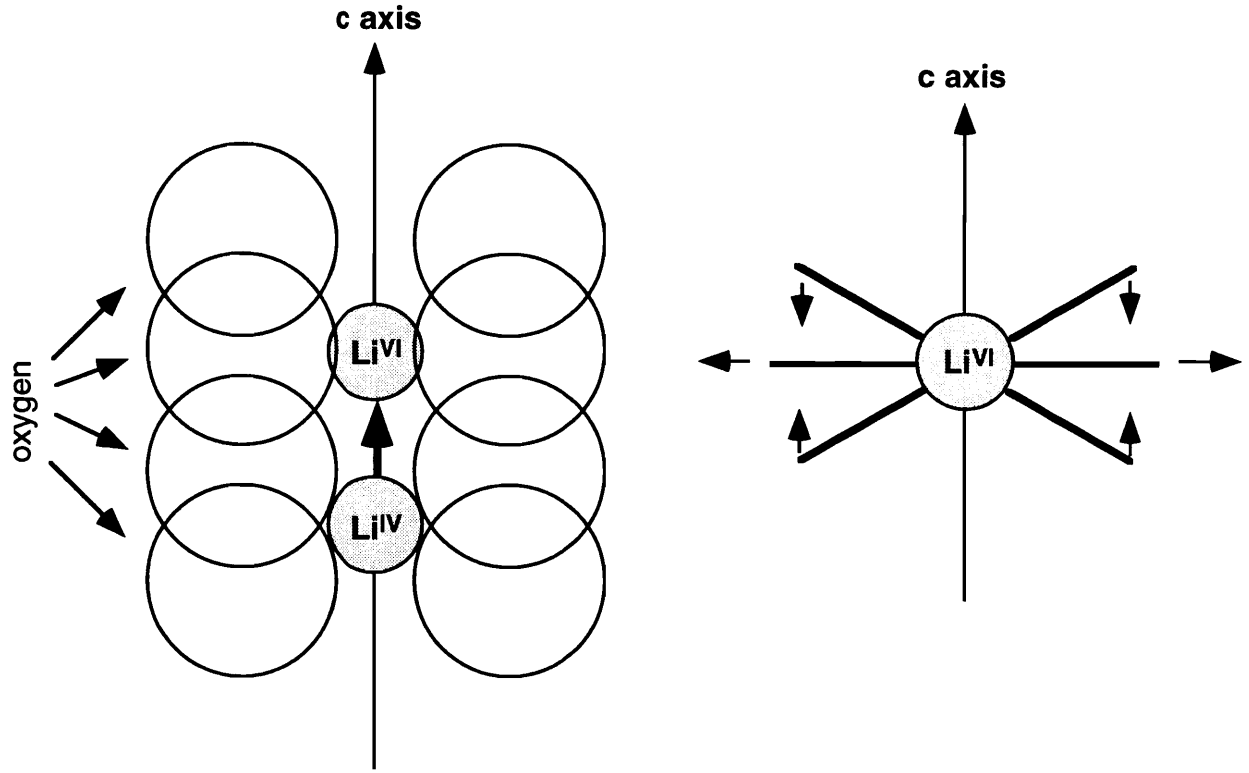

Figure 2.2 Influence of the disordering of an Li atom (from 4- to 6-coordinations) on shifts of oxygen atoms.

Table 2.1. Axial Expansion of β-Eucryptite

CTE along **a** axis ($x10^{-7}$/°C)	CTE along **c** axis ($x10^{-7}$/°C)	Reference
82.1	-176	Gillery *et al.*[11]
81.1	-169	Tien *et al.*[12]
79.0	-152	Tscherry *et al.*[13]

Such high anisotropy of thermal expansion affects the mechanical properties of β-eucryptite. High stresses arise in the polycrystalline sintered β-eucryptite during cooling from the firing temperature; high tensile stress arises along the **a** axis. When this stress exceeds the strength of the crystal or the crystal interface, cracks form. Even though this stress does not exceed the strength of the crystal or the crystal interface, tensile stress can produce microcracks with a small applied load. These cracks cause extensive fracturing of the material, resulting in abnormally poor mechanical properties at room temperature.

2.2 Chemically Modified β-Eucryptite

Many researchers have tried to reduce thermal expansion anisotropy by introducing additives to the β-eucryptite structure. By increasing the SiO_2 content in β-eucryptite solid solutions, Hummel[14] and Moay, Verduch, and Hortal[15] decreased the negative aggregate thermal expansion of those solid solutions. Their results are shown in Figure 2.3.

Hummel and Langensiepen[16] reported the formation of a solid solution between 50 mol% $AlPO_4$ and 50 mol% β-eucryptite which has a thermal expansion as low as that of fused quartz. The structure, inversion temperature, and thermal expansion of $AlPO_4$ are very similar to SiO_2. Perotta[17] reported that a solid solution series extending from 5 to 65 mol% $AlPO_4$ with β-eucryptite can form in the $AlPO_4$-β-$LiAlSiO_4$ system by heating the mixture at 1050°C or higher. The CTE values of this range of compositions varied from $-70x10^{-7}$/°C to $11x10^{-7}$/°C at 1000°C.

Yang[18] measured the coefficient of the axial thermal expansion of the solid solution phase $(Li_{0.41},Mg_{0.035})Al(Si_{0.48},P_{0.52})O_4$, composed of 48 mol% β-$LiAlSiO_4$ and 52 mol% $AlPO_4$ where 20 mol% Li is replaced by Mg. The axial thermal expansion behavior of this $AlPO_4$-modified β-eucryptite solid solution is shown in Figure 2.4. It is

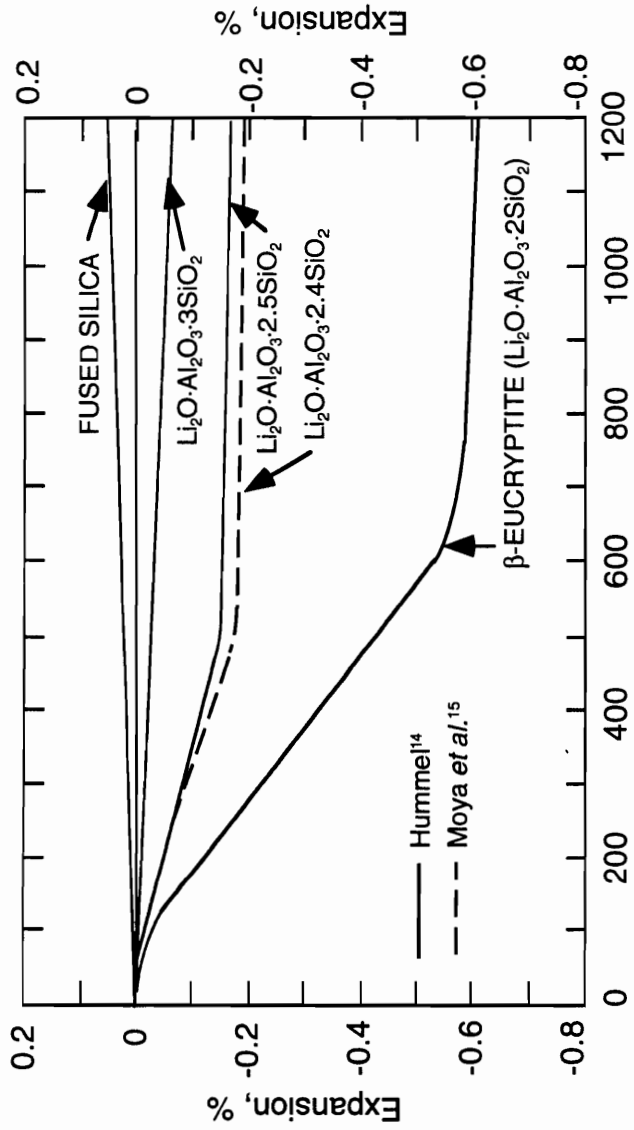

Figure 2.3 Thermal expansion of β-eucryptite and its solid solutions.

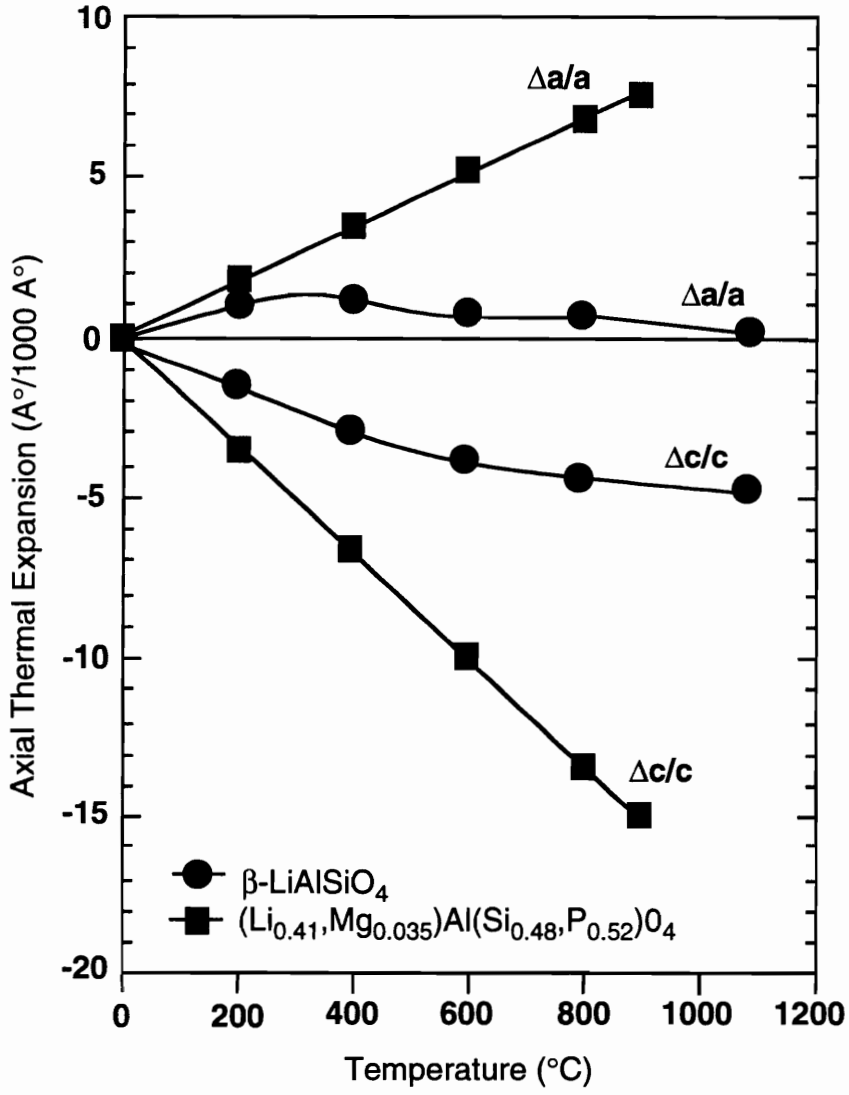

Figure 2.4 Axial thermal expansion of pure β-eucryptite and a modified β-eucryptite.[18]

clearly seen that the $AlPO_4$-modified β-eucryptite solid solution exhibits a near-zero CTE ($-7x10^{-7}/°C$) and lower thermal expansion anisotropy than β-eucryptite.

These facts mentioned above form the basis of this study. Fabrication of a ceramic exhibiting a near-zero CTE suggests superior service capability under severe thermal shock conditions. Lowering thermal expansion anisotropy reduces the possibility of microcrack formation during cooling from sintering or operating temperatures. Therefore, $AlPO_4$-modified β-eucryptite should inherently possess better thermal and mechanical properties than pure β-eucryptite. However, mechanical properties of materials strongly depend on processing conditions. It is experimentally well known that the strength of ceramic materials is strongly dependent on porosity and grain size as described below:[19]

$$\sigma_f = \sigma_o \exp(-nP) \tag{2.1}$$

$$\sigma_f = \sigma_o + kd^{-1/2} \tag{2.2}$$

where n is an experimental constant ranging from 4 to 7, P is the volume fraction porosity, k is an other experimental constant, and d is grain size. The above equations indicate that the strength should increase with decreasing porosity and grain size. A non-porous and fine-grained ceramic body can be obtained by suitable processing techniques. In this study, glass-ceramic processing was selected to produce dense and fine, uniform-grained $AlPO_4$-modified β-eucryptite. Furthermore, during glass-ceramic processing, TiO_2 whiskers are formed throughout the glass-ceramic matrix.

2.3 Glass-Ceramics

Glass-ceramics are polycrystalline solids prepared by controlled heat treatment (usually a two-step process) of appropriate glasses. They consist of a large proportion, typically 95 to 98 vol%, of very small crystals, generally smaller than 1 μm, with a small amount of residual glass phase making up a pore-free body.

Since introduction of the first commercial glass-ceramics, many glass-ceramic materials have been developed for diverse applications such as described by Vogel,[4] Paul,[5] and Strinad,[6] and including machinable glass-ceramics, high-strength glass-ceramics, biomedical glass-ceramics, and optical and electrical glass-ceramics. This literature review focuses on the thermal and mechanical properties of glass-ceramics.

2.3.1 Glass-Ceramic Processing

At one time, crystallization was one of the most serious problems in glass production. The uncontrolled crystallization of glasses initiates at external surfaces, and is followed by crystal growth, producing a non-uniform body of large grain size. However, once crystallization in glasses was controlled and utilized by Stookey,[20] intentionally crystallized glasses became novel materials.

The object of the heat treatment process is to convert a glass into a uniform and fine-grained polycrystalline ceramic having properties superior to those of original glass. The most important feature of glass-ceramics is their high mechanical strength and toughness, which results from their fine-grained and pore-free microstructure. Therefore, in glass-ceramic processing, the question to be answered is, how can a fine-grained microstructure be obtained during conversion from glass to glass-ceramic? Figure 2.5 shows a hypothetical temperature-time cycle for producing a glass-ceramic material. Usually, the controlled heat treatment schedule for producing glass-ceramics

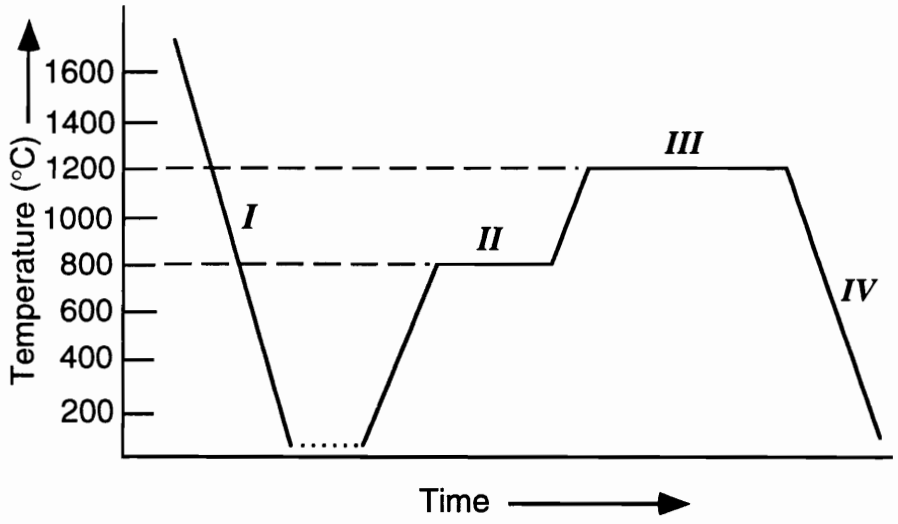

Figure 2.5 Schematic of a glass-ceramic formation as a function of time and temperature.
I: Glass processing
II: Nucleation
III: Crystallization
IV: Annealing of final product

consists of nucleation and crystal growth. To obtain small crystals occupying a large volume fraction of the material, a uniform density of nuclei on the order of 10^{12} to $10^{15}/cm^3$ is required.[19] This in turn means that the nucleation stage of the heat treatment must be carefully controlled.

2.3.2 Nucleation and Crystal Growth (Theoretical Considerations)

(A) Homogeneous and Heterogeneous Nucleation

The nucleation step can probably be singled out as the most critical operation in the glass-ceramic process because it determines whether a uniform crystalline dispersion is achieved. At temperatures below liquidus, the crystalline phase has lower volume free energy than either the liquid or the glass; therefore, substantial thermodynamic and kinetic barriers work against spontaneous and large-scale crystallization. That means crystallization is first initiated at discrete nuclei, with subsequent outward growth from these sites proceeding by migration of the glass/crystalline interface. The nucleation process can be classified as either homogeneous or heterogeneous.

The free energy change upon nucleation, ΔG_r, for the homogeneous nucleation of a spherical crystallite at a temperature below the liquidus temperature is given by:[21]

$$\Delta G_r = \frac{4}{3}\pi r^3(\Delta G_v + \Delta G_s) + 4\pi r^2\gamma \qquad (2.3)$$

where r is the particle radius, γ is the interface energy, ΔG_v is the volume free energy change due to the creation of a volume of thermodynamically stable particle, and ΔG_s is the misfit strain energy. Thus the volume free energy reduction of ΔG_v provides the driving force for nucleation. Note that the misfit strain energy and surface energy terms increase the effective barrier for nucleation. This is shown as a function of r in Figure

2.6. It is clearly seen in Figure 2.6 that a nucleus must have a certain critical size in order to grow. Only when some critical value of radius, r^*, is attained, does the volume free energy term in Equation 2.3 become sufficiently large that incremental nucleus growth beyond r^* results in a net free energy decrease. For this reason, only nuclei with $r > r^*$ will be stable. The critical radius of nucleus and the activation energy barrier for nucleation can be obtained by differentiating the Equation 2.3:[21]

$$r^* = -\frac{2\gamma}{(\Delta G_v + \Delta G_s)} \qquad \Delta G^* = \frac{16\pi\gamma^3}{3(\Delta G_v + \Delta G_s)^2} \qquad (2.4, \text{a,b})$$

where ΔG^*, the free energy change accompanying the formation of the critical-sized nucleus, represents the energy barrier for nucleation.

Nucleation in solids, like in liquids, is almost always heterogeneous. The term "heterogeneous nucleation" refers to the facilitation of nucleation of the main phase by the presence of some alien crystalline nucleus. The formation of a nucleus from the pre-existing surface of a foreign nucleus results in destruction of a defect; free energy (surface free energy) will then be released thus reducing the activation energy barrier, ΔG^*. As depicted in Figure 2.7, if the nucleus forms on the pre-existing surface of the primarily separated solid phase from the glass, then the free energy change connected with the creation of two surface boundaries is given by the relationship:[21]

$$\Delta G_{surface} = \gamma_{GN} A_{GN} + \pi r^2 (\gamma_{NS} - \gamma_{GS}) \qquad (2.5)$$

where γ_{GN}, γ_{NS}, and γ_{GS} are the glass-nucleus, nucleus-solid, and glass-solid interfacial energies, respectively, and A_{GN} is the surface area of the glass-nucleus phase boundary. In Equation 2.5, if $\gamma_{GS} > \gamma_{NS}$, then the overall free energy connected with the formation of

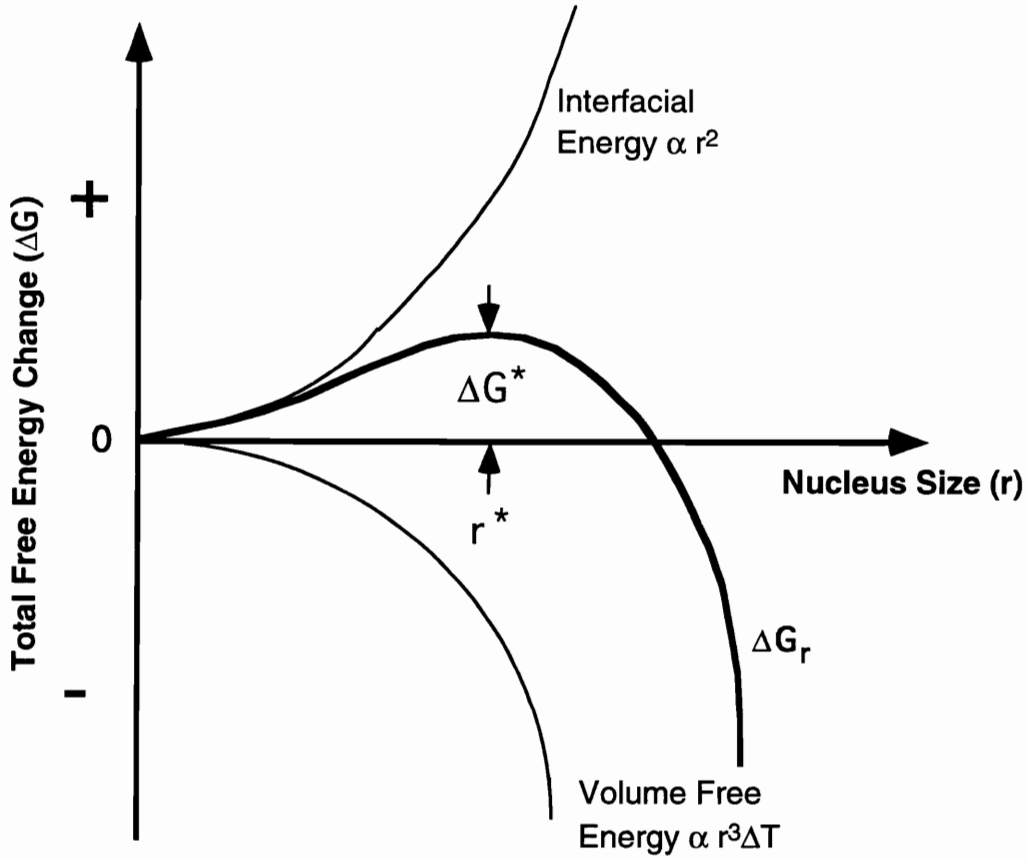

Figure 2.6 Nucleation barrier, ΔG, as a function of radius of a nucleus.[21]

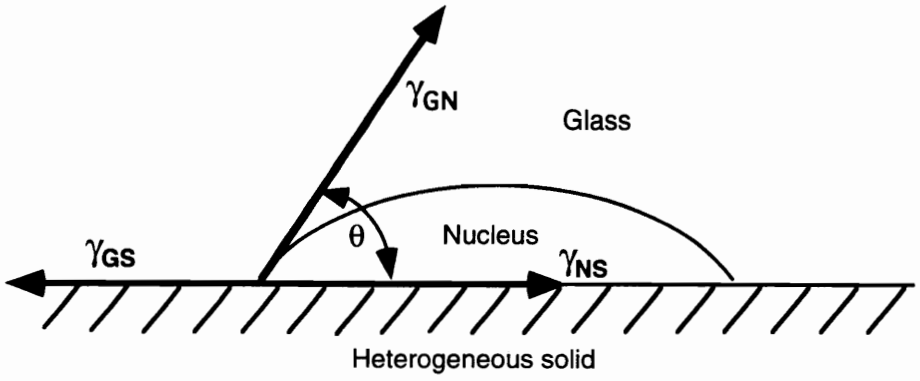

Figure 2.7 Heterogeneous nucleation on a flat heterogeneous solid.[21]

the heterogeneous nuclei is smaller than that for homogeneous nucleation. The above equation can be expressed by wetting angle, θ, and the nucleus cap radius, r, as:[21]

$$\Delta G_{het} = \left\{ \frac{4}{3}\pi r^3 (\Delta G_v + \Delta G_s) + 4\pi r^2 \gamma \right\} f(\theta) \tag{2.6}$$

where $f(\theta) = \dfrac{(2+\cos\theta)(1-\cos\theta)^2}{4}$

Similarly, the activation energy barrier for heterogeneous nucleation will be:[21]

$$\Delta G^*_{het} = \Delta G^*_{\text{hom}} f(\theta) = \Delta G^*_{\text{hom}} \left(\frac{(2+\cos\theta)(1-\cos\theta)^2}{4} \right) \tag{2.7}$$

So, heterogeneous nucleation occurs if the interfacial energy between liquid phase and alien nucleus is less than that between the liquid phase, *i.e.*, $\theta < 180°$. Generally, $0 \le f(\theta) \le 1$,[22] so that heterogeneous nucleation offers a lower free energy barrier to overcome for nucleation.

While thermodynamics predicts whether nucleation is favorable in a given situation, kinetics determines how long it will take if nucleation is favorable. Nucleus growth is limited by the rate at which atoms or molecules arrive at the interface for incorporation into the nucleus. The concentration of critical-sized nuclei, C^*, is given by:[21]

$$C^* = C_o \exp\left(-\frac{\Delta G^*}{kT} \right) \quad clusters\, m^{-3} \tag{2.8}$$

where C_o is the number of atoms per unit volume in the phase, k is Boltzman's constant, and T is the absolute temperature. If each nucleus can be made at a rate of $f = \omega exp(-\Delta G_m / KT)$ per second, nucleation rate can be given by:[21]

$$I = f^* C^* = \omega C_o \exp\left(-\frac{\Delta G_m}{kT}\right)\exp\left(-\frac{\Delta G^*}{kT}\right) \quad Nuclei\ m^{-3}\ s^{-1} \tag{2.9}$$

where ΔG_m is the activation energy for diffusion of atoms across the boundary. The temperature required for the maximum nucleation rate can be predicted by Equation 2.9. Both near the melting point (liquidus) and at much lower temperatures, nucleation rate will be low due to, respectively, the high value of ΔG^* or ΔG_m. Only at a certain intermediate temperature, where the volume free energy driving force is high with rapid diffusion process, will the nucleation rate be a maximum.

(B) Crystal Growth

Crystal growth heat treatment is the next step for producing glass-ceramics once critical-sized nuclei have been attained. Thermodynamic and kinetic factors also determine the crystal growth rate. Atoms must first diffuse to the crystal-glass interface and then must obtain energy sufficient to overcome any energy barrier which is associated with adopting the atomic configuration of the crystal structure. Swift[23] showed an empirical expression for crystal growth rate U of the form:

$$U = \frac{K}{\eta}(T_{liq.} - T) \quad cm\ s^{-1} \tag{2.10}$$

where K is constant, η is the coefficient of viscosity, $T_{liq.}$ is the liquidus temperature, and T is the temperature of interest. The degree of undercooling, $T_{liq.}$ - T, represents the

thermodynamic factors for the crystal growth rate, while the coefficient of viscosity represents the kinetic factors. Like nucleation rate, maximum crystal growth will occur at a certain intermediate temperature where undercooling, $(T_{liq.} - T)$, is high enough to overcome any activation energy associated with atomic arrangement of the crystal structure, and viscosity, η, is low enough to give high diffusion rate.

Nucleation and crystal growth rate curves as a function of temperature for two hypothetical glasses are shown in Figure 2.8. These curves illustrates two extreme cases of nucleation and crystal growth. Figure 2.8(a) shows two rate curves which do not overlap. In this case, a glass-ceramic having uniform and fine crystals can be obtained by two-step heat treatment processing. The first heat treatment stage is nucleation, which produces a sufficiently large number of nuclei throughout the bulk of the glass. The second heat treatment stage is crystallization, which produces uniformly dispersed fine crystals from the nuclei. Figure 2.8(b) shows a system where the two rate curves overlap. In this case, crystals grow immediately once nuclei are formed, so there is no chance to produce a sufficient number of nuclei. Therefore, the end glass-ceramic product will show a small number of non-uniform and coarse grains. The degree of overlapping nucleation rate and growth rate depends on the glass system. Usually, nucleating agents are added to the glass to assure that nucleation occurs well below crystallization in order to produce sufficiently large number of nuclei before crystallization.

(C) Nucleating Agents

The addition of a nucleating agent to a certain glass leads to enhanced rates of uniform crystalline nucleation throughout the entire volume of the glass. Fluorides, phosphates, TiO_2, ZrO_2, and compounds of W, V, Ni, Cr, Mn, Fe, Cu, Ag, Au, and the

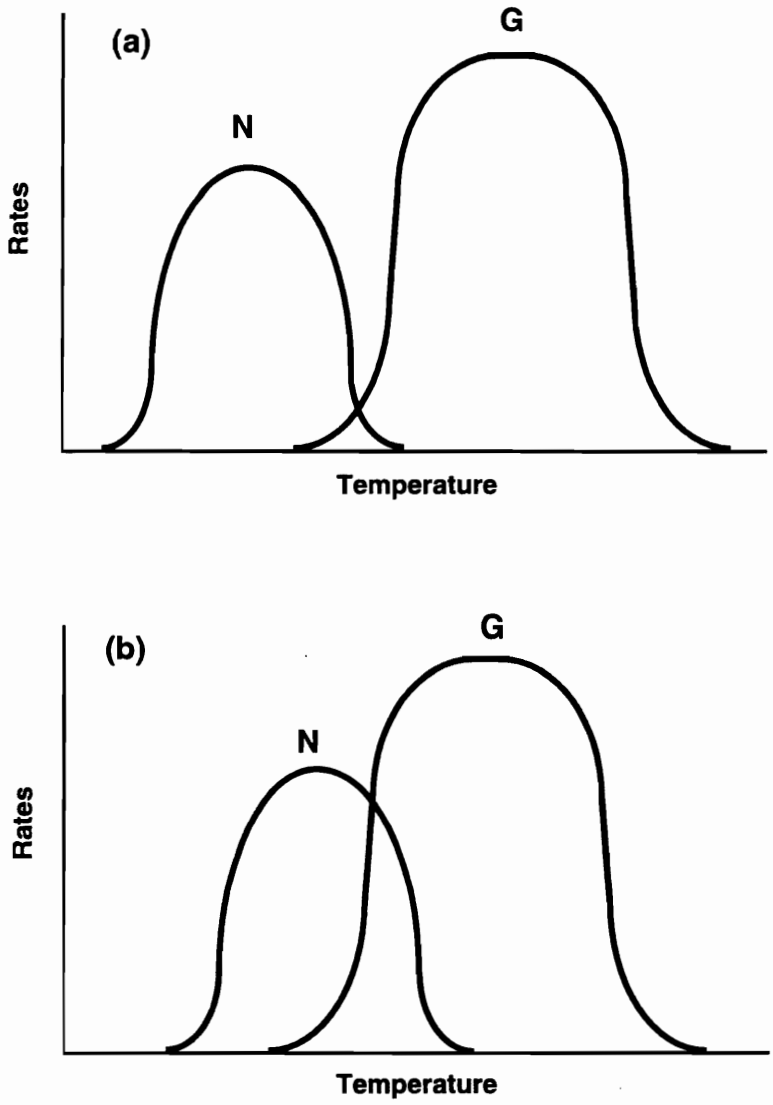

Figure 2.8 Nucleation (N) and crystal growth rate (G) of two hypothetical glasses as a function of temperature.
(a) N and G curves are not overlaped.
(b) N and G curves are overlapped.

platinum metals have been used for nucleating agents. According to Vogel,[4] nucleating agents can be placed into two categories:

(1) Nucleating agents which enhance phase separation (affecting nucleation indirectly) such as fluorides and phosphates.

(2) Nucleating agents which are soluble in the molten glass but precipitate during cooling or upon reheating the glass due to their strong over-saturation.

TiO_2 is the most widely used nucleating agent. This agent is used in lithia aluminosilcates and magnesium aluminosilcates because TiO_2 is quite soluble in silicate glasses and lowers their viscosity considerably. Although many researchers believe that TiO_2 belongs in the second category of nucleating agents, the exact role of TiO_2 in the nucleation of the glass is not clear. Doherty *et al.*[24] found that $Al_2Ti_2O_7$ crystals were precipitated and that these crystals act as heterogeneous nucleation sites for the β-quartz solid solution in a Li_2O-Al_2O_3-SiO_2-TiO_2 system. Also, Maier *et al.*[25] observed the formation of $ZrTiO_4$ type crystallites as the nuclei in a Li_2O-Al_2O_3-SiO_2-ZrO_2 system.

However, there is not much evidence that the crystalline phase which contains TiO_2 is the first phase to precipitate during heat treatment of a glass to form a glass-ceramic. Barry *et al.*[26] found that β-eucryptite and $Li_2O{\cdot}Al_2O_3$ crystals formed in various lithium aluminosilicate glasses containing TiO_2 before any titanate crystal phases were presented. Failure to observe TiO_2 or titanate as the first crystallized phase suggests another nucleation mechanism in which TiO_2 promotes nucleation. Hintz *et al.*[27] suggested that the role of TiO_2 is to promote liquid-liquid phase separation.. Ti^{4+} is tetrahedrally coordinated with oxygen at high temperatures, but the coordination with surrounding oxygen changes to octahedral or cubic symmetry as temperature decreases to near the range of the annealing point of the glass. Changing the coordination number with surrounding oxygens results in microphase separation. Hsu *et al.*[28] observed that

the introduction of TiO_2 in a lithia aluminosilicate glass leads to microphase separation, promoting heterogeneous nucleation. The role of phase separation in the nucleation process is either: (1) the formation of an amorphous phase of relatively high mobility in a temperature range where the driving force for crystallization is large,[29] or (2) the introduction of new interface boundaries between the phase-separated regions where the nucleation of the first crystalline can take place.[30,31] Hillig[32] suggested that perhaps TiO_2 lowers the interfacial tension, γ, between the crystal and the glass, thus increasing the rate of nucleation according to Equation 2.4(b). There is no direct evidence for this mechanism but it is feasible because Ti^{4+} ions which have high field strength can act as a "surface active agent" to lower the interfacial energy.

2.3.3 Physical Properties of Glass-Ceramics

(A) Mechanical Strength

The mechanical strength and elastic moduli of glass-ceramic materials are important characteristics for evaluating suitability of a given substance for a particular application. Similar to the initial glass or ceramics, glass-ceramics are also brittle at room temperature and do not exhibit ductility or plasticity. Considering glass-ceramics as brittle glass-crystal composites, the mechanical properties are strongly dependent on the composition, particle size and volume fraction of crystals, interfacial bonding strength, and thermal expansion mismatch.

The strength of glass-ceramic materials (60-350 MPa) are generally higher than those of the mother glasses (55-70 MPa). This may be due to elastic modulus values (80-140 GPa) of the crystals, which are higher than that of the glass (~70 GPa).[33] Table 2.2 shows bending strength of various types of glass-ceramics.

Table 2.2. Bending Strength (MOR) of Various Glass-Ceramics[6]

Glass-Ceramic Systems (Nucleating Agent)	Main Crystalline Phase	Bending Strength (MPa)
SiO_2-Li_2O		
(photonucleation Ag, Cu, Au)	$Li_2O{\cdot}SiO_2$, $Li_2O{\cdot}2SiO_2$	80-150
Li_20-Al_2O_3-SiO_2		
(TiO_2, ZrO_2)	β-Spodumene (ss)	110-180
(TiO_2, ZrO_2)	β-Quartz (ss)	60-110
MgO-Al_2O_3-SiO_2		
(TiO_2)	Cordierite	150-300
CaO-Al_2O_3-SiO_2		
(fluorides, sulfide)	Anorthite	70-130
ZnO-Al_2O_3-SiO_2		
(TiO_2)	Gahnite	70-130
(ZrO_2, SnO_2)	β-Quartz (ss)	60-110
MgO-K_2O-F-Al_2O_3-SiO_2	Fluorophlogopite	80-105

Furthermore, as discussed previously, their fine-grained and uniform microstructure greatly increases the strength of the glass-ceramics compared to their mother glasses. As indicated by Inglis[34] and Griffith,[35] fracture in brittle solids initiates at micro-levels of flaws, such as microcracks, inclusions, and inherent pores. In other words, the mechanical strength of glass-ceramics is strongly influenced by the microstructure of the glass-ceramic. Equation 2.2 becomes understandable if we consider the Griffith equation:[35]

$$\sigma_f = \left(\frac{2E\gamma}{\pi c}\right)^{1/2} \tag{2.11}$$

where σ_f is the fracture strength of the given material, E is the Elastic Modulus, γ is the fracture surface energy, and c is the microcrack length. This equation implies that the microstructure which has smaller microcracks will have a higher strength value. Microcracks are formed either within the crystalline grain or at the boundary between glass and crystal, thus the length of microcracks is limited by the grain size. Therefore, the glass-ceramic having small grain microstructure will possess smaller microcracks than a glass-ceramic having large grain microstructure. The influence of grain size on strength has been reported for several glass-ceramic systems.[36,37,38]

The fracture strengths of glass-ceramics are also strongly dependent on internal or residual stresses resulting from thermal expansion mismatches between the glass and crystalline phases. By influencing the level of localized stress in the crack tip region, this thermal expansion mismatch can control the conditions for catastrophic fracture. Internal stresses are always present in multiphase materials which have different CTE values. The stress state for multiphase solids after cooling from their fabrication or use temperature was first described by Weyl[39] and later modified by Selsing.[40] The various

stress conditions in the matrix and in a spherical inclusion are listed in Table 2.3. It is clearly seen that regardless of whether the inclusion has a CTE higher or lower than that of the matrix, some component of matrix stress will always be tensile. The presence of a tensile internal stress implies that thermal expansion mismatch may lower fracture strength.

This theoretical approach, however, is not totally supported by literature data on brittle composites. Several investigators examined the strength of glass and ceramic particulate composites fabricated by hot pressing mixtures of glass and ceramic powders. Binns[41] measured fracture strength of glass matrix composites consisting of three different sizes of alumina particles (10, 45, and 180 μm). By changing glass compositions, composites with different amounts of thermal expansion mismatch were fabricated at a given volume fraction and size of alumina particles. According to his results, except for the composite which contained 180-μm alumina particles, the composites showed an increase in fracture strength regardless of the sign or magnitude of the thermal expansion mismatch. Similar results were reported by Frey and Mackenzie.[42] For a single particle size of 120-150 μm, strength values above that of the base glass were obtained regardless of sign or magnitude of the thermal expansion mismatch. More evidence for the strengthening effect of thermal expansion mismatches was reported by Borom *et al.*[43] They found increased fracture strength in a glass-ceramic which contained a $LiSiO_5$ crystal phase of higher CTE value than the glass matrix of the Li_2O-SiO_2 system. Tummala *et al.*[44] reported similar results in that fracture strength was increased for hot-pressed, glass-stabilized zirconia composites when α_p is greater than α_m. In these cases, thermal expansion mismatch has a beneficial effect on strength despite the radial tensile stress component on the matrix.

Thus, the sign and the magnitude of thermal expansion mismatch can act

Table 2.3. Internal Stresses Existing in a Material Containing Spherical Inclusions

Stress State			
Condition	Particle	Matrix	
		σ_{rr}	$\sigma_{\phi\phi}$
$\alpha_p > \alpha_m$	Tension	Tension	Compression
$\alpha_p < \alpha_m$	Compression	Compression	Tension

beneficially. It is clear, however, that if the localized stress due to the thermal expansion mismatch is large enough to create microcracks, strength will be decreased dramatically.[45] In composites where $\alpha_p > \alpha_m$, circumferencial microcracks around inclusions will be formed due to the radial tensile stress in the matrix near the inclusions. In composites with $\alpha_p < \alpha_m$, radial cracks will be formed at particle and matrix interface due to the tangential tensile stress.

In addition to thermal expansion mismatches, the size of a dispersed phase affects the creation of microcracks. Binns[41] reported that at a given thermal expansion mismatch, microcracks would be more likely to form around coarse, rather than fine, particles. Davidge and Green[45] showed the critical size of inclusion radius, R_c, at a given value of thermal expansion mismatch ($\alpha_p > \alpha_m$) to be:

$$R_c \geq \frac{8\gamma_{eff}[(\alpha_p - \alpha_m)\Delta T]^2}{\frac{(1+\nu_m)}{2E_m} + \frac{(1-2\nu_p)}{2E_p}} \tag{2.12}$$

where γ_{eff} is the fracture energy of the matrix, υ is the Poisson's ratio, E_m and E_p are the elastic moduli of the matrix and the particle, respectively, and ΔT is the temperature difference. According to the equation, the presence of particles larger than the critical size will create circumferential microcracks due to thermal expansion mismatch.

(B) Thermal Expansion Behavior of Some Selected Glass-Ceramic Materials

One advantageous aspect of glass-ceramic technology is that a material with a desired CTE can be fabricated. The CTE of glass-ceramic materials depends on the type of crystalline phase and the volume fraction of crystalline phase in the glass-ceramic substance. In a given glass composition, the type and volume fraction of the crystalline

phase can be controlled by the heat treatment. Freiman *et al.*[46] found decrease in the CTE value of the glass-ceramic in Li_2O–SiO_2 system with increasing volume fraction of crystalline phase ($Li_2O{\cdot}2SiO_2$). Therefore, the CTE of a given glass-ceramic can be controlled by crystallization heat treatment temperature and time. The values of the CTE of some phases which can be crystallized in glass-ceramic substances are listed in Table 2.4. As indicated, the CTE of crystalline phases changes in a broad interval from high negative values for β-eucryptite to high positive value for quartz. Therefore, glass-ceramics having near-zero CTE can be obtained by controlling the type and volume fraction of the developed crystalline phase. Besides the mechanical strength and the elastic modulus, the CTE is an important factor determining the resistance to thermal shock. A combination of high strength and low elastic modulus and coefficient of thermal expansion yields a glass-ceramic material with excellent service capability under severe thermal shock.

2.4 Mechanical Properties of Whisker-Reinforced Ceramic Composites

The mechanical properties of whisker-reinforced ceramic composites are strongly influenced by the composite microstructure: matrix grain size and residual porosity, whisker aspect ratio, whisker orientation, and interfacial bonding between the matrix and whisker. Factors influencing the mechanical properties of whisker-reinforced composites and toughening mechanisms are reviewed.

2.4.1 Effect of Whisker Aspect Ratio on Strength

Unlike continuous fiber-reinforced composites, in chopped fiber- or whisker-reinforced composites, both the whiskers and the matrix carry the applied load and there is no direct loading of whiskers. The design of whisker-reinforced composites depends

Table 2.4. CTEs of Selected Polycrystalline Phases[6]

Type of Crystal	CTE (x 10^{-7}/°C)
β-Eucryptite	
$Li_2O \cdot Al_2O_3 \cdot 2SiO_2$	-64 (20-1000°C)
β-Spodumene	
$Li_2O \cdot Al_2O_3 \cdot 4SiO_2$	9 (20-1000°C)
Aluminum Titanate	
$Al_2O_3 \cdot TiO_2$	-19 (20-1000°C)
Cordierite	
$2MgO \cdot 2Al_2O_3 \cdot 5SiO_2$	26 (20-750°C)
Celcian	
$BaO \cdot Al_2O_3 \cdot 2SiO_2$	27 (20-100°C)
Anorthite	
$CaO \cdot Al_2O_3 \cdot 2SiO_2$	45 (100-200°C)
Lithium Disilicate	
$Li_2O \cdot 2SiO_2$	110 (100-600°C)
Gahnite	
$ZnO \cdot Al_2O_3$	72 (20-1300°C)
Quartz	
SiO_2	237 (20-600°C)

upon how the majority of whiskers carry the applied load. Indeed, the attainment of good mechanical properties critically depends on the efficiency of stress transfer from the matrix to the whisker. The efficiency of stress transfer depends on the whisker length and the strength of whisker/matrix interfacial bond. The maximum strengthening by whisker reinforcement can be approached provided that their length exceeds a critical length, ℓ_c, required for transfer of load from matrix.[47] The efficiency of load transfer can be expressed by comparison of actual whisker length to the value of calculated the critical aspect ratio of whisker, $(\ell / d)_c$, the minimum whisker length to diameter ratio necessary to attain the fracture stress of the whisker.

Because the elastic modulus of the whisker is typically much larger than that of the matrix, the axial elastic displacements of two components are different, which creates shear stresses along the length of the whisker. The shear stress developed has its maximum at both ends of the whisker where the maximum elastic displacement has occurred and decreases gradually toward the middle regions of the whisker where the elastic displacement is zero. On the other hand, tensile stress increases from both ends of the whisker and has its maximum at the middle region of the whisker. These stress distribution profiles are strongly dependent on the types of interfacial bonding. In ceramic-ceramic composites, there are two typical bonding types: (1) frictional interfacial bonding, and (2) rigid interfacial bonding. Stress distribution profiles along the whisker in two cases are shown in Figure 2.9.[48]

The case of frictional transfer is simple to analyze because shear stress is constant along the transfer length. If load transfer occurs by a frictional drag at the interface, then the critical aspect ratio of whisker can be determined from simple force balance between the tensile stress and the shear stress to be developed:[47]

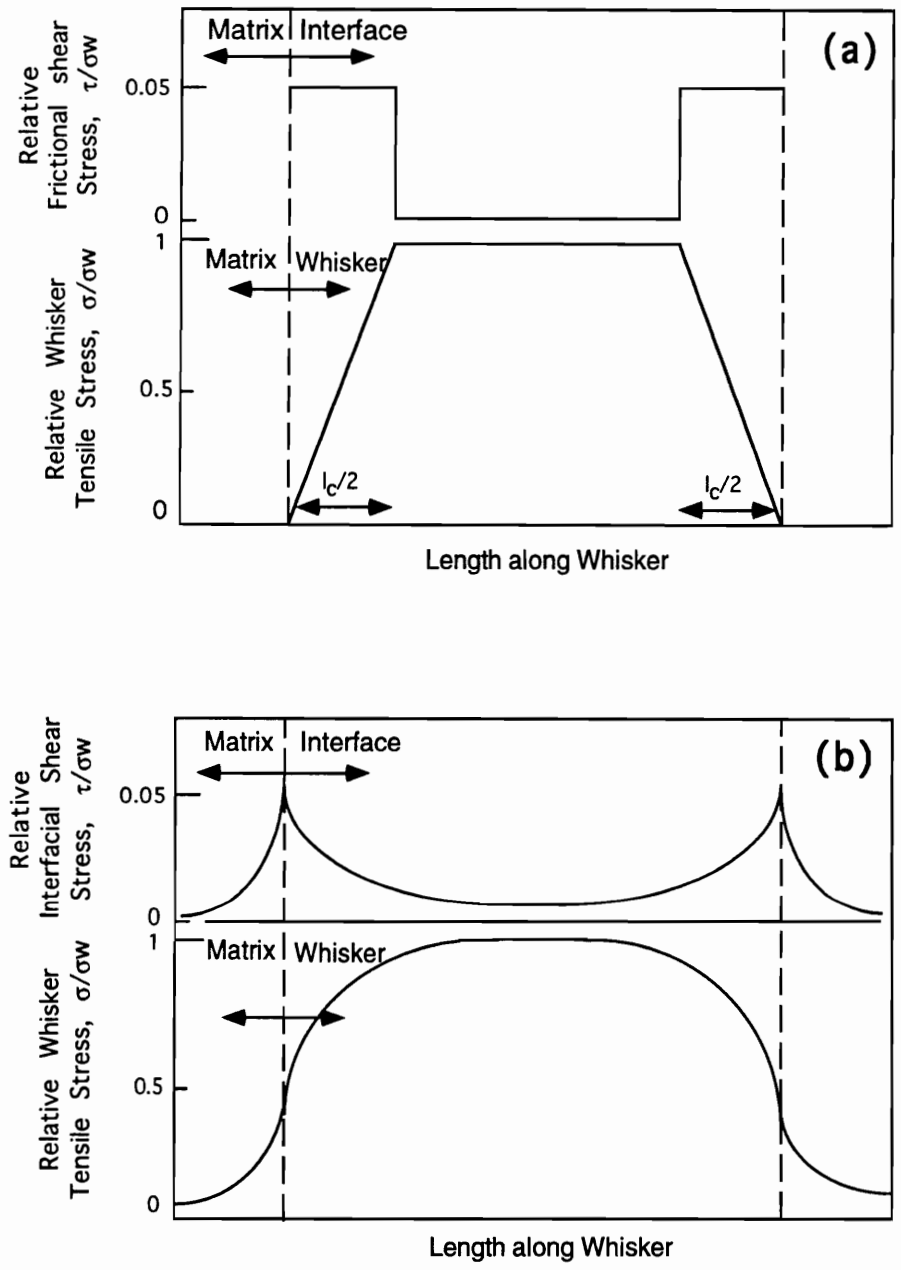

Figure 2.9 Stresses along a whisker in a loaded composite.[48]
(a) frictional bond
(b) rigid bond

$$\left(\frac{\ell}{d}\right)_c = \frac{\sigma_{wu}}{2\tau_f} \tag{2.13}$$

where ℓ and d are the whisker length and diameter, respectively, and σ_{wu} is the whisker fracture strength, and τ_f is the frictional stress.

The overall stress distribution along the whisker can be obtained by integration of the stress distribution:[47]

$$\bar{\sigma}_w = \frac{1}{\ell}\int_o^{\ell} \sigma_w dx = \sigma_w\left(1 - \frac{\ell_c}{2\ell}\right) \tag{2.14}$$

The overall composite strength can then be determined by applying the rule of mixtures:

$$\sigma_c = \sigma_w V_w\left(1 - \frac{\ell_c}{2\ell}\right) + \sigma_m V_m \tag{2.15}$$

If the whisker has the length $\ell = 10\ell_c$, then the composite attains 95% of the strength of the continuous fiber-reinforced composite. Thus, the reinforcement by continuous fibers can be achieved using whiskers if the whisker lengths are much greater than the critical lengths.

The case of rigidly-bonded (perfectly-bonded) whiskers with elastic shear transfer at the interface requires very complicated analysis but yields a similar pattern to the frictionally-bonded case (Fig. 2.9).[49] According to Termonia[49] who studied the stress transfer in single-short fiber embedded composites by using the finite-difference method, the critical whisker length for efficient stress transfer to the short fiber is a unique function of the ratio between the elastic moduli of fiber (E_w) and matrix (E_m):

$$\left(\frac{\ell}{d}\right)_c = \frac{2E_w}{E_m} \tag{2.16}$$

Here, the critical length is based on a transfer length required to give 97% of the full transfer stress, σ_f. In ceramic matrix composites, the ratio of whisker and matrix moduli, E_w/E_m, is generally low and can be as unity.[47] Therefore, for the rigid bonding case, very low critical aspect ratios are predicted.

2.4.2 Whisker Orientation (Randomly-Oriented Whiskers)

Whiskers in ceramic matrix composites are usually randomly-oriented due to their blending process with the ceramic powder. Therefore, the analysis of the fracture stress of a randomly oriented whisker-embedded composite is very complicated.

The applied stress which respect to each randomly-oriented whisker can be expressed by the modified Tsai-Hill equation:[50]

$$\sigma_\theta = \left[\frac{\cos^4\theta}{\sigma_L^2} + \left(\frac{1}{\tau^2} - \frac{1}{\sigma_L^2}\right)\sin^2\theta\cos^2\theta + \frac{\sin^4\theta}{\sigma_T^2}\right]^{-1/2} \tag{2.17}$$

where σ_L is the longitudinal tensile strength, τ is the shear strength, σ_T is the transverse strength, and θ is the angle between the loading direction and the fiber axis. Then the strength of the composite, σ_c, can be obtained by integration of σ_c with its density distribution function, $\rho(\theta)$, where whisker orientation angle is measured with respect to the loading axis:[51]

$$\sigma_C = \int_{-\pi/2}^{\pi/2} \sigma_\theta \rho(\theta) d\theta \tag{2.18}$$

where

$$\int_{-\pi/2}^{\pi/2} \rho(\theta) d\theta = 1$$

The modulus of a randomly-oriented whisker-reinforced composite can be calculated using the empirical relation:[51]

$$E_C = \frac{3}{8} E_L + \frac{5}{8} E_T \tag{2.19}$$

where E_L is the longitudinal modulus, and E_T is the transverse modulus of an oriented whisker composite. Both E_L and E_T can be estimated from Halpin-Tsai equations:[52]

$$\frac{E_L}{E_m} = \frac{1 + 2(\ell / d)(\eta_L V_f)}{1 - \eta_L V_f} \tag{2.20a}$$

and

$$\frac{E_T}{E_m} = \frac{1 + 2\eta_T V_f}{1 - \eta_T V_f} \tag{2.20b}$$

where

$$\eta_L = \frac{E_f / E_m - 1}{E_f / E_m + 2(\ell / d)}$$

and

$$\eta_T = \frac{E_f / E_m - 1}{E_f / E_m + 2}$$

2.4.3 Thermal Expansion Mismatch

As discussed in section 2.3.3, thermal expansion mismatch between the matrix and the whisker is a very important parameter in composite processing since it determines the residual stress distribution after fabrication which affects the mechanical properties of the composite. Because ceramics have limited ductility and the fabrication temperatures of ceramic matrix composites are very high, if the thermal expansion mismatch between the whisker and the matrix is large, microcracks can form throughout the composite during cooling after fabrication and the composite can be very weak. In the case of whiskers, their thermal expansion behavior along the axial and the radial direction is not the same. Donaldson *et al.*[53] summarized four possible residual stress distributions due to the axial and radial thermal expansion mismatch in a given uniaxially-embedded short fiber composite.

(1) *Axial direction,* $\Delta\alpha_a = \alpha_f - \alpha_m$ *is negative*: on cooling from the fabrication temperature, the matrix is in tension along the axial direction. Ceramics are easily broken under tensile stress; thus, if the magnitude of the thermal expansion mismatch is large enough to cause matrix microcracking, then a network of fine microcracks will be formed perpendicular to the axial direction of the whiskers. In the uniaxially-aligned continuous fiber composite case, even though there are transverse microcracks in the matrix, fibers may still hold the matrix together, and the fibers carry the applied load so that the composite can have the desired strength. On the other hand, in randomly-oriented whisker composites, microcracks can form in all directions and the composite exhibits lower strength.

(2) *Axial direction,* $\Delta\alpha_a$ *is positive*: if the interfacial bonding strength is high then the matrix is in compression, which is beneficial because this will increase overall stress required to initiate matrix failure and hence, overall strength of the composite will increase. However, if interfacial bonding strength is too weak to withstand induced

stress, then voids will be formed at the ends of each whisker and cause degradation of the composite strength.

(3) *Radial direction,* $\Delta\alpha_r = \alpha_f - \alpha_m$ *is negative*: the interface between the whisker and the matrix will be in compression which will produce strengthening of the interface.

(4) *Radial direction,* $\Delta\alpha_r$ *is positive*: the fiber tries to shrink away from the matrix on cooling, which will result in decreased bonding strength. Thus, if the interfacial bonding is not strong enough to withstand the induced stress, interfacial debonding will occur.

Therefore, to improve the fracture strength of the composite, $\Delta\alpha_a$ should be positive, $\Delta\alpha_r$ should be negative, and the interfacial strength should be strong enough to withstand the induced stresses.

However if increased fracture toughness at the expense of fracture strength is desired, then whiskers that have CTE less than the matrix should be selected. The decrease of strength is dependent upon the magnitude of the thermal expansion mismatch and the interfacial bonding strength. For example, Claussen *et al.*[54] reported that the fracture toughness increased from 6.2 to 13.5 $MNm^{-3/2}$ when 20 vol% of SiC whiskers were incorporated in an Al_2O_3-15% tetragonal ZrO_2 matrix. However, the corresponding fracture strength decreased from 1100 MPa to 700 MPa, attributed to the formation of microcracking along the weak interface due to the thermal expansion mismatch between the whisker and the matrix. Shalek *et al.*[55] reported that the strength increased in SiC whisker-reinforced tetragonal zirconia polycrystals (TZP) at 1000°C when the thermal expansion mismatch effect disappeared. In this case, the loss of the fracture strength at room temperature resulted from the formation of tensile stress in the matrix during cooling from fabrication temperatures due to the thermal expansion mismatches.

2.4.4 Toughening Mechanisms

Researchers have reported evidence of increased fracture toughness of ceramics when reinforced by whiskers.[56,57,58,59] Most authors observed evidence of both crack deflection and pull-out on the fracture surface.

As shown in Figure 2.10, four commonly encountered toughening mechanisms in composites containing short and randomly-oriented whiskers are deflection, bridging, pull-out, and microcracking.

(1)*Crack deflection*: A crack can be deflected around a whisker if the whisker exhibits an appropriate combination of inclination to the crack plane and relatively moderate interfacial strength (not strong enough to cause whisker fracture; not weak enough to allow whisker pull out).[60] Also, as discussed in section 2.4.3, thermal expansion mismatch can assist crack deflection.[61]

A whisker having higher CTE than the matrix produces compressive tangential stresses near whisker/matrix interface and diverts cracks around the whisker. On the other hand, a whisker having lower CTE than the matrix produces tangential tensile stresses and causing crack propagation toward the whisker.

(2)*Crack bridging*: Crack propagation in a composite can be hindered by the bridging of a crack surface by strong intact whiskers in a zone behind the crack tip.[50]

(3)*Whisker pull-out*: Whiskers resist crack opening by frictional sliding. The contribution of pull-out to toughening is simply estimated by considering the fracture energy of the work involved in pulling out the whisker against the interfacial bonding. Whisker pull-out depends on the length of whiskers and the type of the interfacial bonding. Generally, whiskers shorter than critical length and which are frictionally-bonded to the matrix will be pulled out.[47]

(4)*Microcracking*: When the crack tip hits a microcrack, then fracture energy is released and the crack does not extend.[62] In some cases, whiskers can act as

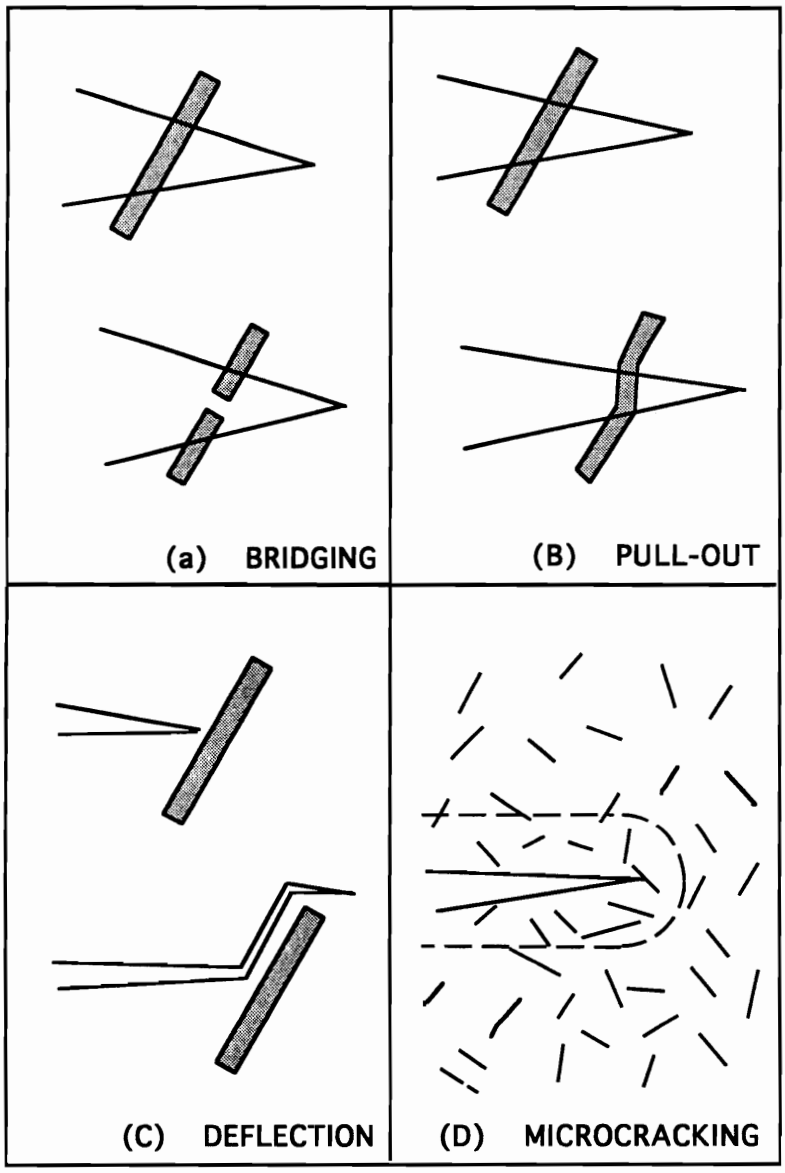

Figure 2.10 Various toughnening mechanisms in whisker-reinforced ceramics.

microcracking sites through tensile failure of the interface at the ends of the whisker, through shear failure along the length of the whisker, and through cracking of the matrix due to the thermal expansion mismatch.

CHAPTER III

EXPERIMENTAL PROCEDURE

$(Li_{0.4},Ca_{0.05})Al(Si_{0.75},P_{0.5})O_{4.5}$ and $(Li_{0.41},Mg_{0.035})Al(P_{0.52},Si_{0.48})O_4$ were prepared and evaluated using different techniques. Therefore, experimental procedure and results/discussion for each composition are described separately.

3.1 Sample Preparation Composition 1: $(Li_{0.4},Ca_{0.05})Al(Si_{0.75},P_{0.5})O_{4.5}$

3.1.1 Single Phase Preparation

Samples of $AlPO_4$-modified β-eucryptite of composition $(Li_{0.4},Ca_{0.05})Al(Si_{0.75},P_{0.5})O_{4.5}$ were prepared by typical glass-ceramic processing. To obtain a homogeneous glass, single phase modified β-eucryptite was prepared by solid-state reaction methods prior to melting. Reactant materials used in processing and compositions of batches for 1 mol of composition 1 are listed in Table 3.1. Samples were prepared by calcining the mixture of $AlPO_4$ and β-eucryptite solid solution phase, $(Li_{1.6},Ca_{0.2})O{\cdot}Al_2O_3{\cdot}3SiO_2$. $(Li_{1.6},Ca_{0.2})O{\cdot}Al_2O_3{\cdot}3SiO_2$ was obtained by mixing $Al(OH)_3{\cdot}nH_2O$, Li_2CO_3, CaO, and SiO_2, then calcining the mixture at 1250°C for 50 hours. $AlPO_4$ was obtained by mixing $Al(OH)_3{\cdot}nH_2O$ and $NH_4H_2PO_4$, then calcining at 1200°C for 30 hours. After obtaining $AlPO_4$ and $(Li_{1.6},Ca_{0.2})O{\cdot}Al_2O_3{\cdot}3SiO_2$, the powders were mixed in the same mole ratio, then calcined at 1150°C for 50 hours to obtain the desired final composition. The resulting phase was confirmed by powder x-ray diffraction. Often a small amount of unreacted $AlPO_4$ or SiO_2 was detected but these phases were usually not observed in the glass-ceramic samples. The resulting calcined composition was pulverized using an alumina mortar and pestle, then ground by ball milling.

Table 3.1. Reactant Materials Used in Processing and Compositions of Batches for 1 Mole of Modified β-Eucryptite Material

	Weight Percent for 1 Mole	
	Composition 1	Composition 2
Li_2O	4.26	4.93
Al_2O_3	36.33	41.02
SiO_2	32.12	23.21
P_2O_5	25.29	29.70
MgO	—	1.14
CaO	2.00	—

3.1.2 Glass Formation

The resulting $(Li_{0.4},Ca_{0.05})Al(Si_{0.75},P_{0.5})O_{4.5}$ powder was mixed with 4 wt% TiO_2 powder, then melted at 1620°C for 3 hours in a vertical tube furnace (Rapid Furnace, CM Furnaces, Inc., Bloomfield, NJ). The glass melt was then either poured into a Cr-Ni-based alloy mold (12 x 60 x 65 mm) or was drawn into a rod, and promptly annealed at 650°C for 2-3 hours. After annealing, the glass showed no sign of devitrification and was stress-free. The resulting rectangular-shaped glass samples were cut and heat treated for mechanical testing, and the rod shaped glass samples were used for differential thermal analysis (DTA), thermal expansion measurements, X-ray diffraction (XRD) phase identification, and scanning electron microscopy (SEM) observations.

3.2 Differential Thermal Analysis (DTA)

Glass transition temperature (T_g), crystallization temperature(T_c), temperature of maximum nucleation rate, and the activation energy for crystallization (E_c) of annealed $AlPO_4$-modified β-eucryptite glass $[(Li_{0.4},Ca_{0.05})Al(Si_{0.75},P_{0.5})O_{4.5}]$ containing 4 wt% TiO_2 were determined using DTA (1700 System, Perkin-Elmer Corp., Norwalk, CT). Platinum-rhodium crucibles were used as the sample and reference holder. Al_2O_3 powder was used as the reference material.

(A) Determination of T_g and T_c

Determination of T_g and T_c is very important in developing the glass-ceramic process because T_g and T_c points can provide important information, such as possible temperature region for nucleation, and crystallization initiation temperature. For determining T_g and T_c, DTA runs were perfomed with -200 mesh glass powders using a 10°C/min ramping rate.

(B) Determination of the Maximum Nucleation Temperature

To measure the temperature of maximum nucleation rate, the bulk glass samples (diameter=2 mm, thickness=2 mm) were cut from the annealed glass rod. Because surface of a glass is the most favorable nucleation site; in order to give the same surface area to each sample, samples were prepared to be exactly the same size and shape. Al_2O_3 powder was placed between the sample and the sample holder in order to promote better heat transfer. The DTA experiments were conducted at a 20°C/min ramping rate in order to prevent formation of nuclei during the ramping. The temperature which yields the maximum nucleation rate was determined using equations developed by Marotta *et al.*[63]

(C) Determination of the Apparent Activation Energy for Crystallization

To determine the apparent activation energy for crystallization, E_c, the bulk glass samples were tested by DTA with various ramping rates. According to Kissinger,[64] the apparent activation energy for crystallization, E_c, can be obtained with the following equation:

$$\ell n\left(\frac{\phi}{T_c^2}\right) = -\frac{E_c}{R}\frac{1}{T_c} + constant \qquad (3.1)$$

where ϕ is the heating rate of the DTA and T_p is the crystallization temperature corresponding to the heating rate in the DTA runs. Plot of $\ell n\left(\frac{\phi}{T_c^2}\right)$ versus $1/T_c$ gives a straight line; and the slope of the line represents the apparent activation energy for crystallization.

3.3 Glass-Ceramic Processing

Glass-ceramic processing of the glass [96%$(Li_{0.4},Ca_{0.05})Al(Si_{0.75},P_{0.5})O_{4.5}$, 4% TiO_2] was conducted using a two-step heat treatment. First, heat treatment was conducted at 740°C for 2-3 hours in order to form a sufficiently large number of nuclei. This temperature was obtained from the DTA study and will be discussed in section 4.2 in detail. Second, heat treatment was conducted at various temperatures above 800°C at 1°C/min ramping rate in order to prevent sample failure. After heat treatment, crystallized glass samples were cooled in the furnace at a 1°C/min in order to prevent the formation of microcracks in the samples due to thermal expansion mismatch between the crystallized phase and residual glass.

3.4 Glass-Ceramics Characterizations

3.4.1 Linear Thermal Expansion

The influence of heat treatment on the thermal expansion behavior of $(Li_{0.4},Ca_{0.05})Al(Si_{0.75},P_{0.5})O_{4.5}$ glass containing 4 wt% TiO_2 was investigated using a dilatometer (Dual Push Rod Differential Dilatometer Model-II, Netzsch. Inc., Exton, PA) with a fused-silica reference. A DIN-silica rod was used to correct for system errors and a software package computed CTE. After heat treatment, bar samples 25 mm long were cut with a diamond saw from the heat-treated block. The relative bulk CTE was measured between 30°C and 700, 800, 900, or 1000°C (depending on the heat treatment of the material) with a 10°C/min heating rate .

3.4.2 X-Ray Analysis

The phases developed during crystallization of the glass were determined by using an X-ray diffractometer (Compact XRD Analyzer System 1840, Phillips Electronic Instruments, Mahwah, NJ). Heat-treated samples were ground using an alumina mortar and pestle, mounted in an aluminum sample holder, and scanned from 15° to 70° (2θ) at a scanning rate of 0.02°/sec. Detected phases were identified using JCPDS Powder Diffraction Files.

3.4.3 Scanning Electron Microscopy

(A) Observation of the Morphologies of the Developed Phases

The morphology of the developed phases during heat treatment was investigated using a scanning electron microscope (Stereo Scan 90, Cambridge Instrument, Cambridge, U.K.). Samples for SEM analysis were prepared by either polishing and etching, or by fracturing. For sample polishing, samples were ground using 240, 320, 400, and 600-grit silicon carbide paper and then polished using 1, 0.5, and 0.03-μm alumina powder. Sample etching was conducted using 2% hydrofluoric acid for 20 seconds.

(B) Determination of Maximum Nucleation Temperature

Maximum nucleation temperature was also determined by SEM. The glass samples were isothermally heat treated at various temperatures from the glass transition temperature (T_g) and crystallization temperature (T_c) for 0.5 hour in order to allow nuclei formation. These samples were then further heated at 950°C for 0.5 hour to allow nuclei growth to a certain measurable size under SEM observation. The grain size of the resulting crystallized glass was then measured. The resulting grain size varied from 1-15 μm depending on the nucleation temperatures. Maximum nucleation temperature was

estimated by comparing grain size of the specimens. The temperature rendering the smallest grains in the sample was selected as the maximum nucleation rate temperature.

(C) Determination of Volume Fraction of the Developed Crystal Phases

Volume fraction of the crystallized phase with different temperatures and times was also determined using an Image analyzer (Zeiss SEM-IPS, Carl Zeiss. Inc., Thornwood, NY) interfaced with a Cambridge Stereoscan 120 scanning electron microscope. Secondary electron images were digitized by the Image analyzer to 256 gray level resolution, and displayed as a 512 x 512 pixel gray level image. After etching, areas of the sample that contained crystalline phases remained as high points relative to the glass matrix and, therefore, appeared as bright areas in the image. Based on this gray level difference, the image analyzer was used to discriminate the crystalline phases from the glass. This resulted in a binary image in which the crystals were at a grey level of 255 and all other pixels were converted to a grey level of zero. The number of pixels at a gray level of 255 versus the total pixel count in the image was then used to determine the percent of crystalline phase in the sample.

3.4.4 Density Measurement

Bulk density values were determined by the Archimedes method (ASTM C20-87), with suspended weights obtained with a wire basket immersed in water. The value of bulk density, ρ, for each sample was calculated from:

$$\rho = \frac{D}{D-S}\rho_{H_2O} \tag{3.2}$$

where D and S are the dried and suspended weights of the sample, respectively, and ρ_{H_2O} is the density of water.

3.4.5 Measurement of Mechanical Properties

Tests were performed to examine the effect of different heat treatments and morphological changes on mechanical properties of the material.

(A) Determination of Flexural Strength

Flexural strength was determined using Military Standard 1942 B four point bending test with 20/40 mm spans and a cross head speed of 0.02 mm/min using an universal testing machine (Model UTM 1100, Applied Test Systems, Inc., Butler, PA) (see Figure 3.1). Bars 3 x 4 x 50 mm in size (Military Standard 1942 B) were cut with a diamond saw from the rectangular slabs of glass and glass-ceramics which had been heat treated at 850, 950, and 1040°C. Prior to flexure testing, samples were polished by 0.5 μm alumina powder and edges were chamfered. Polished samples were annealed at 700°C for 2-3 hours in order to relieve stresses formed during the polishing. For each heat treatment, five to eight specimens were tested. The following equation was used to compute the modulus of rupture (MOR):

$$MOR = \frac{3}{2}\frac{P(L_O - L_I)}{WT^2} \tag{3.3}$$

where P is the load at fracture(N), L_O and L_I are the outer and the inner span size (mm), respectively, and W is the width of the sample (mm), and T is the thickness of the sample (mm).

(B) Determination of Elastic Modulus

Elastic moduli of the original glass and the glass-ceramics heat treated at different temperatures and times were determined by measuring the deflection of the flexure bars. For each heat treatment, five specimens were tested. The elastic modulus was calculated using the following equation:

$$E = \left(\frac{11}{64}\right)\left(\frac{PL^3}{WT^3D}\right) \tag{3.4}$$

where P is the applied load, L is the support span size, W is the width of the flexure bar, T is the thickness of the sample, and D is the deflection.

(C) Determination of Fracture Toughness

Fracture toughness, K_{IC}, for glass and glass-ceramics was determined by the Vickers indentation method. Like other composite materials, it is expected that in situ TiO_2 whisker-reinforced $AlPO_4$-modified β-eucryptite glass-ceramic exhibits R-curve behavior (increase in crack resistance with crack extension). The R-curve behavior of the material was determined by measuring the fracture strength of specimens after indentations.

To determine fracture toughness, surface cracks were introduced using a diamond indenter with a microhardness tester (LECO DM-400, LECO Corp., St. Joseph, MI). Eight to fifteen indents were made on each glass and glass-ceramic specimen. The K_{IC} values were calculated using the following equations:

$$K_{IC} = 0.028H\sqrt{a}\left(\frac{E}{H}\right)^{0.5}\left(\frac{c}{a}\right)^{-1.5}, MPa\cdot\sqrt{m} \quad ^{65} \tag{3.5}$$

$$K_{IC} = 0.016\left(\frac{E}{H}\right)^{0.5}\left(\frac{P}{c^{1.5}}\right), MPa \cdot \sqrt{m} \quad [66] \tag{3.6}$$

where H is the Vickers hardness, E is the elastic modulus, a is the half size of the indent, c is the radial crack size, and P is the load on indenter (9.8N). Cracks did not always form at all four corners of the indents. In this case, only those cracks actually observed were measured.

A increasing fracture toughness (R curve) of the in situ TiO_2-reinforced $AlPO_4$-modified β-eucryptite glass-ceramic was measured at ambient temperature in air using the indentation-strength measurement technique. The indentation-strength measurements were carried out on the samples prepared according to Military Standard 1942 B. The prospective tensile surfaces of the samples were polished with a mixture of water and 0.5-μm alumina powder for microscopic observation after indentation. After polishing, the samples were annealed at 750°C for 2 hours to relieve any processing stresses.

Three controlled surface flaws were produced 5 mm apart in the center of the prospective tensile surface of each flexure bar using a Vickers microhardness indenter in air for 15 seconds. During these indentations, care was taken to orient one set of the radial cracks of an indent parallel to the cross section of the flexure bar where the rupture would occur. Indentation loads of P = 2.94, 4.9, and 9.8 N were used.

The subsequent strength tests were conducted by four point bending (span size were 20/40 mm) at room temperature using an ATS universal test machine with crosshead speed of 0.02 in./min. At least seven bars which exhibited fracture initiation at one of the three indentations were obtained for each indentation load. Indentation geometry on the surface of the flexure bar is illustrated in Figure 3.1.

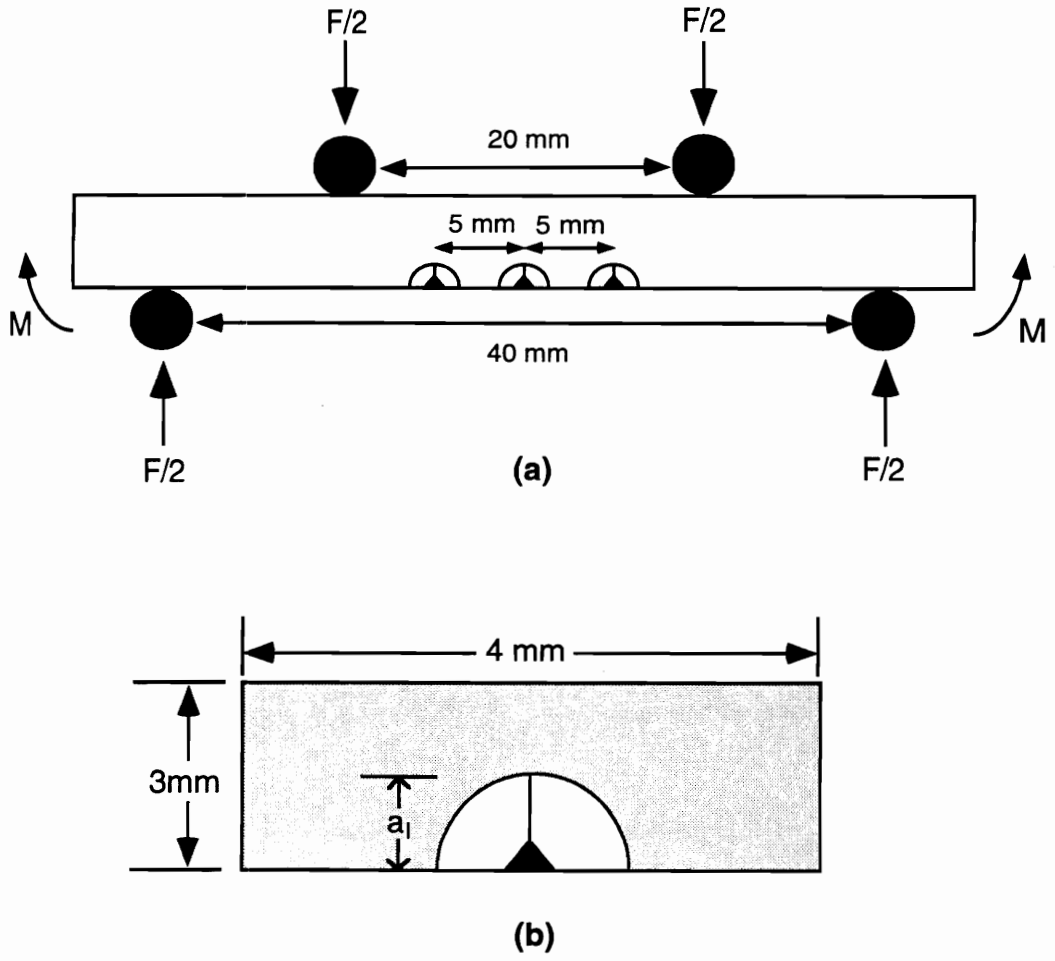

Figure 3.1 Schematic of geometry of (a) sample for indentation-fracture test and (b) surface flaw made by Vickers indentations on fracture surface.

3.5 Sample Preparation Composition 2: $(Li_{0.41},Mg_{0.035})Al(Si_{0.48},P_{0.52})O_4$

3.5.1 Single Phase Preparation

Single phase $(Li_{0.41},Mg_{0.035})Al(Si_{0.48},P_{0.52})0_4$ was prepared by solid-state reaction of the raw materials without the prior formation of $AlPO_4$ and β-$LiAlSiO_4$. Reactant materials are listed in Table 3.1. Amounts of reagent-grade $Al(OH)_3 \cdot nH_2O$, silicic acid, $NH_4H_2PO_4$, $MgSO_4$, and Li_2CO_3 were calculated to produce one mole of $(Li_{0.41},Mg_{0.035})Al(Si_{0.48},P_{0.52})0_4$. Included in this calculation is the weight loss factor for silicic acid and $Al(OH)_3 \cdot nH_2O$. The mixture was ground with acetone using a glass mortar and pestle, then allowed to dry completely. After drying, the mixture of raw materials underwent a series of heat treatments. The mixture was first heated at 200°C for 2 hours, then ground again with acetone using a glass mortar and pestle. The heating and grinding were repeated at 400°C, 600°C, and 800°C. This early heat treatment gradually drove off water and carbon dioxide such that the oxides were thoroughly mixed. Finally, the mixture was heat treated at 1070°C for 100 hours to produce the desired phase. Single phase formation was verified by XRD.

3.5.2 Glass Formation

The resulting calcined material was ground into a powder using an alumina mortar and pestle. The powder was mixed with 0, 6, 8, 10, 12 wt% TiO_2 by ball-milling. The mixture was placed in an alumina crucible and heated at 1620°C for 2 hours in a vertical tube furnace. After heating, the glass melt was quenched in water in order to obtain glass fragments. The glass melt which contained 12 wt% TiO_2 showed a certain degree of devitrification during the quenching. However, clean glass fragments were obtained. These glass fragments were ground using an alumina mortar and pestle, then

wet-milled for 4 hours with Al_2O_3 balls and ethyl alcohol as a mixing fluid. The average particle size of the glass after milling was measured by a particle size analyzer (Electrozone-Celloscope 80XY, Particle Data, Inc., Elmhurst, IL) and the result is shown in Figure 3.2. After 4 hours of ball-milling, resultant glass particles had an average particle size of 10 μm.

3.5.3 Densification and Sintered Glass-Ceramic Process

Conventional glass-ceramic processing, *i.e.*, converting a solid piece of glass to a glass-ceramic, could not be applied to this composition because of severe microcracking (sometimes the sample was shattered after heat treatment) resulting from the large thermal expansion mismatch between the glass and the crystallized phase. Therefore, for composition 2, $(Li_{0.41},Mg_{0.035})Al(Si_{0.48},P_{0.52})0_4$, glass-ceramic processing was conducted by sintering the glass powder compact in order to convert it to a glass-ceramic.

The glass compact was obtained by filtration of the mixture of glass powder, acetone, and alcohol. The glass powder with an average particle size of 10 μm was mixed with acetone and alcohol, made into a slurry, then poured into a glass die with a paper filter at the bottom (Figure 3.3). During sedimentation of the glass powder, acetone and alcohol were drained from the bottom part of the mold to leave a glass compact. The compact was then carefully removed from the die and heat treated as shown in Figure 3.4.

3.5.4. Sample Characterization

Flexural strength and bulk CTE values of the sintered glass-ceramic specimens containing different amounts of TiO_2 (0, 6, 8, 10, and 12 wt%) were measured. Flexural strength was determined by a three-point bending test (30 mm span size) using an Instron

machine (Model 4204, Instron Corp. Canton, MA) with 0.02 in./min crosshead speed and calculated using the equation:

$$MOR = \frac{3}{2}\frac{PS}{WT^2} \tag{3.7}$$

where P is the load at fracture (N), S is the span size (mm), W is the width of the specimen (mm), and T is the thickness of the specimen (mm). Five to six samples were tested for the material having different amounts of TiO_2. Bulk CTE values (30°C to 1000°C) of the samples containing various amounts of TiO_2 were measured using a dilatometer with a 10°C/min heating rate.

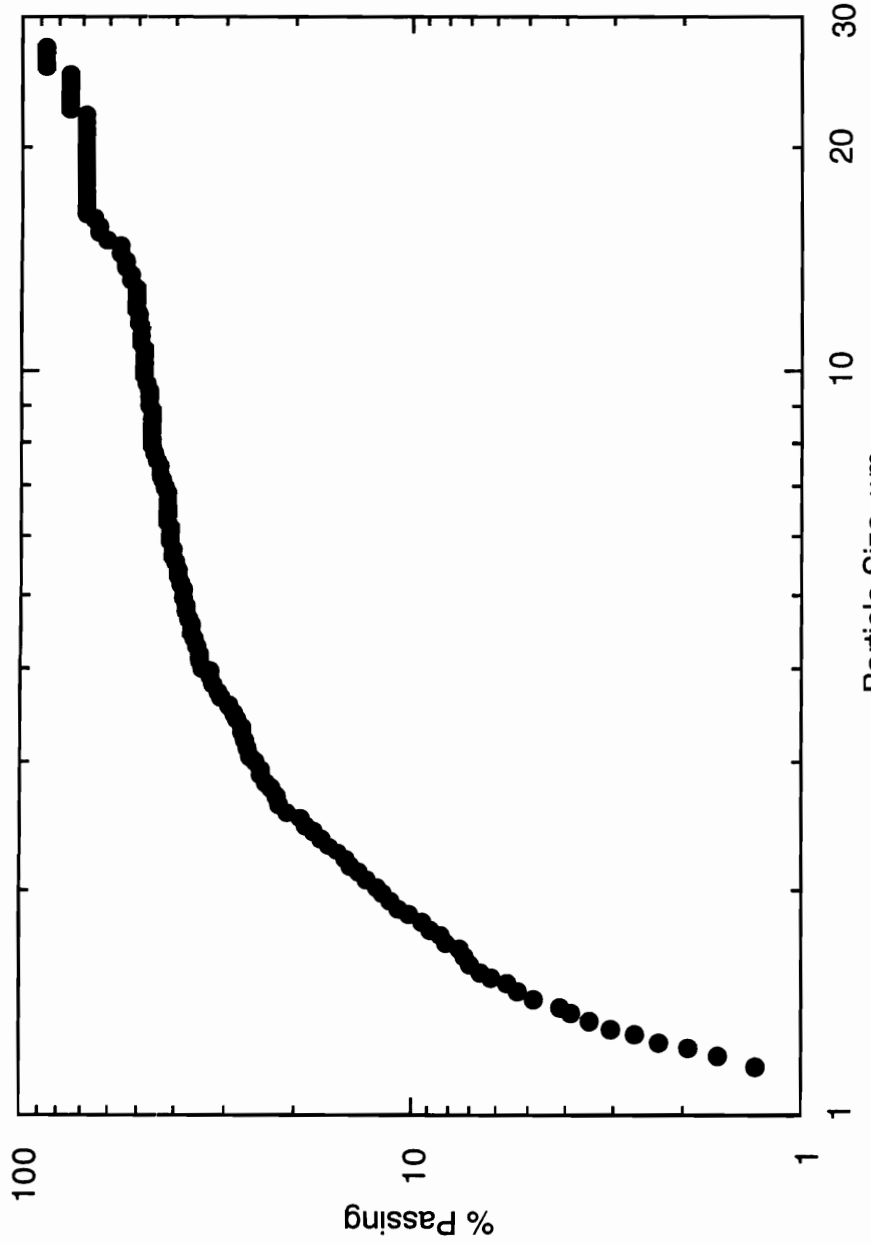

Figure 3.2 Particle size distribution of $[(Li_{0.41},Mg_{0.035})Al(Si_{0.48},P_{0.52})O_4$ glass after wet-milling for 4 hours.

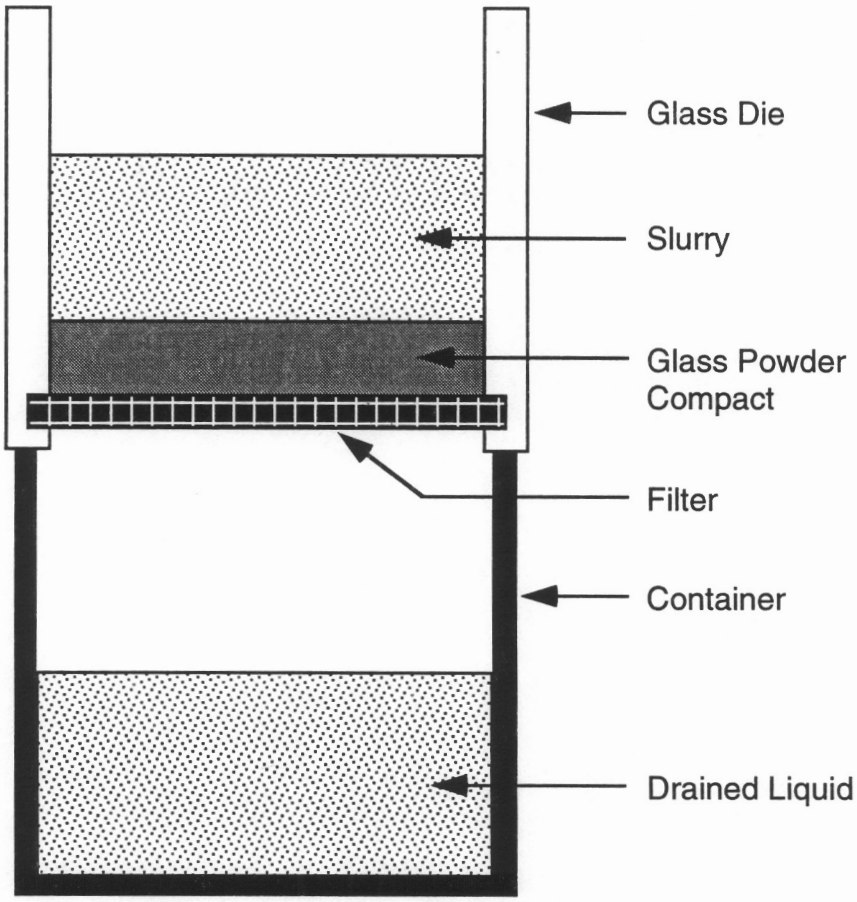

Figure 3.3 Slurry filtration process.

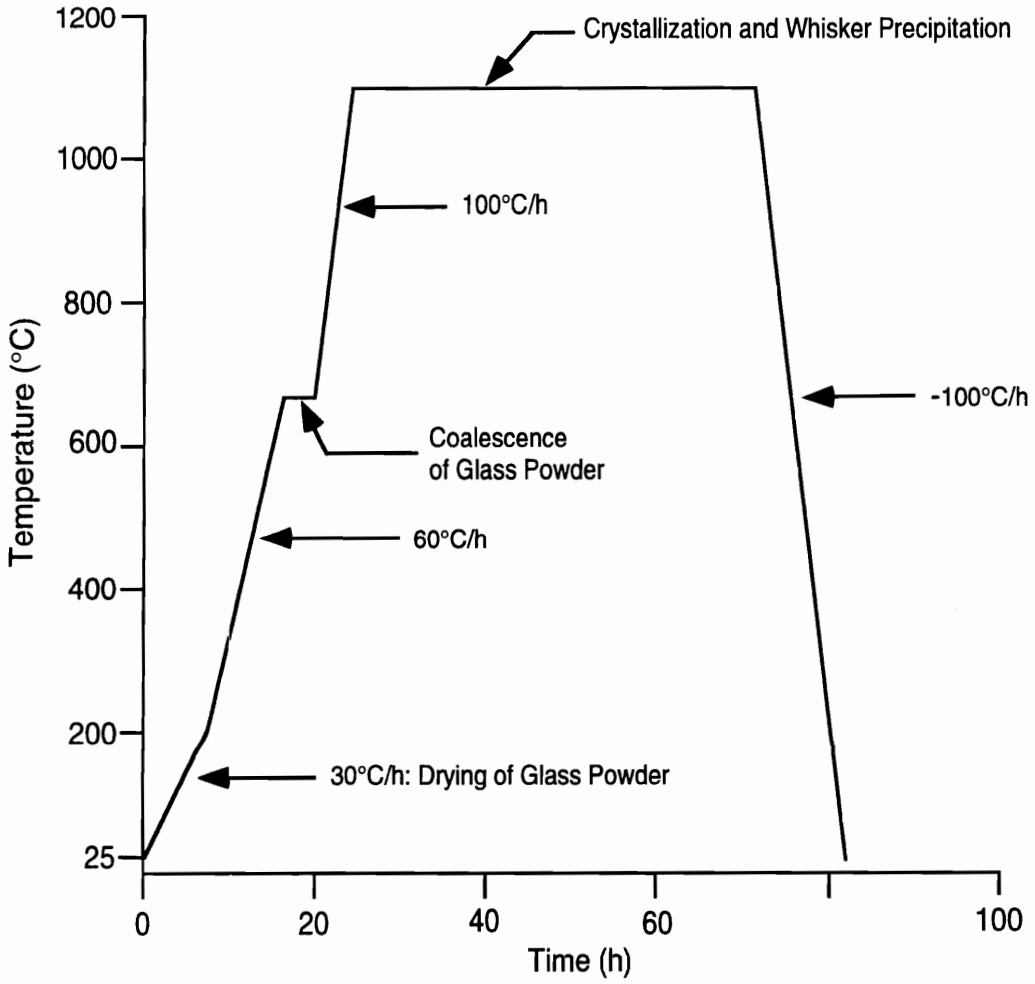

Figure 3.4 Heat-treatment schedule for the [94% $(Li_{0.41},Mg_{0.035})Al(Si_{0.48},P_{0.52})O_4$ and 6% TiO_2] glass compact.

CHAPTER IV

RESULT AND DISCUSSION FOR COMPOSITION 1

4.1 Glass Formation

After melting at 1620°C for 2-3 hours, the glass obtained was examined by x-ray diffractometer which showed that there was no sign of devitrification during cooling. The DTA thermogram for the glass containing 96% $(Li_{0.4},Ca_{0.05})Al(Si_{0.75},P_{0.5})O_{4.5}$ and 4% TiO_2 is shown in Figure 4.1. The small endothermic peak at 670°C corresponds to the glass transition temperature, T_g, and an exothermic peak at 807°C is associated with the crystallization of the glass phase. DTA results indicate that the maximum nucleation temperature will be between 670°C and 807°C, and that crystallization begins around 800°C.

4.2 Determination of Maximum Nucleation Temperature

(A) DTA study

Glass samples containing different numbers of nuclei show different crystallization peak temperatures as shown in Figure 4.2. Maximum nucleation rate temperature can be determined based on the equations described below.

The nonisothermal devitrification of a glass is the result of two processes: nucleation and crystal growth. The number of nuclei per unit volume after DTA test (N_{TOTAL}) is the sum of surface nuclei (N_s), nuclei formed during the DTA run (N_{DTA}), and bulk nuclei formed from heat treatment prior to the DTA run (N_n):[64]

$$N_{TOTAL} = N_s + N_{DTA} + N_n \tag{4.1}$$

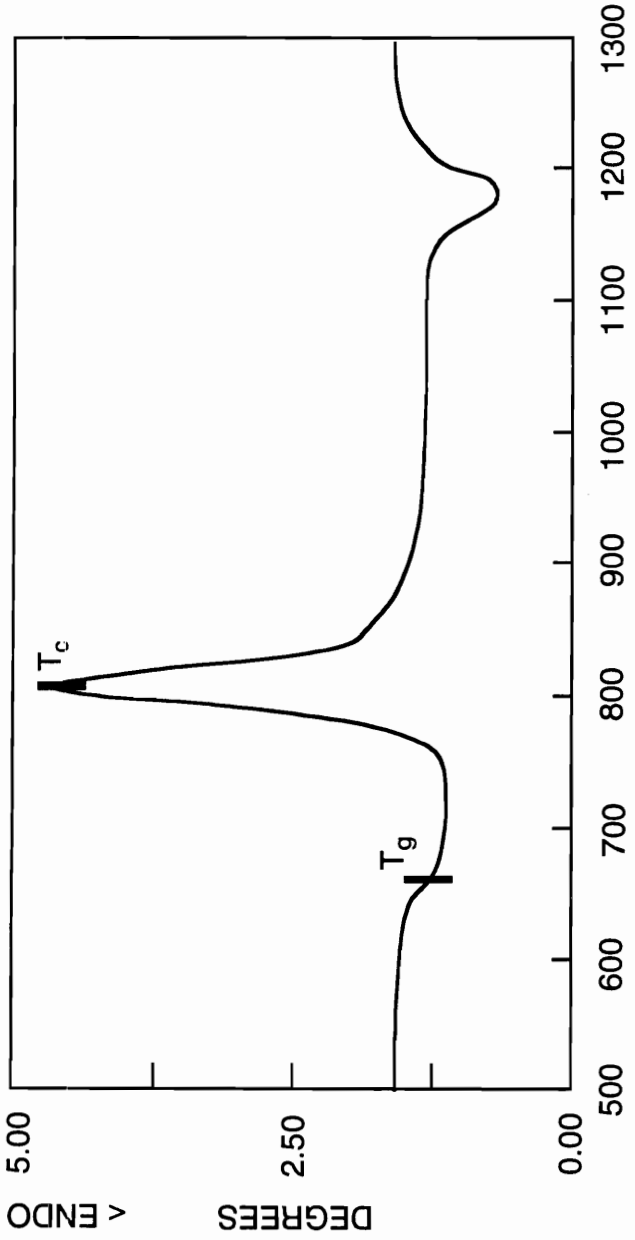

Figure 4.1 DTA curve for the [96% $(Li_{0.4},Ca_{0.05})Al(Si_{0.75},P_{0.5})O_{4.5}$, 4% TiO_2] glass.

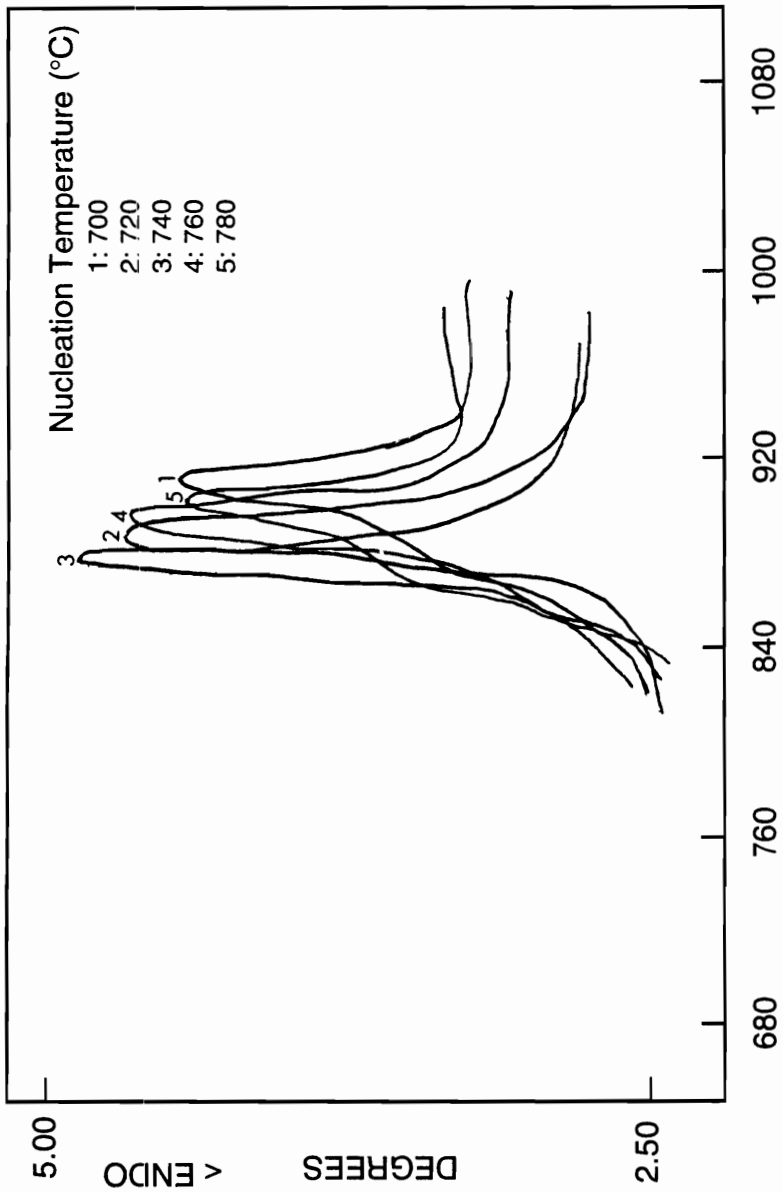

Figure 4.2 Variation of the crystallization peak as a function of the nucleation temperature.

N_s, N_{DTA}, and N_n are strongly dependent on the specific surface area of the sample, DTA heating rate, amount of nucleating agent, and previous nucleation heat treatment time and temperature. All samples were prepared in the same shape and size, thus the specific surface area was fixed as constant for each sample. The nucleating agent, TiO_2, was added as a fixed amount of 4 wt%. In previous nucleation heat treatments, heat treating time was fixed as constant. During the DTA runs, the heating rate was fixed at 20°C/min. Therefore, N_{TOTAL} is solely a function of previous heat treatment temperature, *i.e.*, among the samples heat treated at different nucleation temperatures, the temperature which yielded the maximum number of nuclei in the sample is the maximum nucleation rate temperature.

The condition for maximum crystallization peak in the DTA run is:[67]

$$AN\exp\left(-\frac{E_c}{RT}\right)t = 1 \tag{4.2}$$

where A is a constant, N is the number of nuclei, E_c is the activation energy for crystallization, R is the gas constant, T is the absolute temperature, and t is the DTA heating time which is proportional to the reciprocal of the DTA heating rate. Taking logarithms of the equation yields:

$$\ell nN - \ell n\beta = \frac{E_c}{R}\frac{1}{T_c} + constant \tag{4.3}$$

where β is the reciprocal of the heating rate which is fixed as constant, and T_c is the crystallization peak temperature in the DTA run. Let's suppose there are two samples: (1) a previously nucleated sample, and (2) an as-quenched sample with no prior nucleation heat treatment. These samples are tested using DTA with the same heating

rate. The relationship between the number of nuclei and the crystallization temperature for the pre-nucleated sample can be expressed as:

$$\ell nN = \frac{E_c}{R}\frac{1}{T_c} + constant \tag{4.4}$$

for the as-quenched glass as:

$$\ell nN_o = \frac{E_c}{R}\frac{1}{T_c^o} + constant \tag{4.5}$$

where T_c^o is the crystallization peak temperature of the as-quenched glass. The following equation can be derived from the above equations:[6,7]

$$\ell nI = \frac{E_c}{R}\left(\frac{1}{T_c} - \frac{1}{T_c^o}\right) + constant \tag{4.6}$$

where the nucleation rate, I, is the number of nuclei per unit time. Therefore, the prior nucleating heat treatment temperature which shows the maximum value of $[(1/T_c)-(1/T_c^o)]$ is the maximum nucleation temperature. Figure 4.3 shows a nucleation rate-like curve with the maximum $[(1/T_c)-(1/T_c^o)]$ at 740°C. Therefore, 740°C was determined to be the temperature which yields a maximum nucleation rate. Microscopic observation indicates that crystallization starts from the bulk of the sample, and this implies that the material has a high Avrami parameter, n, which is related to the directionality of crystal growth. The Avrami exponent is determined from the shape of the DTA crystallization exotherm of as-quenched glass containing 4 wt% TiO_2 and found to be $n=4.2$ using the equation:[68]

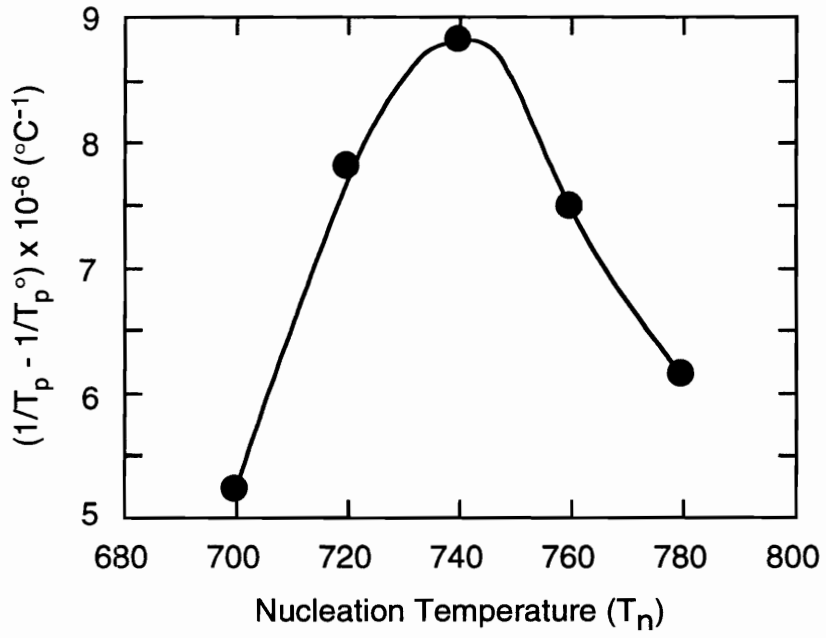

Figure 4.3 Nucleation rate curve determined using Marrotta method.[60]

$$n = \left(\frac{2.5}{\Delta T}\right)\left(\frac{RT_c^2}{E_c}\right) \tag{4.7}$$

where ΔT is the width of the crystallization peak at half the maxima. A value of n close to 1 denotes surface crystallization while a value of 3 or more implies bulk crystallization.

(B) SEM study

The maximum nucleation temperature, 740°C, determined using DTA was confirmed by SEM based on observing the microstructures formed by nucleation/isothermal crystallization heat treatments. The sample nucleated at 740°C shows the smallest and most uniform grains after crystallization at 900°C for 0.5 hour. The scanning electron micrographs in Figure 4.4 show two extreme cases; Figure 4.4(a) shows the small and uniform grain morphology after nucleation at 740°C and crystallization at 900°C, and Figure 4.4(b) shows the large (≈20 μm) grain morphology after nucleation at 780°C and crystallization at 900°C.

4.3. Determination of Activation Energy for Crystallization

The apparent activation energy for crystallization of a glass is one of the key factors affecting how easily the structural rearrangement will occur during conversion from a glass to a glass-ceramic. The smaller the activation energy is, the easier structural rearrangement will occur. The apparent activation energy for crystallization of $[(Li_{0.41},Ca_{0.05})Al(Si_{0.75},P_{0.5})O_{4.5}]$ glass is determined using an equation developed by Kissinger *et al.*:[65]

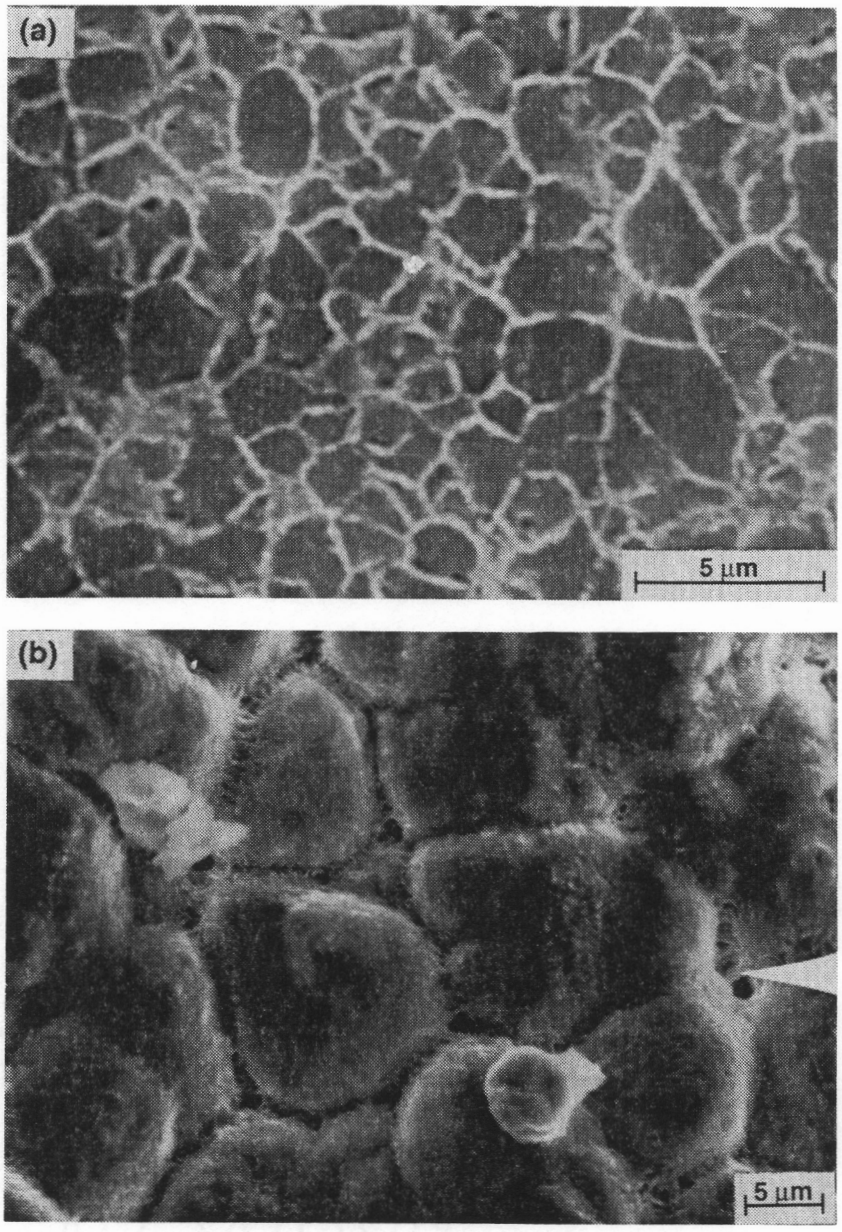

Figure 4.4 Scanning electron micrographs showing glass-ceramics having different size of grains due to different nucleation heat treatments. (a)740°C/2 h + 900°C/0.5 h and (b)780°C/2 h + 900°C/0.5 h.

$$\ell n\left(\frac{\phi}{T_C^2}\right) = -\frac{E_c}{R}\frac{1}{T_C} + constant \qquad (4.8)$$

where ϕ is the DTA heating rate, and T_c is the crystallization peak temperature corresponding to the heating rate in each DTA run. The plot of $\ell n(\phi / T_C^2)$ versus $1/T_c$ is shown in Figure 4.5. The linearity of the curve indicates that crystallization occurs on a fixed number of nuclei. The apparent activation energy for crystallization of the glass was determined to be 285 KJ/mol. This value is less than the kinetic parameters for other glass systems (362 KJ/mol for $18.4CaO{\cdot}78.6Ga_2O_3{\cdot}3SiO_2$[69]; 325 KJ/mol for $40Li_2O{\cdot}60SiO_2$[70]; and 357 KJ/mol for $16.7Na_2O{\cdot}33.3Cao{\cdot}50SiO_2$[71]) which indicates that structural rearrangement during crystallization for this system occurs more easily than for those cited.

Volume crystallization for the glass at various crystallization temperatures is shown in Figure 4.6. As can be seen in the figure, the volume-time crystallization curves are typically sigmodial for isothermal transformation controlled by nucleation and growth. The glass converts to the fully-crystallized glass within 0.3 hour when the glass is heat treated at 1040°C.

4.3 In Situ Whisker-Reinforced Glass-Ceramic Processing

Glass-ceramic processing was conducted by a two-step heat treatment. First, the annealed glass samples were nucleated at 740°C for 2 hours and crystallized at temperatures above 800°C for varying times. The final morphologies of the resultant glass-ceramics are dependent upon heat-treatment temperature and time. Scanning electron micrographs of the polished and etched glass-ceramics which were heat treated at different temperatures and times are shown in Figure 4.7. The glass-ceramic heat

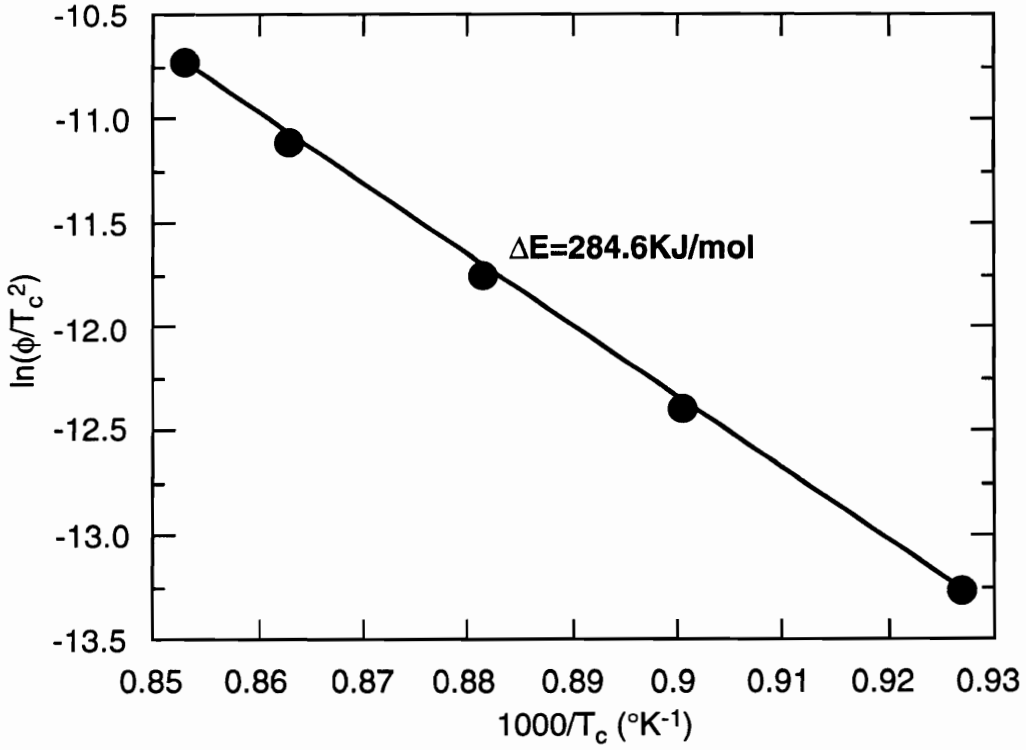

Figure 4.5 Apparent activation energy determined using Kissinger method.[64]

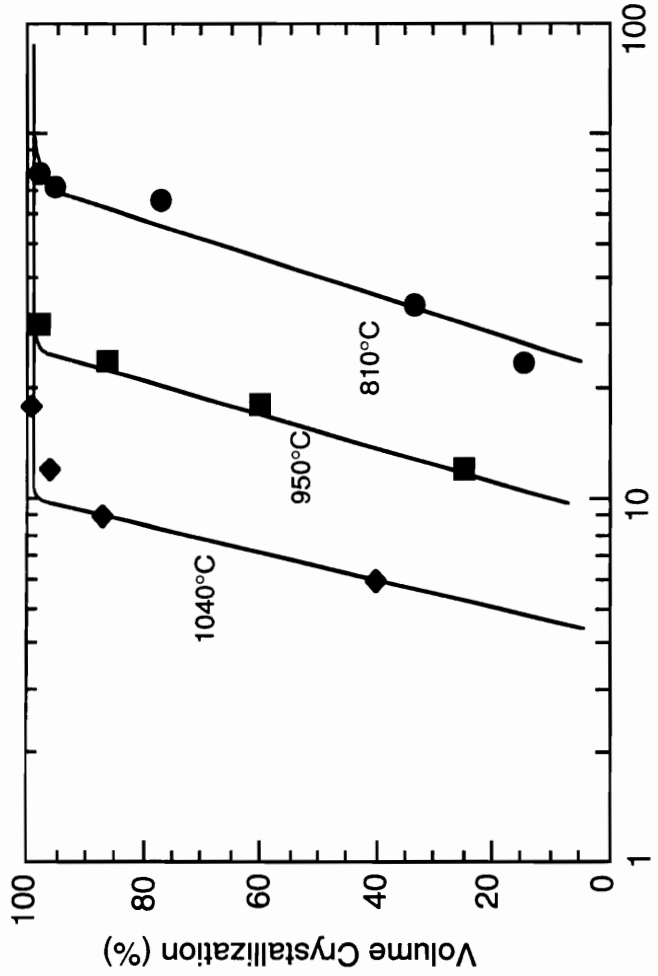

Figure 4.6 Volume crystallization as a function of heat-treatment temperature and time.

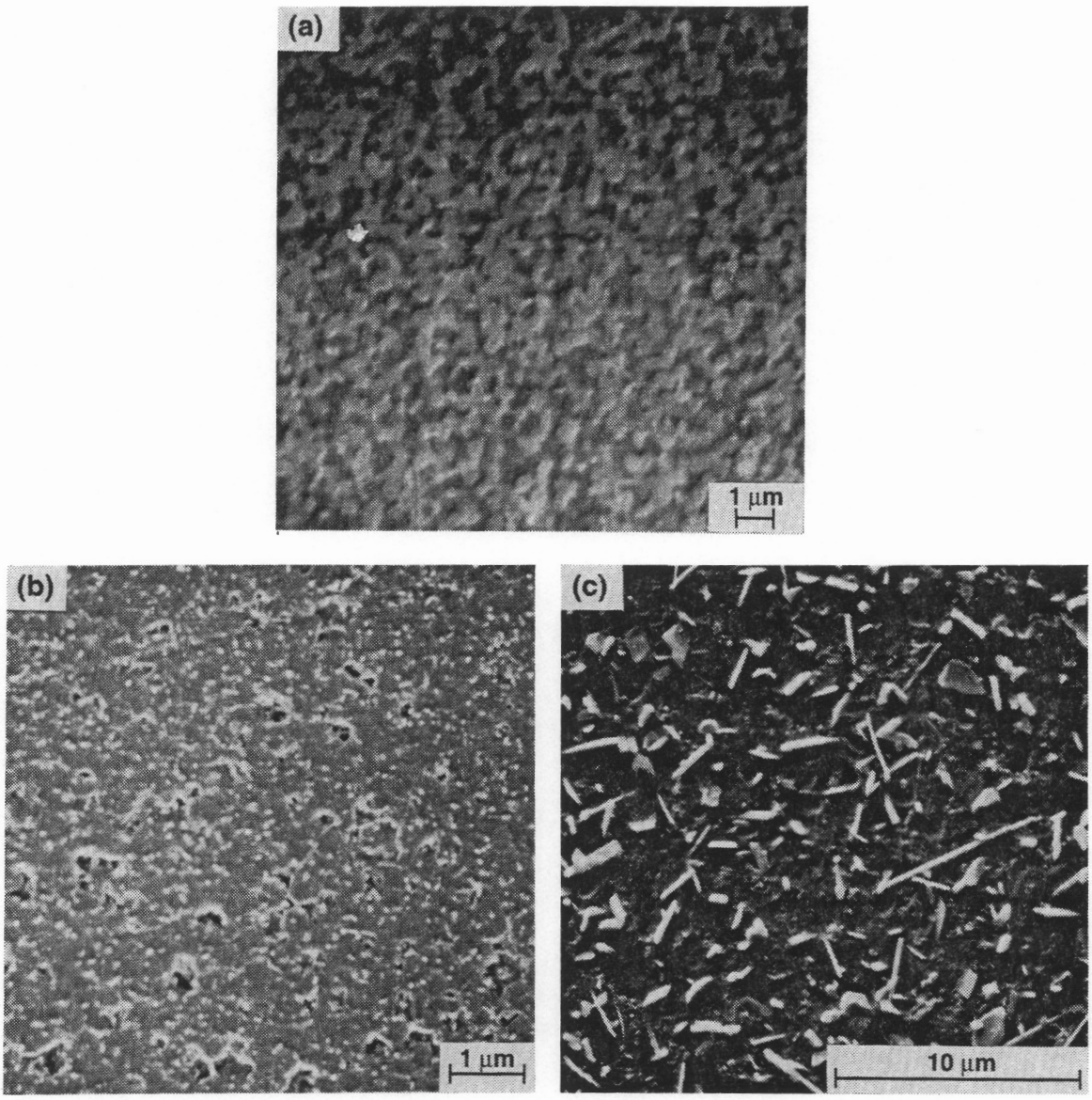

Figure 4.7 Scanning electron micrographs of etched glass-ceramics after nucleation at 740°C/2 h and crystallization at (a)800°C/1 h (b)850°C/1h, and (c)1040°C/20 h.

treated at 800°C for 1 hour (Figure 4.7(a)) shows that a uniformly distributed, large number of crystals was precipitated throughout the glass matrix as a consequence of maximum nucleation heat treatment at 740°C for 2 hours. Crystals are less than 1 μm in size and are somewhat inter-connected; the material exhibits 76% volume crystallization. Figure 4.7(b) shows a near-fully crystallized glass sample after heat treatment at 850°C for 1 hour. The crystals are in contact, and only small portions of the glass phase (dark areas in the figure) remain. There was no significant crystal growth, and the crystal size is still less than 1 μm. Figure 4.7(c) shows glass which was crystallized at 1040°C for 20 hours. At this point, the randomly-oriented whisker-like grains are developed throughout the modified β-eucryptite glass-ceramic matrix.

Crystal phase development during glass-ceramic formation monitored by XRD is presented in Table 4.1 $AlPO_4$-modified β-eucryptite solid solution phase, $[(Li_{0.4},Ca_{0.05})Al(Si_{0.75},P_{0.5})O_{4.5}]$, begins to crystallize at 800°C, and is the dominant phase up to higher temperatures. In some samples, unreacted $AlPO_4$ phase was detected above 950°C as a minor phase. Above 950°C, TiO_2 is detected as a secondary phase. The precipitation of modified β-eucryptite solid solution phase as a first crystalline phase indicates the role of TiO_2 in the nucleation of the material as promoting phase separation during either cooling of the glass melt or reheating of the glass. The modified β-eucryptite solid solution phase is then crystallized from one of the separated phases and, at higher temperatures, TiO_2 phase diffuses out from the modified β-eucryptite phase. Figure 4.7(b) shows secondary phase precipitation (white areas) throughout the crystallized modified β-eucryptite solid solution phase and it is believed that the secondary phase is TiO_2.

Development of TiO_2 phase at high temperatures may be related to the developed whisker phase. Elemental x-ray mapping (Figure 4.8) using an electron microprobe analyzer (SX50, Zameza, Paris, France) indicates that the whisker-shaped grains are

Table 4.1. Phases Developed in $(Li_{0.4},Ca_{0.05})Al(Si_{0.75},P_{0.5})O_{4.5}$ Glass Containing 4 wt% TiO_2 after Nucleation at 740°C for 2 Hours and Crystallization at Various Temperatures and Times

Temperature (°C)	Time (h)	Phase
800	0.1	Glass
800	0.5	mod. β-eucryptite, glass
850	1.0	mod. β-eucryptite
850	2.0	mod. β-eucryptite
950	10.0	mod. β-eucryptite, TiO_2, $AlPO_4$
1040	0.5	mod. β-eucryptite, TiO_2
1040	20.0	mod. β-eucryptite, TiO_2

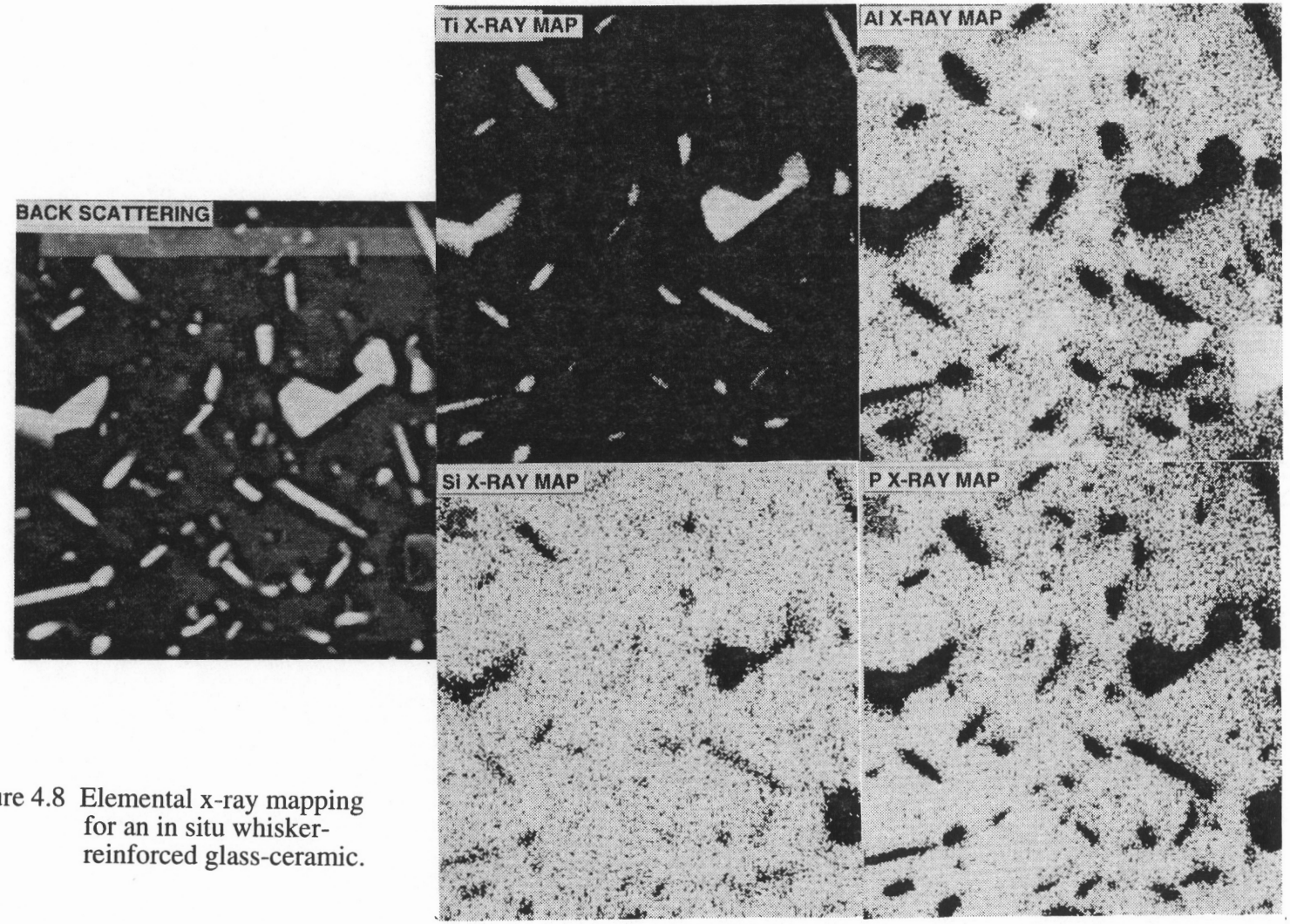

Figure 4.8 Elemental x-ray mapping for an in situ whisker-reinforced glass-ceramic.

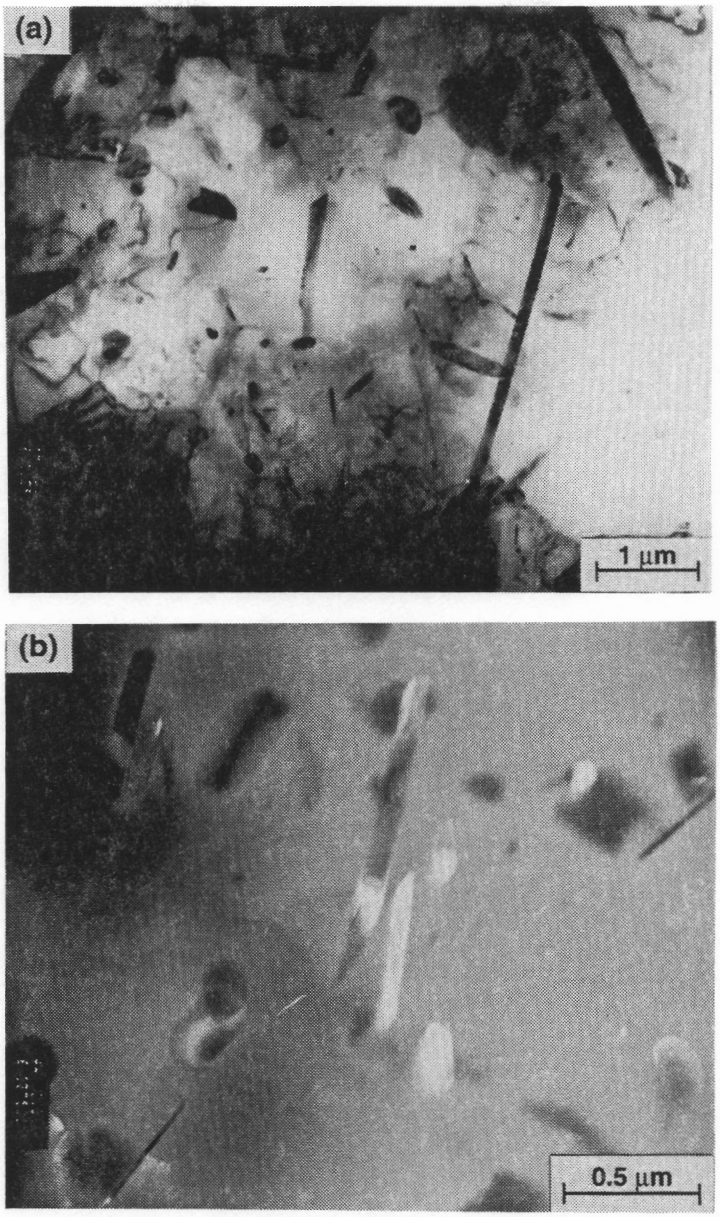

Figure 4.9 Transmission electron micrographs showing (a)precipitated TiO_2 whiskers and (b)dark-field image of TiO_2 whisker

TiO_2. TEM study (STEM 420-T, Phillips, Holland) indicates that the precipitated whisker-shaped TiO_2 crystal is a single crystal (Figure 4.9 (b))and there are no microcrack formations at the interface between the matrix and the TiO_2 whisker (Figure 4.9 (a)). Thus, at low temperatures, TiO_2 which had been added as a nucleating agent acts to create a sufficiently large number of nucleation sites; at high temperatures, TiO_2 phase is also crystallized and grown in whisker-shaped grains and the glass becomes an in situ TiO_2 whisker-reinforced glass-ceramic composite.

4.5 Physical Property Characterizations

4.5.1 CTE and Bulk Density

The influence of heat treatment on the thermal expansion behavior of the [96% $(Li_{0.41},Ca_{0.05})Al(Si_{0.75},P_{0.5})O_{4.5}$, 4% TiO_2] glass was investigated and the results are shown in Figure 4.10. The CTE of the original glass was determined to be about $50x10^{-7}$/°C averaged over from 30 to 700°C. When the glass is heat treated at 850°C, the material exhibits slightly negative thermal expansion behavior ($-2.8x10^{-7}$/°C) due to formation of crystal phase of $AlPO_4$-modified β-eucryptite. However, the glass-ceramic which was heat treated at 950°C exhibits a positive thermal expansion ($4.7x10^{-7}$/°C) due to the formation of a small amount of $AlPO_4$ phase as detected by XRD. The structure, inversion temperature, and CTE of $AlPO_4$ are very similar to that of SiO_2. The precipitation of $AlPO_4$ results in positive thermal expansion of bulk modified β-eucryptite glass-ceramic. However, the glass-ceramic which was heat treated at 1040°C consists of only modified β-eucryptite phase and TiO_2 phase.

The glass-ceramic after heat treating at 1040°C has a slightly negative CTE value ($-1.7x10^{-7}$/°C) which is slightly higher than that of the sample heat treated at 850°C. This is due to the development of 12 vol% of TiO_2 phase which has a positive CTE ($7.3x10^{-6}$/°C).

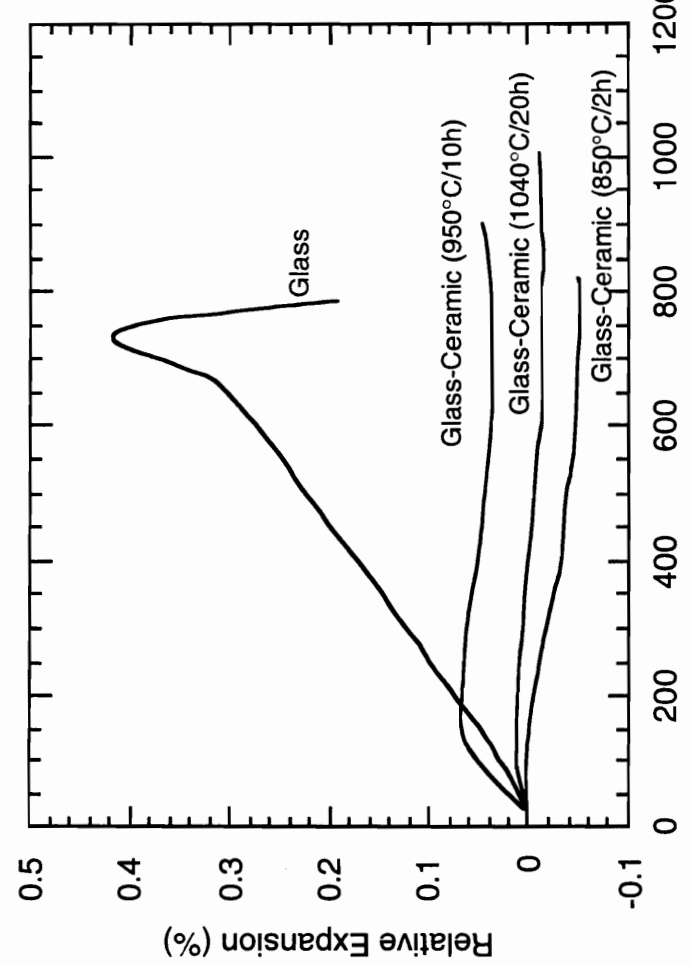

Figure 4.10 Relative thermal expansion of the glass and glass-ceramics heat treated at various temperatures and times.

Bulk density is increased with heat treatment time and temperature(see Table 4.2). Since the original glass has a more open structure than the crystallized glass, the original glass exhibits the lowest density. Among the glass-ceramics, the glass-ceramic crystallized at 1040°C for 20 hours exhibits the highest density value due to the formation of TiO_2 whiskers which have a higher bulk density (4.25 g/cm^3) than the matrix. However, the density (2.51 g/cm^3) of the in situ TiO_2 whisker-formed $AlPO_4$-modified β-eucryptite glass-ceramic is still lower than that of other structural ceramics, Si_3N_4 (3.44 g/cm^3) and SiC (3.22 g/cm^3) for example.

4.5.2 Effect of TiO_2 Whiskers on Flexural Strength of $AlPO_4$-Modified β-Eucryptite

Flexural strength measurement of the glass and the glass-ceramics with and without TiO_2 whisker precipitation was conducted using four-point bending tests and the results are shown in Figure 4.11. The flexural strength of the original glass is 67 MPa. When the glass is fully crystallized at 850°C for 2 hours, flexural strength is increased to 81 MPa due to the development of uniform crystals less than 1 μm in size which have higher elastic modulus than the glass. In this system, however, full-crystallization must occur in order to increase the flexural strength after crystallization. When the glass was only partially crystallized, the sample broke into pieces during machining due to the development of very high tangential tensile stresses in the glass matrix resulting from the severe thermal expansion mismatch ($\alpha_{glass} > \alpha_{crystal}$) between the glass ($50 \times 10^{-6}$/°C) and the precipitated crystal phase (-2.8×10^{-7}/°C). However, when the glass is crystallized at 850°C for 2 hours, the glass is almost fully crystallized with only a small amount (≈2vol%) of discontinuous glass phase. In this case, the developed crystal phase serves as the matrix, thus compressive stress, which is beneficial to strengthening, is created in the matrix. The flexural strength of the glass-ceramic heat treated at 950°C for 10 hours decreased from 81 to 72 MPa due to grain coarsening and the presence of $AlPO_4$ phase.

Table 4.2. Bulk Density for Various Heat Treatments of $AlPO_4$-Modified β-Eucryptite Glass-Ceramic

Heat Treatment (Temperature and Time)	Bulk Density (g/cm^3)
Original Glass	2.44
740°C/2h + 850°C/2h	2.47
740°C/2h + 950°C/10h	2.48
740°C/2h + 1040°C/20h	2.51

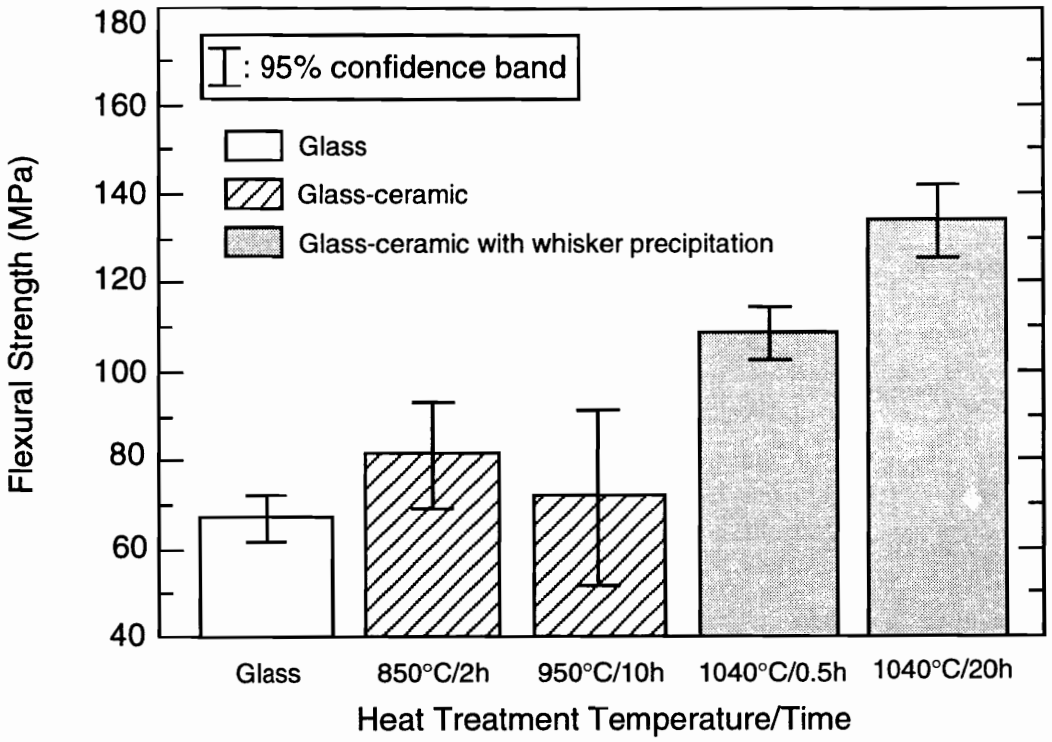

Figure 4.11 Effect of heat treatment temperature and time on flexural strength of the glass and the glass-ceramics.

However, glass-ceramics heat treated at 1040°C exhibit increasing strength values, with the glass-ceramic heat treated at 1040°C for 20 hours exhibiting the highest strength value (134 MPa). This clearly indicates that the precipitated TiO_2 whiskers improve the strength of the $AlPO_4$-modified β-eucryptite glass-ceramic.

Elastic modulus and fracture strength values for TiO_2 whiskers are not available in existing literature, however the values can be estimated from published studies which give the mechanical strength of 99% densified hot-pressed polycrystalline TiO_2 as a function of grain size. The elastic modulus and fracture strength of a densified polycrystalline TiO_2 were found to be 283 GPa[72] and 350 MPa,[73] respectively. Since the TiO_2 whisker is single crystal (see Figure 4.9) and no handling or processing defects are formed during precipitation, it can be assumed that the whiskers possess a strength value greater than 350 MPa.

The strengthening requirements for whisker-reinforced composites are: first, whiskers must be stiffer and stronger than the matrix; and second, the aspect ratio of the whisker must be larger than the critical aspect ratio because the basic mechanism of strengthening in whisker composites is load transfer from the matrix to the whiskers through shear at whisker ends. The amount of load transfer from the matrix to the whisker depends on the aspect ratio of the whiskers. Therefore, to strengthen composites, the aspect ratio must be larger than the critical aspect ratio. Strengthening of in situ formed TiO_2 whisker-reinforced $AlPO_4$-modified β-eucryptite glass-ceramic can be explained by the following:

(1) Precipitated TiO_2 whiskers are stiffer and stronger than the $AlPO_4$ modified β-eucryptite glass-ceramic matrix.

(2) Average aspect ratios of the precipitated TiO_2 whiskers for the glass-ceramics heat treated at 1040°C for 0.5 hour and 20 hours are 10 and 28, respectively. These values

are greater than the critical aspect ratio ($\ell/d=8$) which is determined from an empirical equation developed by Termonia[49] (refer to the section 2.4.1 for details).

Therefore, when a load is applied to the material, the stiffer and stronger TiO_2 whiskers carry the majority of the applied load, and overall flexural strength of the material is improved. In addition to this, as can be seen in Figure 4.11, in situ TiO_2 whisker-precipitated glass-ceramic heat treated at 1040°C for 20 hours shows a higher strength value compared to the glass-ceramic composite heat treated at 1040°C for 0.5 hour. The higher strength is due to the higher aspect ratio of the precipitated TiO_2 whiskers heat treated for a longer time. As aspect ratio increases, more load can be carried by the whiskers and overall strength is increased.

(3) Residual stresses on the composite can affect the strength of the material. As mentioned in section 4.1.2, the bulk CTE of the $AlPO_4$-modified β-eucryptite glass-ceramic is less than $4.0x10^{-7}$/°C. However, according to the literature, the bulk CTE of TiO_2 is larger, approximately $7.3x10^{-6}$/°C. Therefore, during cooling from the fabrication temperature, the matrix is under compressive stress along the axial direction of the TiO_2 whiskers. This compressive stress strengthens the matrix if no interfacial debonding is caused by the thermal expansion mismatch between the precipitated TiO_2 whisker and the matrix. Since no microcracks were observed between the whisker and the matrix by transmission electron microscopy, residual compressive stress in the matrix along the axial direction of the whisker is beneficial for strengthening.

4.5.3 Effect of TiO_2 Whiskers on Elastic Modulus of $AlPO_4$-Modified β-eucryptite

Elastic moduli of the original glass, the glass-ceramics heat treated below 1000°C (and hence contain no TiO_2 whisker precipitation), and the glass-ceramic heat treated at

1040°C for 20 hours (and contains TiO_2 whisker precipitation) were determined by measuring the deflection of the flexural bars. The results are shown in Figure 4.12.

As can be seen, the in situ TiO_2 whisker-reinforced glass-ceramic exhibits the highest elastic modulus value. On the other hand, the original glass shows the lowest elastic modulus value. The increases in elastic modulus value during glass to glass-ceramic transition results from the formation of $[(Li_{0.41},Ca_{0.035})Al(Si_{0.75},P_{0.5})O_{4.5}]$ crystal phase which has a higher elastic modulus than the glass phase. Generally, in a glass-ceramic composition, the crystalline phase has a higher elastic modulus than the glass phase. Increase in the elastic modulus of the glass-ceramic without in situ TiO_2 whisker precipitation compared to that of the glass-ceramic with in situ TiO_2 whisker precipitation is due to the incorporation of the very stiff (E=283 GPa) TiO_2 phase.

Theoretically, the modulus of the randomly-oriented TiO_2 whisker-reinforced $AlPO_4$-modified β-eucryptite glass-ceramic composite can be estimated using equations.[51,52] When the glass is crystallized at 1040°C for 20 hours, about 12 vol% of randomly-oriented TiO_2 whiskers with an average aspect ratio of 28 are precipitated throughout the modified β-eucryptite glass-ceramic matrix. Using E_w = 283 GPa, E_m = 67 GPa, V_w = 0.12, and (ℓ/d) = 28 in the Halpin-Tsai equations (Equation 2.20(a) and (b)), the modulus of randomly-oriented TiO_2 whisker-reinforced modified β-eucryptite glass-ceramic composite is calculated as E_c = 84 GPa which confirms the value measured experimentally (85 GPa).

4.5.4 Effect of TiO_2 Whiskers on the Fracture Toughness

Fracture toughness, K_{IC}, for the original glass and the glass-ceramics with and without TiO_2 whisker precipitation was measured by the indentation method using a 9.8N load. For the in situ TiO_2 whisker-reinforced glass-ceramic case, R-curve behavior was also examined by the indentation-strength method.

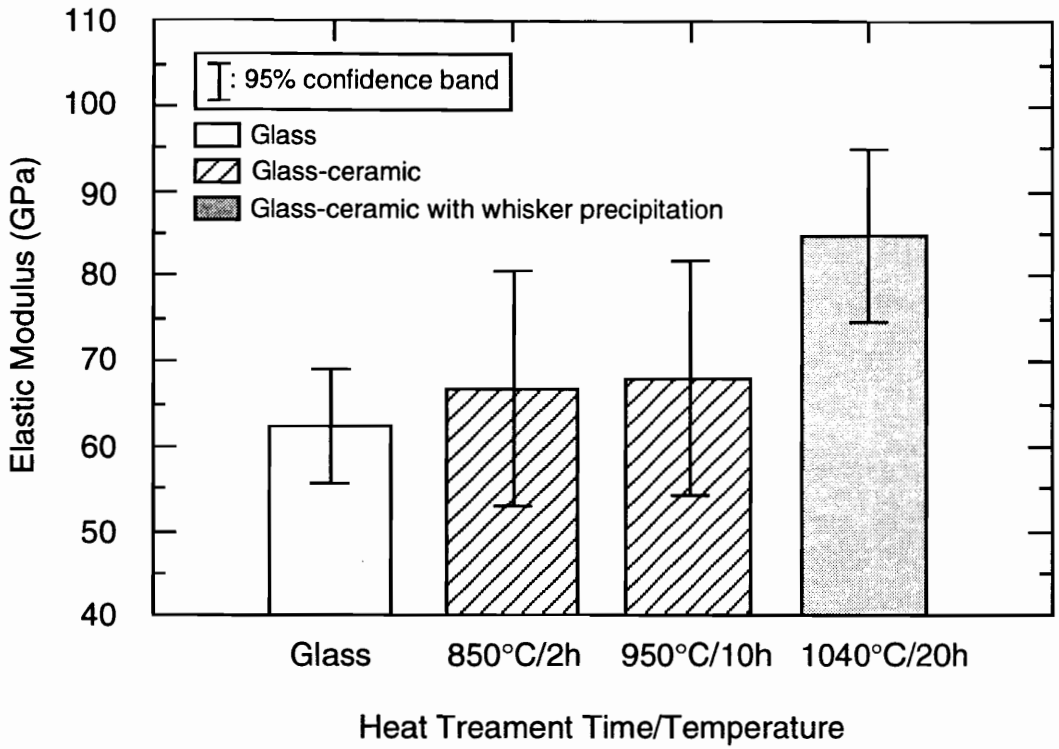

Figure 4.12 Effect of heat treatment temperature and time on elastic moduli of the glass and the glass-ceramics. All glass-ceramics were heat treated at 740°C/2h prior to heat treatments.

(A) Determination of Indentation Fracture Toughness

Generally, there are two different crack geometries after Vickers indentation in ceramic systems. The one known as the Palmqvist cracks and the other known as the radial cracks. Fracture toughness value analysis of a material is related to the type of crack which develops after Vickers indentation. In the present study, the glass and the glass-ceramics exhibit radial cracks after Vickers indentations in the indentation load range from 0.98N to 9.8N. The radial crack size, measured along the crack from the center of the indent to the crack tip, is plotted on a $\ell n - \ell n$ scale as a function of Vickers indentation load in Figure 4.13. As can be seen in the figure, the linear regression slope of the ℓn indentation load versus ℓn crack size is close to 2/3 which implies radial crack development.[74] SEM observation of the fracture surface of the in situ TiO_2 whisker-reinforced $AlPO_4$-modified glass-ceramic after indentation reveals the development of a radial crack in Figure 4.14.

The literature abounds with fracture toughness determination methods using Vickers indentations; two equations were used for determination of fracture toughness values of the modified β-eucryptite glass and glass-ceramics.[66,67] Fracture toughness results obtained are shown in Figure 4.15. For the given material, the equations did not give the same K_{IC} value. For example, for the original glass, the equation developed by Lawn *et al.*[66] gave $K_{IC} = 0.662$ MPa·√m. However, the equations of Antis *et al.*[67] gave 0.809 MPa·√m for the K_{IC} value of the original glass. It is difficult to decide which is more suitable equation for calculating K_{IC} of the present materials.

According to Wiederhorn,[75] fracture toughness values of silicate glasses are in the range 0.7 - 0.9 MPa·√m. Therefore, the equation by Antis *et al.*[67] (K_{IC} for the glass = 0.81) may be more suitable for calculating the fracture toughness of the $AlPO_4$-modified β-eucryptite glass and glass-ceramics.

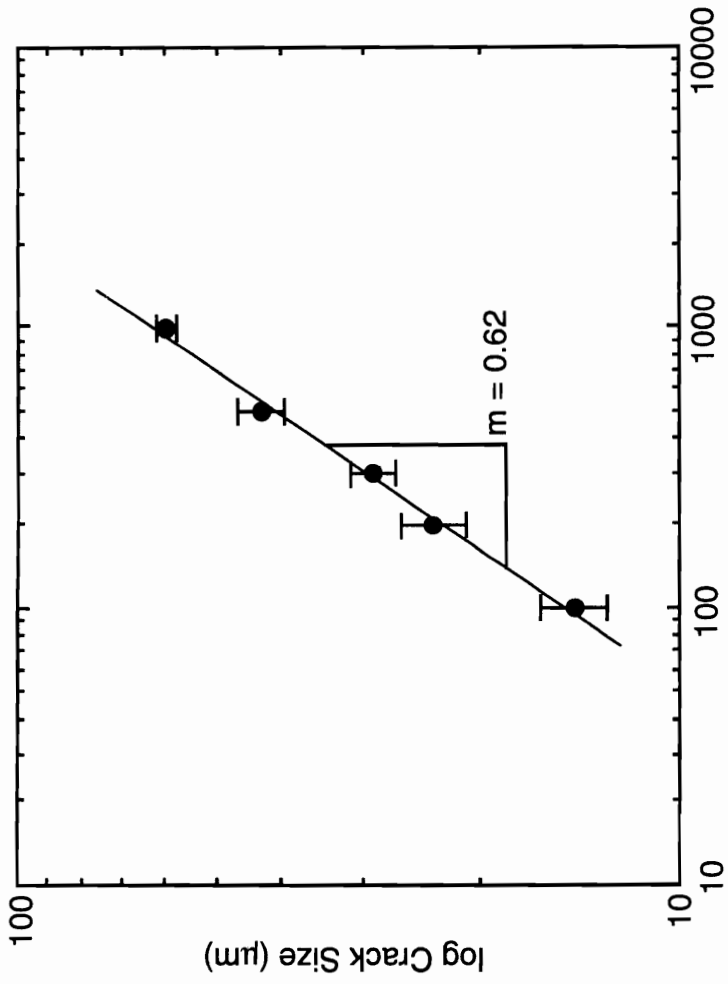

Figure 4.13 Crack size as a function of indentation load for $AlPO_4$-modified β-eucryptite heat treated at 1040°C for 20 hours.

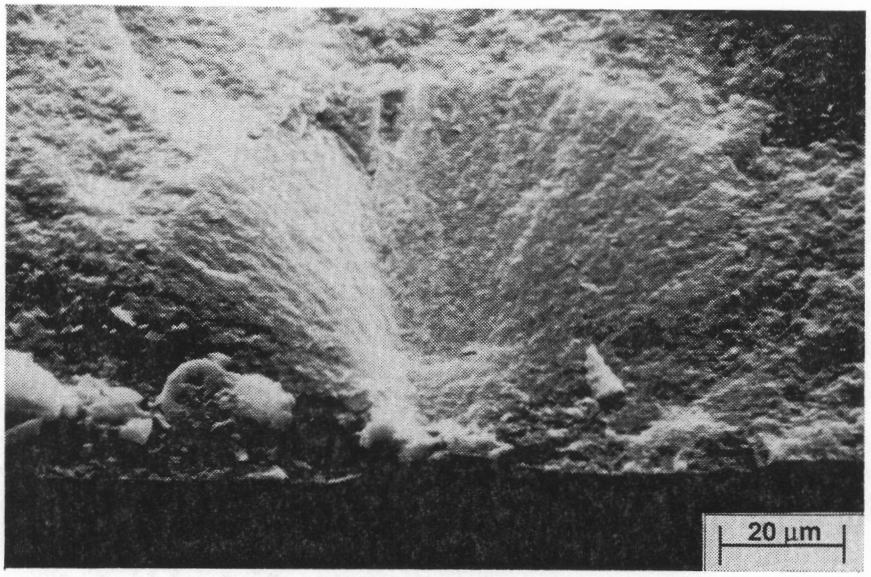

Figure 4.14 Scanning electron micrograph showing the development of a radial crack on the fracture surface of the material after indentation with 9.8N load.

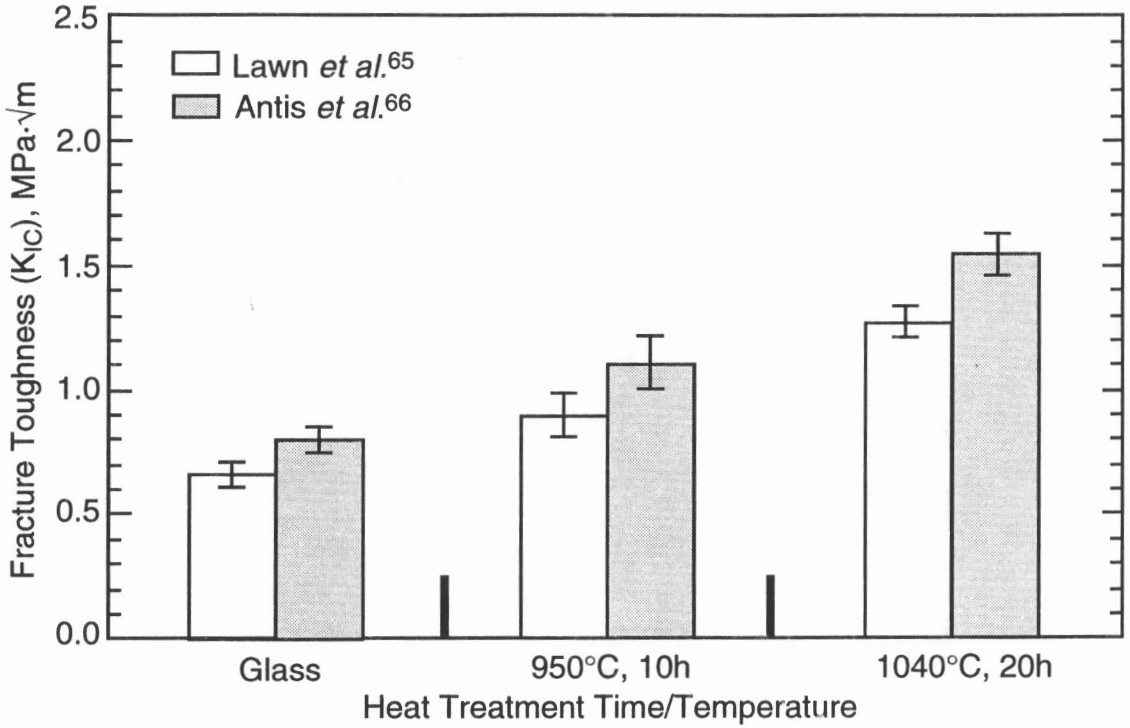

Figure 4.15 Fracture toughness, K_{IC}, for the $AlPO_4$-modified β-eucryptite glass and glass-ceramics determined by using different equations. 95% confidence band is also shown.

As shown in Figure 4.15, for a given equation, the glass exhibits the lowest fracture toughness value. On the other hand, the in situ TiO_2 whisker-reinforced glass-ceramic exhibits the highest fracture toughness value. In glass, fracture toughness is dependent on the fracture energy, γ, which is related to the atomic bonding strength of a glass and there are no possible toughening mechanisms because there are no media (grain boundary, second phase, etc.) to deflect the crack. When the glass is crystallized and becomes a glass-ceramic, there is increasing fracture toughness due to increasing fracture energy, γ, with increasing elastic modulus. The maximum K_{IC} value of the in situ glass-ceramic composite indicates that toughening mechanisms are involved.

SEM observation of the indentation cracks on the polished surface of the in situ TiO_2 whisker-reinforced $AlPO_4$-modified β-eucryptite glass-ceramic indicates that the main toughening mechanism is crack deflection. Figure 4.16 shows cracks deflected where the crack tip approaches the TiO_2 whiskers. TiO_2 whiskers located near a propagating crack alter the direction of crack growth, causing a reduction in stress intensity. Some of the whiskers are broken where they intersect the crack tip. This, too, contributes to reducing stress intensity by absorbing fracture energy when the crack tip breaks the whiskers because the whiskers have a higher elastic modulus than does the matrix. Figure 4.17 shows fracture surfaces of the original glass, and modified β-eucryptite glass-ceramics with and without in situ TiO_2 whisker formation. The in situ TiO_2 whisker-formed glass-ceramic exhibits the roughest fracture surface, indicating that cracks are deflected by the whiskers. Consequently, when the TiO_2 whiskers are precipitated throughout the $AlPO_4$-modified β-eucryptite glass-ceramic matrix, there is a 40% increase in the fracture toughness, K_{IC}, value. According to Freiman,[76] increases of ≈40% in K_{IC} can be achieved by crack deflection. However, Faber *et al.*[60] derived a model for the effect of crack deflection around an elongated second particle and their

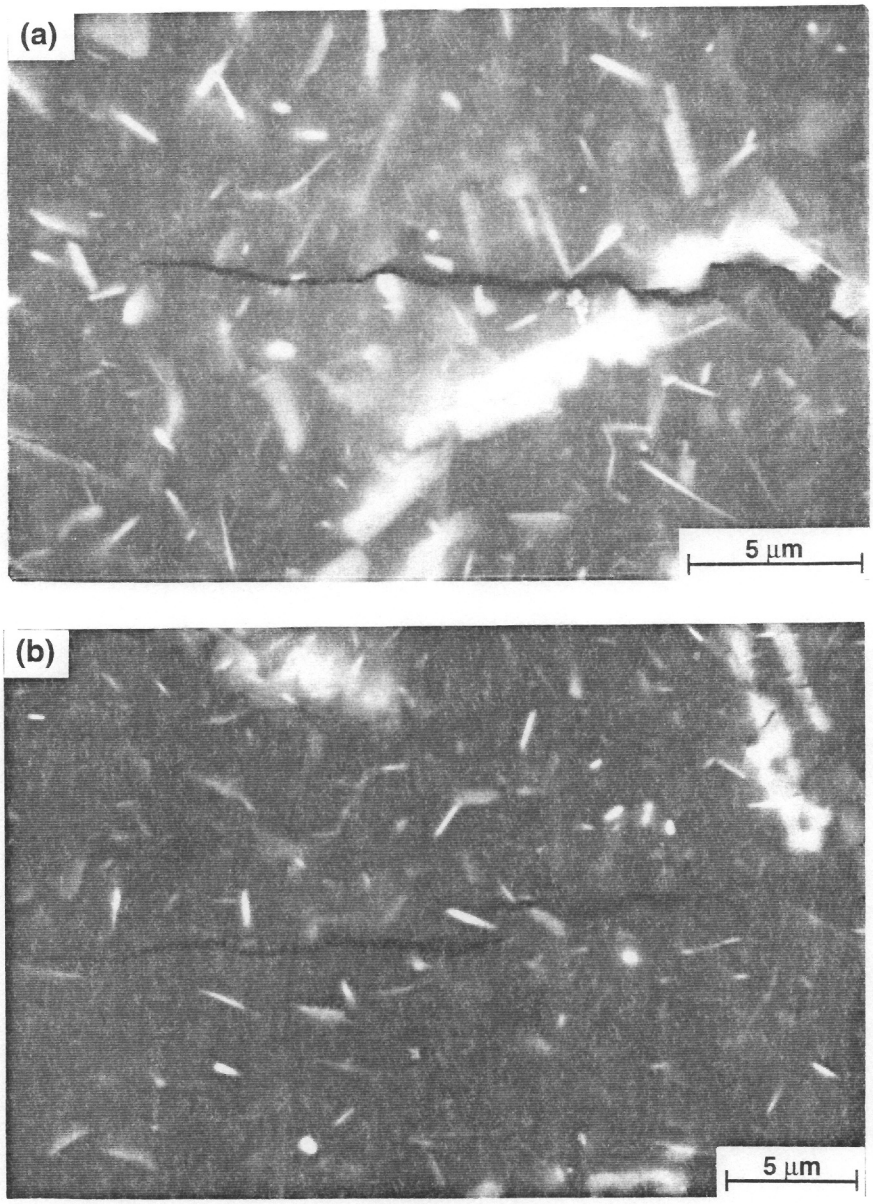

Figure 4.16 Scanning electron micrographs showing indentation crack propagation in an in situ TiO_2 whisker-reinforced modified β-eucryptite glass-ceramic.

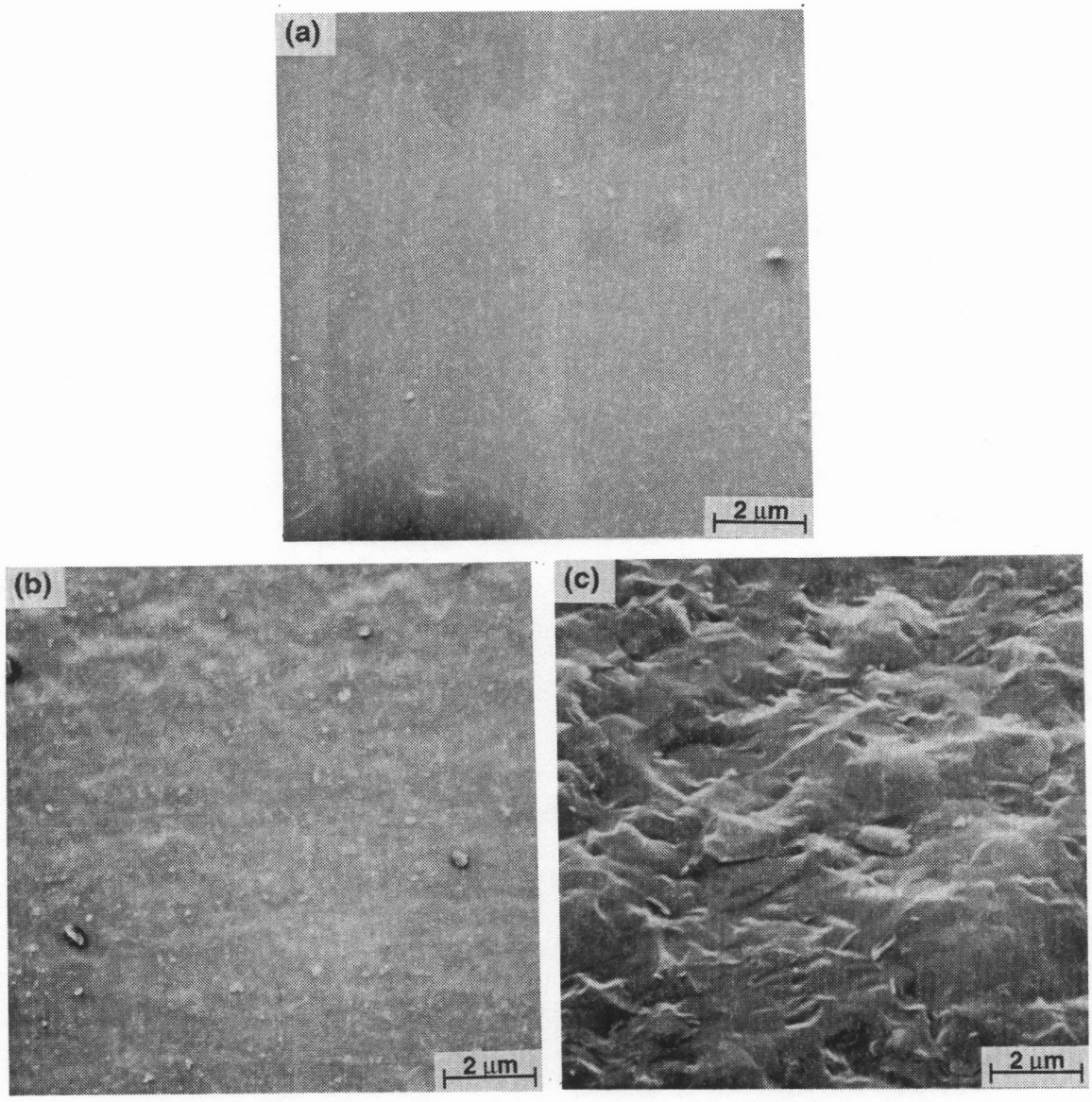

Figure 4.17 Scanning electron micrographs showing fracture surface of (a)glass (b)glass-ceramic without TiO_2 whisker precipitation, and (c) glass-ceramic with TiO_2 whisker precipitation.

model indicates increases in K_{IC} value greater than 40% when a crack is deflected by an elongated second phase.

Deflection toughening arises whenever interaction between the crack tip and the second phase produces a non-planar crack.[60] The formation of a non-planar crack by deflection at a particulate phase arises either from weak interface bonding or from the residual stress in the matrix due to thermal expansion/elastic modulus mismatches between the matrix and the particulate phase.

Since the TiO_2 whisker has higher CTE and elastic modulus values than $AlPO_4$-modified β-eucryptite glass-ceramic matrix, a tangential compressive stress is created near the TiO_2 whisker/matrix interface during cooling from the fabrication temperature; this compressive stresses diverts the crack around the whisker. However, the actual experimental result reveals that the residual compressive strain has no significant influence on the K_{IC} of in situ TiO_2 whisker-reinforced $AlPO_4$-modified β-eucryptite. In order to examine the residual stress effect on K_{IC}, an experimental study was conducted with samples quenched in air. Samples of in situ TiO_2 whisker-reinforced $AlPO_4$ modified β-eucryptite glass-ceramic were cut into blocks (4 x 5 x 15 mm) and polished. Since the magnitude of thermal expansion mismatch can not be changed, the blocks were quenched from 400, 600, 800, and 1000°C in order to introduce different levels of residual compressive stress according to the following relationship:[40]

$$\sigma_{tangential} = \frac{\Delta\alpha\,\Delta T}{2\left[\left(1+\frac{\upsilon_m}{2E_m}\right)+\left(1-\frac{2\upsilon_w}{E_w}\right)\right]} \tag{4.9}$$

where $\Delta\alpha$ is the thermal expansion mismatch ($\alpha_{matrix} - \alpha_{TiO_2}$); υ_m and υ_w are the Poisson's ratios of the matrix and whisker, respectively; E_m and E_p are the elastic moduli of the

matrix and whisker, respectively; and ΔT is the temperature change. When the material is quenched from 800°C to 25°C, compressive residual stress is two-fold greater than that in the material quenched from 400°C to 25°C. After quenching from the various temperatures, critical fracture toughness, K_{IC}, was determined using Vickers indentations (eight indents for each quenched specimen) with a 9.8N load; results are shown in Figure 4.18. The data indicate that the magnitude of the compressive stress developed has no effect on crack propagation, and therefore no impact on fracture toughness. However, the results also indicate the excellent thermal shock resistance of the material quenched from the 1000°C in air.

In order to produce non-planar cracks during crack propagation, the bond strength of the interface between matrix and TiO_2 whisker is the most critical factor. Strong interface bonding will prevent whisker pull-out and, consequently, there will not be a great energy absorption by the whiskers. On the other hand, too weak an interface bond will not produce very much energy absorption during whisker pull-out and therefore will cause little enhancement in fracture toughness. The fracture surface of in situ TiO_2 whisker-reinforced $AlPO_4$-modified β-eucryptite (Figure 4.17(c)) shows no significant whisker pull-out, indicating strong interfacial bonding between the whisker and the matrix. Therefore, in situ formed TiO_2 whiskers, due to strong bonding to the matrix, are beneficial for increasing fracture strength because of efficient load transfer from the matrix to the whiskers, but causes little significant improvement in fracture toughness.

Fracture toughness is typically a single-value parameter which describes fracture resistance, *i.e.*, a constant resistance value to fracture. However, variation of K_{IC} with crack length (so-called rising fracture toughness or R-curve behavior) was observed in the in situ TiO_2 whisker-reinforced $AlPO_4$-modified β-eucryptite. Fracture strength as a function of indentation load for the in situ TiO_2 whisker-reinforced glass-ceramic

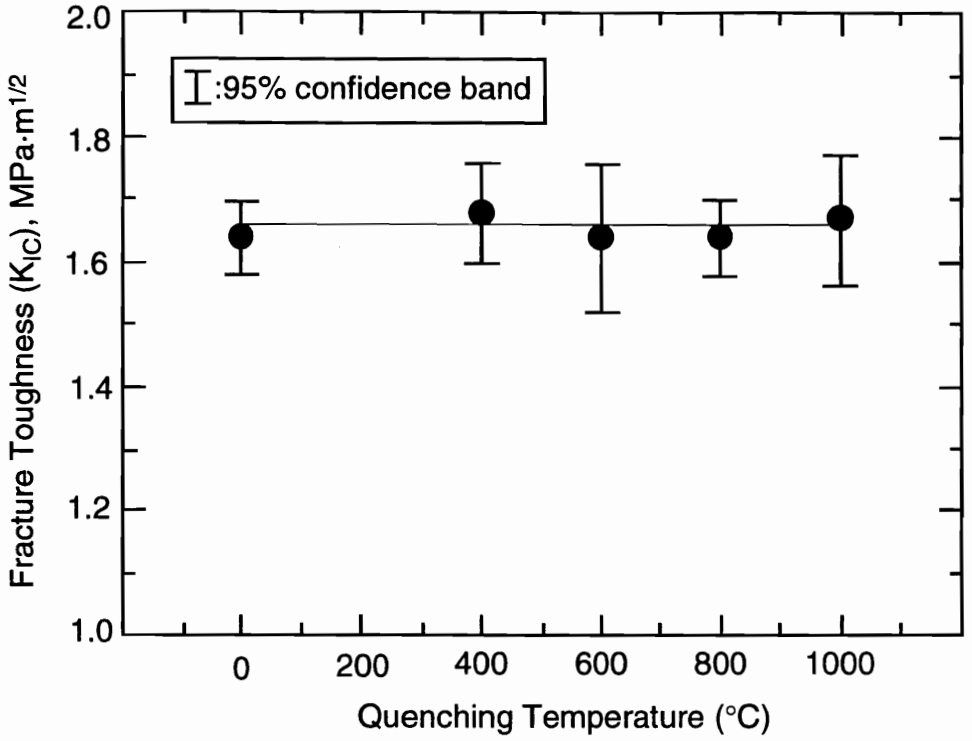

Figure 4.18 Fracture toughness after TiO_2 whisker-reinforced modified β-eucryptite glass-ceramic was quenched in air.

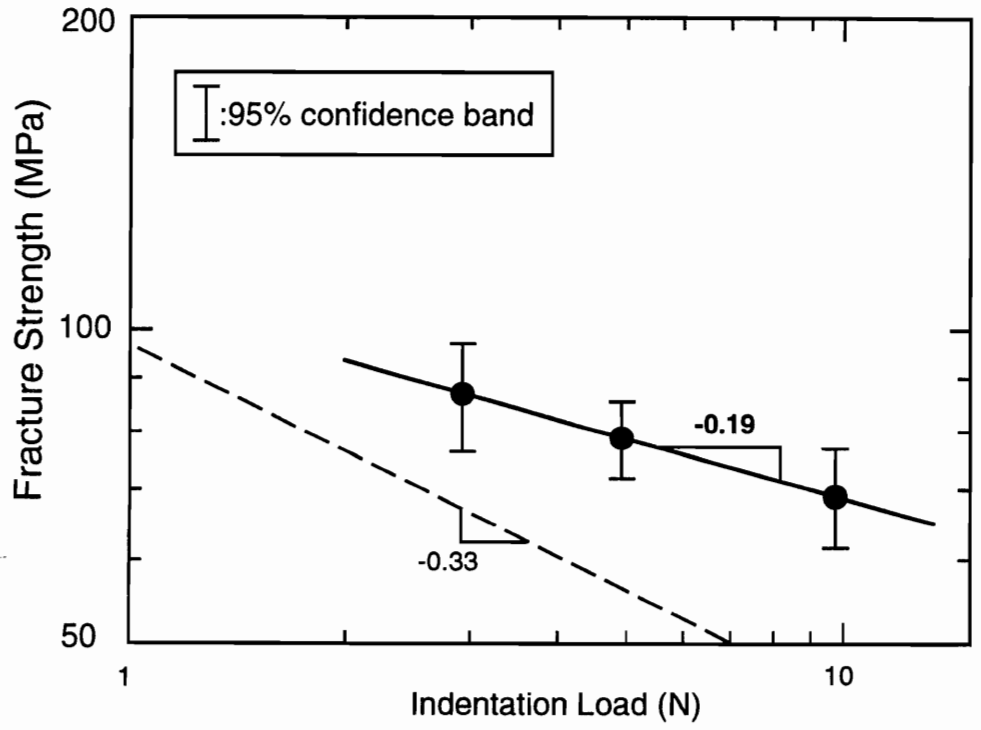

Figure 4.19 Fracture strength as a function of indentation load. The dashed line represents an ideal slope for no R-curve behavior.

composite is shown in Figure 4.19. R-curve behavior of the material can be estimated from the indentation-strength data shown. A material which exhibits no R-curve behavior shows the following relationship for strength loss accompanying indenter contact:[77]

$$\sigma_f = \left[\left(\chi_r K_{IC}^4\right)^{1/3} Y^{-1/2}\right] P^{-1/3} \tag{4.10}$$

where σ_f is the fracture strength, χ_r is the dimensionless constant related to the residual field about the indentation, K_{IC} is the fracture toughness, Y is a crack-geometry constant, and P is the indentation load. The $\sigma_f \propto P^{-1/3}$ relationship indicates that fracture strength is independent of contact load. In other words, fracture toughness, K_{IC}, does not change with crack extension. However, if the material does not follow the $\sigma_f \propto P^{-1/3}$ relationship, then the material will exhibit R-curve behavior. As shown in Figure 4.19, the slope of the curve ($d\ell og\sigma / d\ell ogP$) is -0.19 which is about 57% less than the -1/3 slope. This indicates that fracture toughness of the material would change with the crack extension. The fracture resistance of the material can then be calculated by the following equations:[78]

$$\sigma_f = \alpha P^{-\beta} \tag{4.11}$$

$$\begin{aligned} K_R &= k(\Delta a)^{(1-3\beta)/(2+2\beta)} \\ &= \left[Y\alpha(\beta\gamma)^{-\beta}(1+\beta)^{1+\beta}\right](\Delta a)^{(1-3\beta)/(2+2\beta)} \end{aligned} \tag{4.12}$$

where Y is a dimensionless configuration coefficient dependent on the boundaries of the specimen, α is a constant, β is the slope of $\ell og\sigma$ *vs.* ℓogP, γ is a constant, and Δa is the crack extension. Values of these parameters which define fracture resistance, K_R, of in

Table 4.3. Parameter Values which Define K_R of the Material

Parameter	Value
β	0.19
α	106
$\log \gamma$	6.856
Y	1.292

situ TiO_2 whisker-reinforced modified β-eucryptite glass-ceramic are listed in Table 4.3. The α value was determined by measuring the intercepting value of $\ell og\sigma_f$ axis in the $\ell og\sigma$ *vs.* ℓogP curve. The γ was determined using the following equation:

$$\gamma = \frac{P}{a_I^{2/(1+\beta)}} \tag{4.13}$$

where P is the indentation-load, and a_I is the indentation-crack length. Y was determined from published stress-intensity factor equations for a surface crack on a specimen subjected to a bending moment.[79] As shown in Figure 4.14, after indentation, the crack developed was semicircular. If it is assumed that this semicircular crack does not change its shape during the bending test, Y value is determined to be 1.292. Crack resistance, K_R, can then be calculated as $11.54(\Delta a)^{0.18}$. Crack resistance as a function of crack extension, Δa, is shown in Figure 4.20. For the given crack extension, K_R is increased from 1.89 to 2.5 MPa·√m over the crack extension range from 40 to 200 μm. As shown in Figure 4.16(b), R-curve behavior of in situ TiO_2 whisker-reinforced glass-ceramic arises due to the crack bridging between whiskers in the wake of the crack tip.

When TiO_2 whiskers are precipitated throughout $AlPO_4$-modified β-eucryptite glass-ceramic, mechanical strength and fracture toughness increase. However, increases in flexural strength and fracture toughness do not necessarily reduce strength scatter. If the material exhibits R-curve behavior, then a significant increase in Weibull modulus, *i.e.*, a reduction in strength scatter can be expected.[80,81,82] The results of strength measurement of the glass-ceramics with and without TiO_2 whisker precipitation (see Figure 4.11) show that the in situ TiO_2 whisker-reinforced glass-ceramic exhibits narrower strength distribution. The result suggests that when the TiO_2 whiskers are precipitated throughout the matrix, the Weibull modulus can increase significantly. This

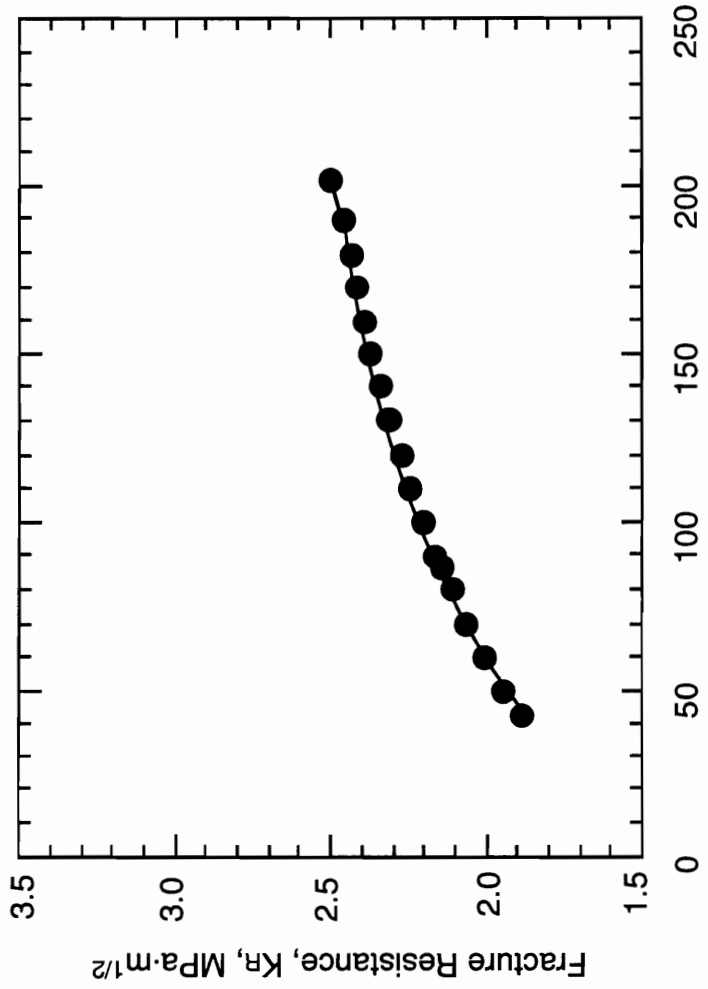

Figure 4.20. Fracture resistance as a function of crack extension.

is because R-curve toughening indicates that cracks can have a certain stable crack growth prior to catastrophic failure; larger cracks can have longer stable crack growth than smaller cracks. In materials which exhibit R-curve behavior, failure stress will be relatively insensitive to crack size. Further, in the material which exhibits R-curve behavior, larger cracks require higher stresses to propagate. Therefore, the material exhibits a narrow strength distribution, hence an increase in Weibull modulus. The higher the Weibull modulus, the lower the amount of scatter, and consequently, the higher the probability of successful operation at a given stress level, *i.e.*, improved reliability of the material. The higher the value of the slope of the rising R curve, $dK_R / d(\Delta a)$, the more narrow a strength distribution can be expected.[81]

CHAPTER V

RESULT and DISCUSSION for COMPOSITION 2

5.1 Glass Formation

Glass powders which contain 6~10 wt% TiO_2 were melted at 1620°C for 2-3 hours then poured into water. XRD examination indicated that devitrification did not occurred during the water quenching. However, the glass powder containing 12 wt% TiO_2 showed slight devitrification during cooling but clean glass fragments were collected for further treatment. A DTA thermogram for the glass containing 94% $(Li_{0.41},Mg_{0.035})Al(Si_{0.48},P_{0.52})O_4$ and 6% TiO_2 is shown in Figure 5.1. The small endothermic peak at 596°C corresponds to the glass transition temperature, Tg, and an exothermic peak at 730°C is associated with crystallization of the glass phase. These points change very little, even with increasing amounts of TiO_2. The DTA result also indicates that densification heat treatment of the glass powder must be conducted between 596°C and 730°C.

5.2 Densification and Sintered Glass-Ceramic Process

Densification of glass powder is accomplished by simply heat treating the glass powder above its glass transition point so that each glass particle becomes viscous and coalesces. However, the coalescence of the glass powder must be conducted below the crystallization temperature. If crystallization starts before completion of the densification, the crystallized external area of each glass particle hinders viscous flow, and full-densification can not be obtained. The schematic sequence of densification and crystallization is illustrated in Figure 5.2. However, coalescence of the glass powder is not simple for the composition $(Li_{0.41},Mg_{0.035})Al(Si_{0.48},P_{0.52})O_4$. As mentioned in

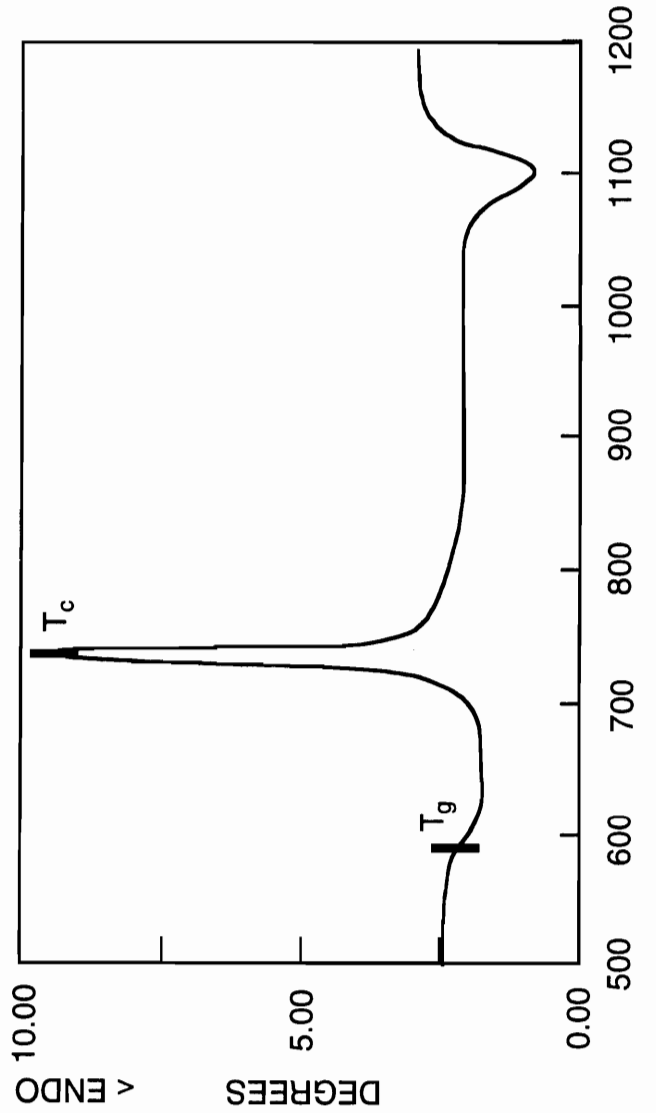

Figure 5.1 DTA curve for the [94% $(Li_{0.41},Mg_{0.035})Al(Si_{0.48},P_{0.52})O_4$, 4% TiO_2] glass.

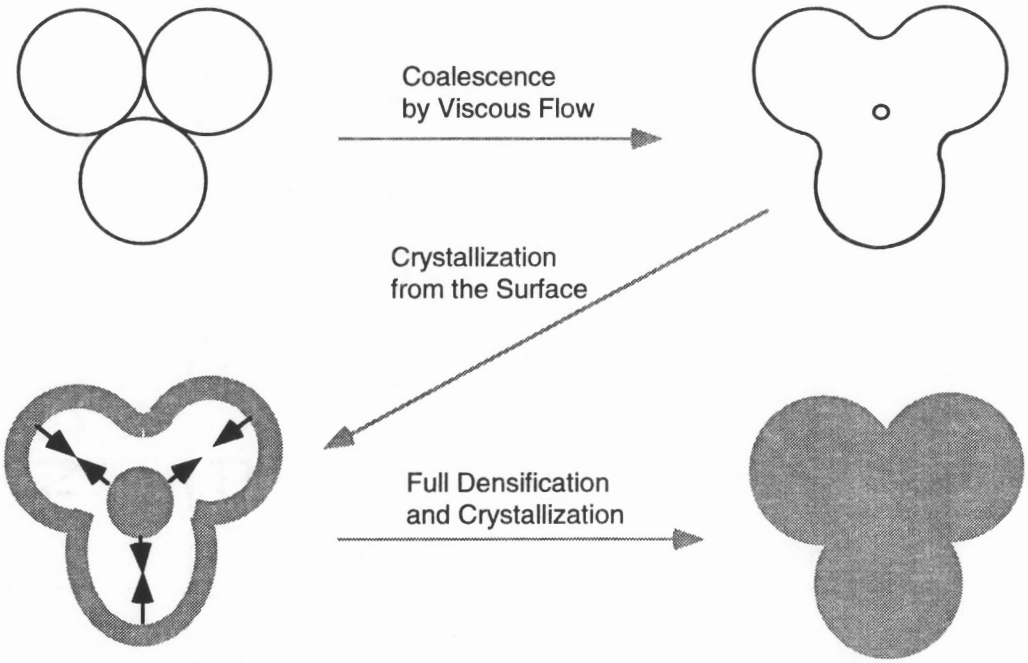

Figure 5.2 Schematic of coalescence and crystallization sequence of $(Li_{0.41},Mg_{0.035})Al(Si_{0.48},P_{0.52})0_4$ glass.

Section 3.5.3, this composition can not proceed through the conventional glass-ceramic process, *i.e.*, nucleation and crystallization heat treatment of solid glass sample is not possible due to catastrophic failure of the sample resulting from thermal expansion mismatch between the glass and the crystal phase developed. If the densification of the powder is too high, then the situation is the same as dealing with a solid glass sample, and cracking occurs during crystallization. Optimal degree of densification was obtained by heat treating the glass powder compact at 680°C for 3 hours. Figure 5.3 shows a green compact after sedimentation, and coalesced glass powder after heat treatment at 680°C for 3 hours. Individual glass particles coalesced with ≈7 vol% of pores. After that, final densification was conducted at 1200°C for 50 hours with crystallization. During heat treatment at 1200°C, TiO_2 whiskers were also precipitated. Figure 5.4 shows the final morphology of the sample after heat treatment. The precipitated TiO_2 whiskers have a higher aspect ratio than the whiskers precipitated in composition 1 which contains 4 wt% TiO_2 due to the higher TiO_2 content (6 wt%). Also, in this case, diffusion is easier because of the presence of pores, thus the higher aspect ratio of the TiO_2 whiskers is expected.

5.3 Physical Property Characterizations

5.3.1 Effect of TiO_2 Whisker Content on CTE of $AlPO_4$-Modified β-Eucryptite

CTE values of the in situ composite with various TiO_2 contents, shown in Figure 5.5, indicate that the CTE of the in situ composite increases linearly with increasing TiO_2 content. This would be expected because of the incorporation of TiO_2 which has a higher CTE value (7.8×10^{-6}/°C) than the matrix (-7.4×10^{-7}/°C). For example, for up to 6 wt% of TiO_2 content, the in situ composite exhibits negative aggregate CTE values for temperatures between 30 and 1000°C. However, the in situ composite containing 8 or higher wt% TiO_2 exhibits positive CTE values. The in situ composite containing 8~10

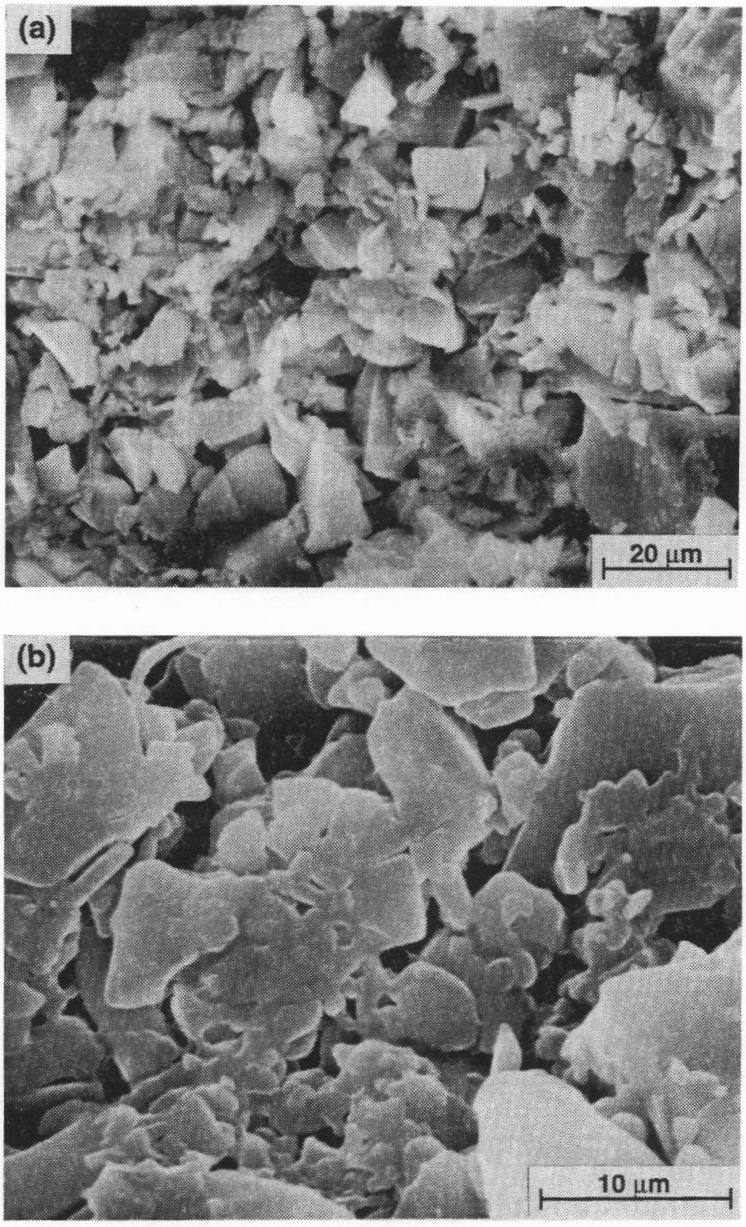

Figure 5.3 Scanning electron micrographs showing the microstructure of glass particles of (a)as-sedimented and (b)heat treated at 680°C/3 h.

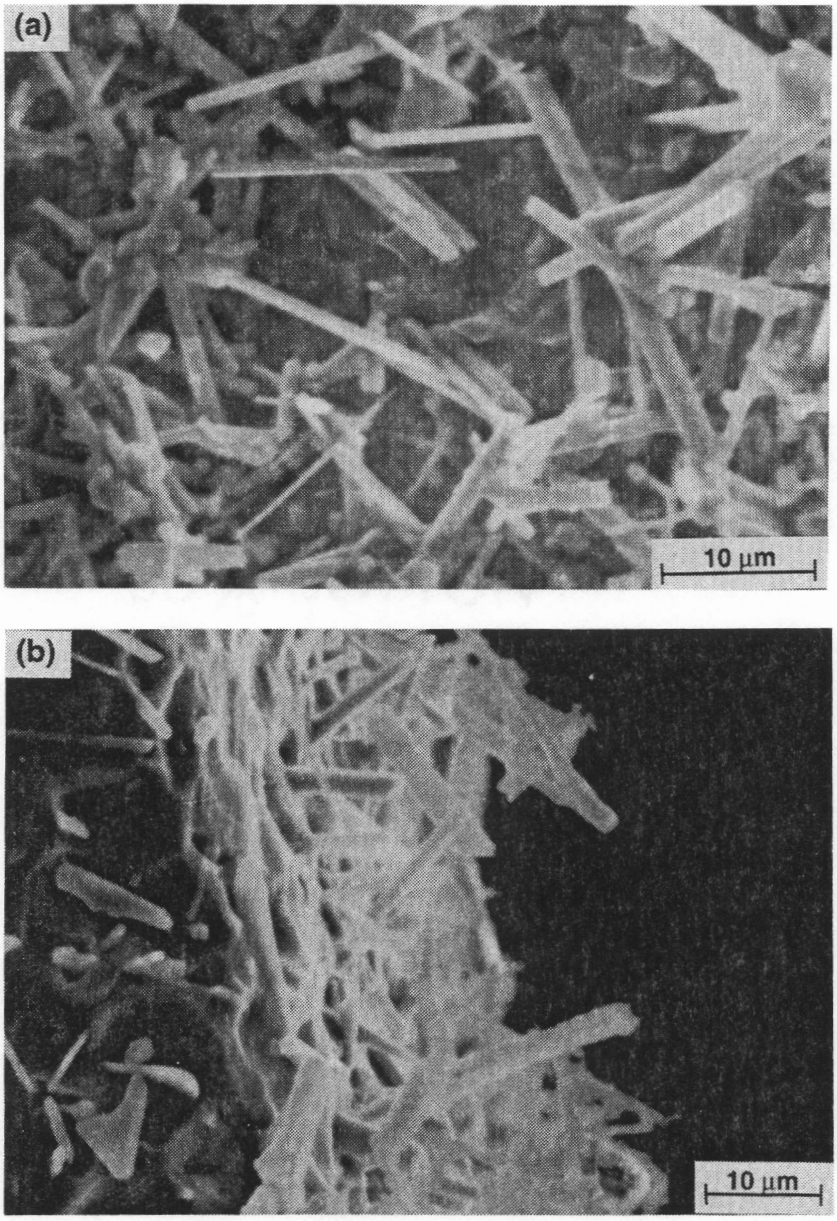

Figure 5.4 Scanning electron micrographs showing the microstructure of glass particles after crystallization at 1200°C/50 h. (a)front view of the fracture surface and (b)side view of the fracture surface.

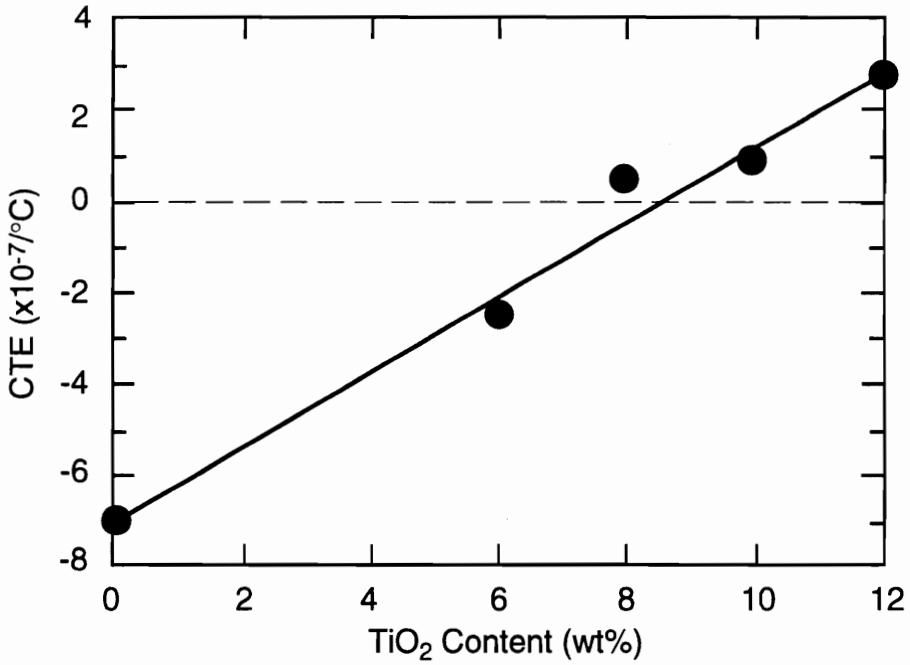

Figure 5.5 CTE (30 to 1000°C) values of $(Li_{0.41},Mg_{0.035})Al(Si_{0.48},P_{0.52})O_4$ glass-ceramic as a function of TiO_2 content.

wt% TiO_2 exhibits almost zero CTE values up to 1000°C. Microstructure observations indicate that incorporation of up to 12 wt% TiO_2 does not produce microcracks during heating and cooling of the material. Therefore, even though there is a thermal expansion mismatch between the $(Li_{0.41},Mg_{0.035})Al(Si_{0.52},P_{0.48})0_4$ glass-ceramic matrix and the TiO_2 whiskers, this mismatch does not have a detrimental effect on mechanical properties.

5.3.2 Effect of TiO_2 Whisker Content on Flexural Strength

As discussed earlier, the TiO_2 grown in situ throughout the $(Li_{0.4},Ca_{0.05})Al(Si_{0.75},P_{0.5})0_{4.5}$ glass-ceramic matrix improves the mechanical strength of the glass-ceramic. Theoretically, if whisker incorporation does not cause microcracking due to thermal expansion mismatch or inappropriate composite processing, then the mechanical strength of the composite increases with increasing volume fraction of the whisker according to the following relationship:[47]

$$\sigma_c = \sigma_w V_w \left(1 - \frac{1-\beta}{\ell/\ell_c}\right) + \sigma_m (1 - V_w) \qquad (5.1)$$

where σ_c, σ_m, and σ_w are the fracture strength of the composite, matrix, and whisker, respectively, V_m and V_w are the volume of the matrix and the whisker, respectively, ℓ_c is the critical whisker length, and β is the load transfer function.

In the case of the composition 1, $(Li_{0.4},Ca_{0.05})Al(Si_{0.75},P_{0.5})O_{4.5}$, the maximum amount of TiO_2 which can be incorporated is around 5 wt%, therefore it is very difficult to study of effect of TiO_2 content on the mechanical strength. On the other hand, in the case of composition 2, $(Li_{0.41},Mg_{0.035})Al(Si_{0.48},P_{0.52})0_4$, up to 12 wt% of TiO_2 can be incorporated. Therefore, the effect of TiO_2 content on the strength of the material was

examined by varying the TiO_2 amount. After sintering and crystallization, the sample exhibited 93% theoretical density with TiO_2 whisker precipitation throughout the sintered glass-ceramic matrix. Flexural strength of the sintered $(Li_{0.41},Mg_{0.035})Al(Si_{0.48},P_{0.52})0_4$ glass-ceramic with 0~12 wt% of TiO_2 was measured. The results, shown in Figure 5.6, indicate that the flexural strength increases with increasing TiO_2 content according to Equation 5.1. For example, when 12 wt% TiO_2 is incorporated, there is a three-fold increase in flexural strength compared to the sample without TiO_2 incorporation.

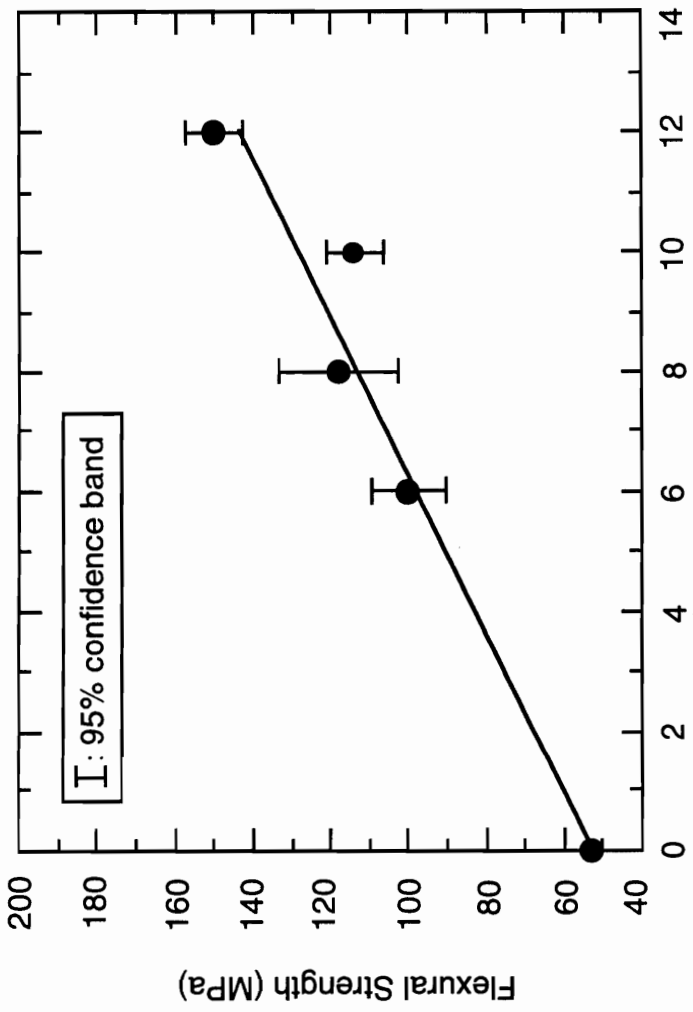

Figure 5.6 Effect of TiO_2 content on flexural strength of the modified β-eucryptite glass-ceramic.

SUMMARY AND CONCLUSIONS

In situ TiO_2 whisker-reinforced glass-ceramics in the Li_2O-Al_2O_3-P_2O_5-SiO_2 system were produced using either conventional glass-ceramic processing or sintering of the glass powder.

The in situ TiO_2 whisker-reinforced $AlPO_4$-modified β-eucryptite glass-ceramic with the composition [96% $(Li_{0.4},Ca_{0.05})Al(Si_{0.75},P_{0.5})O_{4.5}$, 4% TiO_2] was produced by heat treating the glass sample at 740°C for 2 hours to obtain the maximum number of nuclei, and 1040°C for 20 hours to crystallize the modified β-eucryptite phase and to precipitate TiO_2 whiskers throughout the glass-ceramic matrix. The maximum nucleation temperature, 740°C, was determined using a DTA method and the result was confirmed by SEM observation of the microstructures formed by nucleation/isothermal crystallization heat treatments. The apparent activation energy for crystallization of the material is 283 KJ/mol. TiO_2 whiskers which are grown in situ drastically improve mechanical strength, fracture toughness, and reliability of the material in operation under severe thermal shock conditions.

When TiO_2 whiskers (≈12 vol%) are precipitated from the $AlPO_4$-modified β-eucryptite glass-ceramic matrix, flexural strength is improved from 72 to 134 MPa. Elastic modulus of the material is also increased from 67 to 85 GPa. Fracture toughness, K_{IC}, is increased from the 1.1 to 1.6 MPa·√m due to crack deflection by the TiO_2 whiskers. The in situ composite exhibits rising fracture resistance with increasing crack extension. R-curve behavior of the material was determined from the relationship $K_R = k(\Delta a)^m$ where k and m are constant, and Δa is the crack extension. The fracture resistance is increased from 1.89 to 2.5 MPa·√m over the crack extension range of 40 to 200 μm, respectively. Because the in situ composite exhibits R-curve behavior, the material shows a narrow failure strength distribution.

The effect of TiO_2 whisker content on mechanical strength and CTE was determined using the composition $(Li_{0.41},Mg_{0.035})Al(Si_{0.48},P_{0.52})O_4$ with the amount of TiO_2 varying from 0 to 12 wt%. The glass compact was sintered at 1200°C for 50 hours. The resulting material exhibits 93% theoretical density with TiO_2 whisker precipitation throughout the glass-ceramic matrix. CTE value of the material changes from a negative to a positive value with increasing TiO_2 content. For example, the in situ composite containing 8~10 wt% TiO_2 exhibits near-zero CTE values up to 1000°C. This indicates excellent service capability of the material under severe thermal shock conditions. Results of flexural strength tests using three-point bending indicate that flexural strength of the sintered glass-ceramic increases with increasing TiO_2 content. When 12 wt% TiO_2 is precipitated as whiskers, there is a three-fold increase in flexural strength compared to the sample without TiO_2.

Improvement in mechanical strength, toughness, reliability, and thermal shock resistance is due to the development of TiO_2 whiskers which have higher strength, elastic modulus, and CTE values than those of the $AlPO_4$-modified β-eucryptite glass-ceramics without whiskers.

This unique method of improving mechanical properties of ceramic materials via in situ whisker reinforcement has resulted in a patent (*U.S. Patent No. 5,186,729*).

REFERENCES

1. F. L. Kennard, R. C. Bradt and V.S. STUBICAN, "Eutectic Solidification in the System MgO-$MgAl_2O_4$," J. *Am. Ceram. Soc.,* **56**[11] 566-69 (1973).

2. M. Fragneau and A. Revcolevschi, "Crystallography of Directionally Solidified NiO-CaO Eutectic," *J. Am. Ceram. Soc.*, **66**[9] C-162-C163 (1983).

3. C. C. Sorrel, H. R. Beratan, R.C. Bradt, and V.S. Stubican, "Directional Solidification of (Ti,Zr) Boride Eutectics," *J. Am. Ceram. Soc.*, **67**[3] 190-94 (1984).

4. W. Vogel, Chemistry of Glass, American Ceramic Society, Inc. (1985).

5. A. Paul, Chemistry of Glass, Chapman and Hall, New York (1982).

6. Z. Strinad, Glass-Ceramic Materials, Glass Science and Technology; vol. 8, Elsevier Science Publishing Company, Inc., New York (1986).

7. H. G. F. Winkler, "Synthesis and Crystal Structure of β-Eucryptite, $LiAlSiO_4$," *Acta Crystallogr.*, **1** [1] 27-34 (1948)

8. V. Tscherry and F. Laves, "Synthesis and X-Ray Deflection Pattern of β-Eucryptite," *Naturwissenschaften*, **57** [4] 194 (1970).

9. F. Hummel, "Significant Aspect of Certain Ternary Compounds and Solid Solutions," *J. Am. Ceram. Soc.*, **35** [3] 64-66 (1952).

10. Yu. Kondrat'ev, "Order and Disorder in Lithium Aluminosilicates," *Izv. Akad. Nauk. SSSR Neorg. Matter.*, **1** [5] 1935-1938 (1965).

11. F. Gillery and E. Bush, "Thermal Contraction of β-Eucryptite ($Li_2O{\cdot}Al_2O_3{\cdot}2SiO_2$) by X-Ray and Dilatometer Methods," *J. Am. Ceram. Soc.*, **42**[4] 175-7 (1959).

12. T. Tien and F. Hummel, "Studies in Lithium Oxide System: VIII, $Li_2O{:}Al_2O_3{:}2SiO_2$ - $Li_2O{:}Al_2O_3{:}2GeO_2$,"*J. Am. Ceram. Soc.*, **47**[11] 582-84 (1964).

13. V. Tscherry and H. Schulz, M. Czank, "Thermal Expansion of the Lattice Constants of β-Eucryptite Single Crystals," *Ber. Deut. Keram. Ges.*, **49**[5] 153-4 (1972).

14. F. Hummel, U.S. Pat., Re.24,795 (1960).

15. J. S. Moay, A. G. Verduch, and M. Hortal, "Thermal expansion of Beta-Eucryptite Solid Solutions," *Trans. J. Brit. Ceram. Soc.*, **73** [6] 177-178 (1974).

16. F. Hummel and J. B. Langensiepen, "Elimination of α to β Cristoballite Inversion of $AlPO_4$," *Korean Cer. Inds. Ass.*, **11**[4], 4-5 (1986).

17. A. J. Perrotta, U.S. Pat., 3,549,394,22 (1970).

18. Y. Yang, Private Communication, Virginia Tech, Blacksburg (1989).

19. W. D. Kingery, H. K. Bowen, and D. R. Uhlmann, Introduction to Ceramics, John Wiley and Sons, New York (1976).

20. S. D. Stookey, "Chemical Machining of Photosensitive Glass," *Ind. Eng. Chem.*, **45**[1] 115-18 (1953).

21. D. A. Porter and K. E. Easterling, Phase Transformations in Metals and Alloys, Van Nostrand Reinhold Co., New York (1981).

22. J. J. Hammel, pp. 1-9 in *Advances in Nucleation and Crystallization in Glasses*, edited by L.L. Hench and S.W. Freiman, American Ceramic Society, Colmbus, OH (1971).

23. J. R. Swift, "Some Experiments on Crystal Growth and Solution in Glasses," *J. Am. Ceram. Soc.*, **30**[6] 165 (1947).

24. P. E. Doherty, D. W. Lee, and R. S. Davis, "Direct Observation of the Crystallization of Li_2O-Al_2O_3-SiO_2 Glasses Containing TiO_2,"*J. Am. Ceram. Soc.*, **55** [2] 77-81 (1970.

25. V. Maier and G. Muller, "Mechanism of Oxide Nucleation in Lithium Aluminosilicate Glass-Ceramics," *J. Am. Ceram. Soc.*, **70** [8] C176-C178 (1987).

26. T. I. Barry, D. Clinton, L. A. Lay, R. A. Mercer, and R. P. Miller, "The Crystallization of Glasses Based on the Eutectic Compositions in the System Li_2O-Al_2O_3-SiO_2, Part I," J. *Mat. Sci.*, **4**, 596-612 (1969).

27. W. Hinz and P. O. Kunth, "Phase Separation and Nucleation in Vitroceram Production," *Glasstech. Ber.*, **34** [9] 431-7 (1961).

28. J. Hsu and R F. Speyer, "Comparison of the Effects of Titania and Tantalum Oxide Nucleating Agents on the Crystallization of $Li_2O{\cdot}Al_2O_3{\cdot}6SiO_2$ Glasses,"*J . Am. Ceram. Soc.*, **72** [12] 2334-41 (1989).

29. D. G. Bernett and R. W. Douglas, "Liquid-Liquid Phase Separation in the Soda-Baria-Silica System," *Phys. Chem. Glasses*, **12**[5] 117-24 (1971).

30. G. H. Beall, B. R. Karstetter, and H. L. Rittler, "Crystallization and Chemical Strengthening of Stuffed β-Quartz Glass-Ceramics," *J. Am. Ceram. Soc.*, **50**[4] 181-89 (1967).

31. R. D. Maurer, "Crystal Nucleation in a Glass Containing Titania," *J. Appl. Phys.*, **33**[6] 2132-39 (1962).

32. W. B. Hillig; pp. 77-89 in *Symposium on Nucleation and Crystallization in Glasses and Melts.* Edited by M. K. Reser, G. Smith, and H. Insley. The American Ceramic Society, Columbus, Ohio, 1962.

33. P. W. McMillan, Glass-Ceramics, 2nd ed. Academic Press, London, 1979.

34. C. E. Inglis, *Trans. Inst. Nav. Archit*, **55** 219-230 (1913)

35. A. A. Griffith, "Phenomena of Rupture and Flow in Solid," *Phil. Trans. Roy. Soc.* (London), **221A** 163-98 (1920).

36. A. J. Stryjak and P. W. McMillan, "Microstructure and Properties of Transparent Glass-Ceramics Part 2: The Physical Properties of Spinel Transparent Glass-Ceramics,"*J. Mat. Sci.*, **13**[8] 1794-1804 (1978).

37. Megumi Tashiro, "Chemical Compositions of Glass-Ceramics: II," *Glass Ind.*, **47**[8] 428-35 (1966).

38. Yoshikazu Utsumi and Sumio Sakka, "Strength of Glass-Ceramics Relative to Crystal Size," *J. Am. Ceram. Soc.*, **53**[5] 286-7 (1970).

39. D. Weyl, "Influence of Internal Strains on Texture and Mechanical Strength of Porcelains," *Ber. Deut. Keram. Ges.*, **36** [10] 319-24 (1958).

40. J. Selsing, "Internal Stresses in Ceramics," *J. Am. Ceram. Soc.*, **44**[8] 419 (1961).

41. D. Binns, pp.315-34 in Science of Ceramics, Vol. 1, Edited by G.H. Stewart, Academic Press, New York (1962).

42. W. J. Frey, and J. D. Mackenzie, "Mechanical Properties of Selected Glass-Crystal Composites," *J. Mater. Sci.*, **2**[2] 124-30 (1967).

43. M. P. Borom, A. M. Turkalo, and R. H. Doremus, "Strength and Microstructure of Lithium Disilicate Glass-Ceramics," *J. Am. Ceram. Soc.*, **58**[9-10] 385-91 (1975).

44. R. R. Tummala, and A. L. Friedberg, "Strength of Glass-Crystal Composites," *J. Am. Ceram. Soc.*, **52**[4] 229-30 (1969).

45. R. W. Davidge and T. J. Green, "The Strength of Two-Phase Ceramic/Glass Materials," *J. Mat. Sci.*, **3**[6] 629-34 (1968).

46. S. W. Freiman and L. L. Hench, "Effect of Crystallization on the Mechanical Properties of Li2O-SiO2 Glass-Ceramics," *J. Am Ceram. Soc.*, **55**[2] 86-90 (1972).

47. K. K. Chawla, Composite Materials, Springer-Verlag, New York (1987).

48. R. Warren and V. K. Sarin, "Fracture of Whisker-Reinforced Ceramics," pp.571-614 in Application of Fracture Mechanics to Composite Materials edited by K. Friedrich, Elsevier Science Publisher, New York (1989).

49. Y. Termonia, "Theoretical Study of the stress transfer in Single Fibre Composites," *J. Mat. Sci.*, **22** 504-8 (1987).

50. R Hull, An Introduction to Composite Materials, Cambridge University Press, Cambridge (1981).

51. B. D. Agrawal and L. J. Broutman, Analysis and Performance of Fiber Composite, Wiley, New York, 1980

52. J. C. Halpin and S. W. Tsai, "Effect of an Environmental Factors on Composite Materials," AFML-TR67-423 (1969).

53. I. W. Donaldson and P. W. McMillan, "Review Ceramic-Matrix Composite," *J. Mat. Sci.*, **11** 949-72 (1976).

54. N. Claussen and G. Petzow, "Whisker-Reinforced Zirconia-Toughened Ceramics," pp. 649-62 in Tailoring Multiphase and Composite Ceramics, edited by R. E. Tressler, G. L. Messing, C. G. Pantano, and R. E. Newnham, Plenum Press, New York, (1986)

55. P. D. Shalek, J. J. Petrovic, G. F. Hurley and F. D. Gac, "Hot Pressed SiC Whisker/Si_3N_4 Matrix Composites,"*Am. Ceram. Soc. Bull.*, **65**[2] 351-56 (1986).

56. K. P. Gadkaree and K. Chyung, "Silicon-Carbide-Whisker-Reinforced Glass and Glass-Ceramic Composites," Am. Ceram. Soc. Bull. **66** [2] 370-76 (1987).

57. W. L. Vaughn, J. C. Homeny and M. K. Ferber, "Mechanical Properties of Silicon Carbide Whisker/Aluminum Oxide Matrix Composites," *Ceram. Eng. Sci. Proc.* **8** 848-59 (1987).

58. C. G. Wei and P. F. Becher, "Development of SiC-Whisker-Reinforced Ceramics," *Am. Ceram. Soc. Bull.* **64**[2] 298-304 (1985).

59. S. T Buljan, J. G. Baldoni and M. G. Huckabee, "Si_3N_4-SiC Composites," *Am. Ceram. Soc. Bull.* **66**[2] 347-52 (1987).

60. K. T. Faber and A. G. Evans, "Crack Deflection Process–I. Theory," *Acta Metall.*, **31**, 577-87 (1983).

61. G. H. Stewart, Science of Ceramics, Academic Press, New York (1962).

62. R. G. Hoagland, C. W. Marschall, A. R. Rosenfield, G. Hollenberg, and R. Ruh, "Microstructural Factors Influencing the Fracture Toughness of Hafnium Titanate," *Mater. Sci. Eng.*, **15**[1] 51-62 (1974).

63. A. Marrotta, A. Buri, F. Branda, and S. Saiello, "Nucleation and Crystallization of $Li_2O{\cdot}2SiO_2$ Glass–A DTA study,"; pp.146-52 in *Advances Nucleation and Crystallization in Glasses*, Edited by J. H. Simmons, D. R. Uhlmann, and G. H. Beall, American Ceramic Society, Inc., Columbus, OH (1982)

64. H. E. Kissinger, "Variation of Peak Temperature with Heating Rate in Differential Thermal Analysis," *J. Res. Natl. Bur. Stand. (U.S.)*, **57**[4] 217-21 (1956).

65. B. R. Lawn, A. G. Evans, and D. B. Marshall, "Elastic/Plastic Indentation Damage in Ceramics: Median/Radial Crack System," *J. Am. Ceram. Soc.*, **63**[9-10] 574-81 (1980).

66. G. R. Antis, P. Chantikul, B. R. Lawn, and D. B. Marshal, "A Critical Evaluation of Indentation Techniques for Measuring Fracture Toughness: I, Direct Crack Measurements," *J. Am. Ceram. Soc.*, **64**[9] 533-43 (1981).

67. T. Ozawa, "Kinetics of Non-Isothermal Crystallization," *Polymer*, **12** 150-58 (1971).

68. J. A. Augis and J. E. Bennett, "Calculation of the Avrami Parameters for Heterogeneous Solid-State Reactions Using a Modification of Kissinger Method," *J. Ther. Anal.*, **13**[2] 283-92 (1978).

69. C. S. Ray and D. E. Day, "Crystallization of Calcia-Gallia-Silica Glasses," *J. Am. Ceram. Soc.*, **67**[12] 806-9 (1984).

70. C. S. Ray, W. Huang, and D. E. Day, "Crystallization Kinetics of Lithia-Silica Glass: Effect of Sample Characteristics and Thermal Analysis Measurement Techniques," *J. Am. Ceram. Soc.*, **74**[1] 60-6 (1991).

71. C. S. Ray and D. E. Day, "Nucleation and Crystallization in Glasses as Determined by DTA," Fourth Symposium on Nucleation and Crystallization, Glass and Optical Meeting, Stone Mt., Georgia (1992).

72. S. Musikant, What Every Engineer Should Know About Ceramics, Marcel Dekker, Inc., New York (1991).

73. H. P. Kirchner and R. M. Grover, "Strength-Anisotropy-Grain Size Relations in Ceramic Oxides," *J. Am. Ceram. Soc.*, **53**[5] 232-6 (1970).

74. R. F. Cook and G. M. Pharr, "Direct Observation and Analysis of Indentation Cracking in Glasses and Ceramics," *J. Am. Ceram. Soc.*, **73**[4] 787-817 (1990).

75. S. M. Wiederhorn, "Fracture Surface Energy of Glass,"*J. Am. Ceram. Soc.*, **52**[2] 99-105 (1969).

76. S. W. Freiman, "Brittle Fracture Behavior of Ceramics," *Ceram. Bull.*, **67**[2], 392-402 (1988).

77. B. R. Lawn and M. V. Swain, "Microstructure beneath Point Indentations in Brittle Solids," *J. Mater. Sci.*, **10**[1] 113-22 (1975).

78. R. F. Krause, "Rising Fracture Toughness from the Bending Strength of Indented Alumina Beams," *J. Am. Ceram. Soc.*, **71**[5] 338-43 (1988).

79. J. C. Newman, Jr., and I. S. Raju, "An Empirical Stress-Intensity Factor Equation for the Surface Crack," *Eng. Fract. Mech.*, **15**, 185-92 (1981).

80. R. F. Cook and D. R. Clarke, "Fracture Stability, R-Curves and Strength Variability," *Acta Metall.* **36**[3] 555-62 (1988).

81. K. Kendal, N. Alford, S. R. Tan, and J. D. Birchall, "Influence of Toughness on Weibull Modulus of Ceramic Bend Strength," *J. Mat. Res.*, **1**[1] 120-23 (1986).

82. N. Ramachandran, L. Y. Chao, and D. K. Shetty, "R-curve Behavior and Flaw Insensitivity of Ce-TZP/Al_2O_3 Composite," *J. Am. Ceram. Soc.*, **76**[4] 961-69 (1993)

VITA

Kyoungho Lee was born in the Republic of Korea, on August 21, 1963. He attended Korea University and received his Bachelor of Science degree in Materials Science in February, 1986. After graduation, he entered the graduate program in Materials Science and Engineering, College of Engineering at Virginia Tech and received his Master of Science degree in May, 1988. After that he returned to Korea and served in the Korean Army as a second lieutenant. He enrolled as a Ph.D. student in Materials Engineering and Science, College of Engineering at Virginia Tech in September, 1989.

Kyoungho Lee